Chem Soc Rev

# Thermo-photo catalysis: A whole greater than the sum of its parts



| | |
|---|---|
| Journal: | *Chemical Society Reviews* |
| Manuscript ID | CS-SYN-08-2021-000782.R2 |
| Article Type: | Review Article |
| Date Submitted by the Author: | 31-Mar-2022 |
| Complete List of Authors: | Fang, Siyuan; Michigan Technological University,<br>Hu, Yun Hang; Michigan Technological University, Materials Science and Engineering |
| | |

ARTICLE

# Thermo-photo catalysis: a whole greater than the sum of its parts

Siyuan Fang and Yun Hang Hu*

Received 00th January 20xx,
Accepted 00th January 20xx

DOI: 10.1039/x0xx00000x

Thermo-photo catalysis, which is the catalysis with the participation of both thermal and photo energies, not only reduces the large energy consumption of thermal catalysis but also addresses the low efficiency of photocatalysis. As a whole greater than the sum of its parts, thermo-photo catalysis has been proven as an effective and promising technology to drive chemical reactions. In this review, we first clarify the definition (beyond photo-thermal catalysis and plasmonic catalysis), classification, and principles of thermo-photo catalysis and then reveal its superiority over individual thermal catalysis and photocatalysis. After elucidating the design principles and strategies toward highly efficient thermo-photo catalytic systems, an ample discussion on the synergetic effects of thermal and photo energies is provided from two perspectives, namely, the promotion of photocatalysis by thermal energy and the promotion of thermal catalysis by photo energy. Subsequently, state-of-the-art techniques applied to explore thermo-photo catalytic mechanisms are reviewed, followed by a summary on the broad applications of thermo-photo catalysis and its energy management toward industrialization. In the end, current challenges and potential research directions related to thermo-photo catalysis are outlined.

## 1. Introduction

Although catalysis widely exists in nature in the form of digestion, fermentation, and some other enzymatic processes, artificial catalysis did not emerge until the early 1800s.[1] Faraday was the first to explore the heterogenous catalytic reaction and indicate the zone of adsorbed material as the catalytic reaction region (Fig. 1).[1] Afterwards, a number of efforts were made in both theoretical construction and experimental exploration of heterogenous (thermal) catalysis.[2, 3] Until 1911, Eibner found the illumination of ZnO led to the bleaching of Prussian blue pigment, which marks the birth of a new type of heterogeneous catalysis driven by photo energy - photocatalysis.[4, 5] Later, in 1972, Fujishima and Honda discovered that ultraviolet (UV) light irradiation of a cell consisting of a $TiO_2$ photoanode and a Pt counter electrode could achieve $H_2$ production from water.[6]

**Siyuan Fang**

*Siyuan Fang is currently a PhD student under the supervision of Prof. Yun Hang Hu at Michigan Technological University. Siyuan received her bachelor's degree in Engineering from Shanghai Jiao Tong University in 2019. Her research interests include the design and application of novel thermo-photo catalytic processes for energy conversion and environmental remediation and the synthesis of advanced carbon materials.*

*Department of Materials Science and Engineering, Michigan Technological University, Houghton, Michigan 49931-1295, United States*
*E-mail: yunhangh@mtu.edu*

**Yun Hang Hu**

*Yun Hang Hu is the Charles and Carroll McArthur Endowed Chair Professor at Department of Materials Science and Engineering, Michigan Technological University. He is fellows of AAAS, ACS, APS, AIChE, ASM, and RSC. He was elected as the chair of the Energy and Fuels Division of the American Chemical Society (ACS) in 2014 and the president of the Hydrogen Storage Division of International Association of Hydrogen Energy (IAHE) in 2015. He is the editor-in-chief of "Energy Science & Engineering" (Wiley journal) and an editorial board member for 8 international journals. His main research interests range from thermo-photo catalysis, heterogeneous catalysis, nanomaterials, clean fuels, solar energy, batteries, supercapacitors, fuel cells, photodegradation of pollutants, natural gas conversion, and hydrogen storage materials to $CO_2$ conversion with about 300 papers published in prestigious journals.*

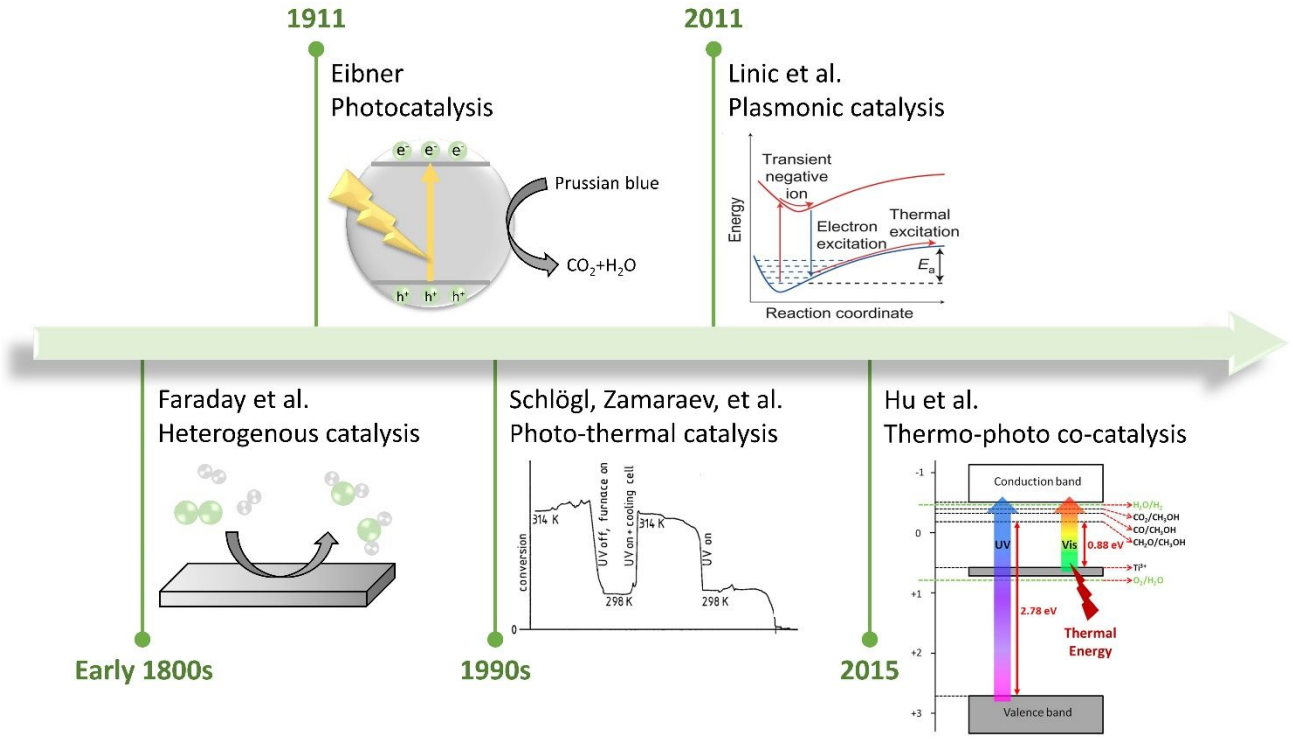


**Fig. 1** Milestones in the development of thermo-photo catalysis. Reproduced with permission from ref. 13, Copyright (1991) Springer; ref. 18, Copyright (2011) Springer Nature; ref. 21, Copyright (2015) American Chemical Society.

Thanks to these pioneering works, both thermal catalysis and photocatalysis have attracted broad research interests to drive reactions for producing chemicals and fuels.[7-10] However, typically, thermal catalysis suffers from large energy consumption and low catalytic selectivity, while photocatalysis demonstrates poor catalytic efficiency and limited solar energy conversion.[9, 11, 12] This dilemma inspired the exploration of synergetic catalytic processes with the participation of both thermal and photo energies.

Since 1990s, some researchers utilized photo-to-thermal conversion to increase reaction temperature and thus the catalytic efficiency.[13-15] These catalytic processes in which the only role of light irradiation is to provide thermal energy are named photo-thermal catalysis, which inherently belongs to thermal catalysis despite the apparent dependence on photo energy.[16, 17] Later, in 2011, Linic and co-workers explored the catalytic reactions over plasmonic nanostructures of Ag under illumination at high temperatures as a new catalysis category entitled plasmonic catalysis.[18] Plasmonic catalysis is based on the localized surface plasmon resonance (LSPR) effect and driven by hot charge carriers and/or thermal energy, while quantifying their respective contributions remains as a challenge.[19, 20]

Distinctively, in 2015, Hu's group revealed the intrinsic contradiction of visible-light photocatalysis on the band gap of catalysts, namely, the visible light absorption requires a smaller band gap, whereas a larger band gap is necessary to obtain a sufficient potential energy as a driving force for photocatalytic reaction.[21] To solve this critical issue, Hu pioneered the strategy of utilizing kinetic energy to compensate insufficient potential energy for driving a reaction in visible-light photocatalysis. Consequently, his group experimentally demonstrated that the introduction of thermal energy (i.e., kinetic energy) into photocatalytic system realized highly efficient visible-light driven thermo-photo catalytic $H_2$ production from water.[21] Since then, a rapid and exciting development in thermo-photo catalysis has been witnessed with an emphasis on catalyst design and catalytic performance enhancement. So far, thermo-photo catalysis, as a whole greater than the sum of its parts (individual thermal catalysis and photocatalysis), has been applied in a wide range of chemical processes such as $CO_2$ reduction,[22-26] $CH_4$ oxidation,[27-33] CO conversion,[34-38] $H_2$ production,[21, 39-42] $N_2$ fixation,[43-46] pollutant degradation,[47-51] and organic synthesis,[52-56] showing high activity, tuneable selectivity, and excellent stability under mild conditions at low cost, owing to the synergetic effects of thermal and photo energies (Fig. 2).

Currently, most research works and published reviews are focused on the resulting catalytic performance while the underlying synergetic mechanism remains confusing.[11, 57-59] Therefore, it is of vital importance to provide an insightful review revealing the synergetic effects of thermal and photo energies, which would act as a valuable guideline for designing highly efficient catalytic processes. Here, different from previous reviews which are focused on a subgroup of thermo-photo catalysis like photo-thermal catalysis[15, 57, 60] and plasmonic catalysis[19, 20, 61, 62] or limited to specific chemical reactions,[11, 58, 63, 64] we will (1) clearly define and classify thermo-photo catalysis, (2) reveal the superiority of thermo-photo catalysis over individual thermal catalysis and photocatalysis, (3) elucidate design principles and strategies for building a highly efficient thermo-photo catalytic system, (4) provide an

 

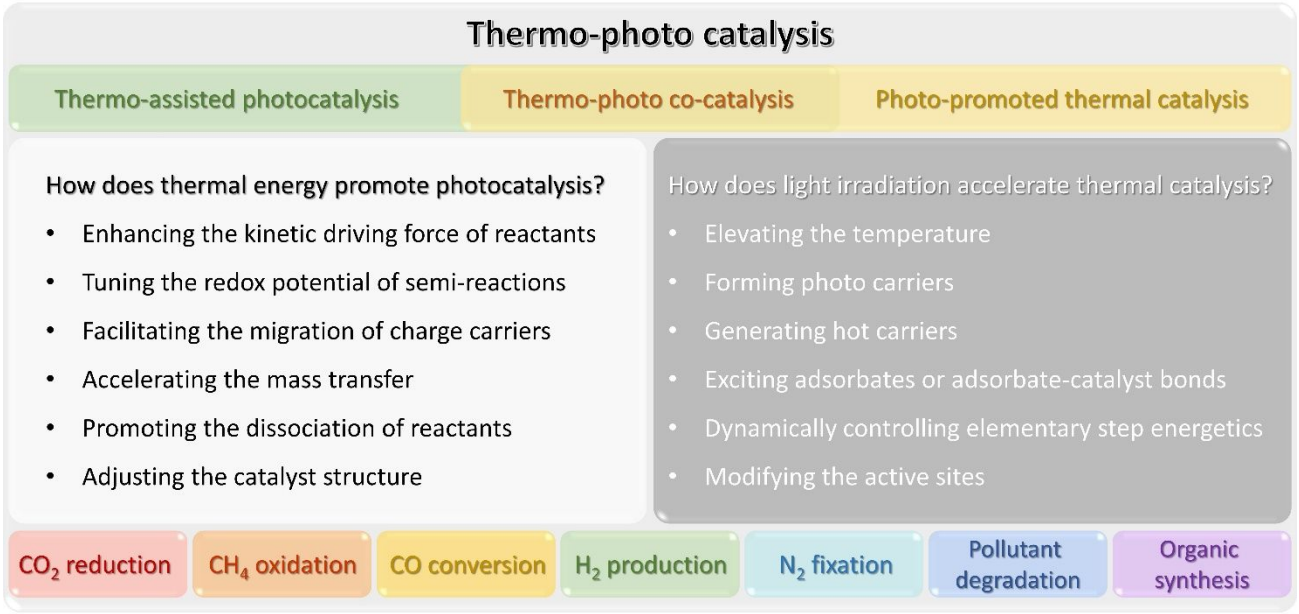


**Fig. 2** Classification, synergetic effect, superiority, and application of thermo-photo catalysis.

up-to-date understanding on the synergetic roles of thermal and photo energies from the perspective of "*How does thermal energy promote photocatalysis?*" and "*How does light irradiation accelerate thermal catalysis?*", (5) comprehensively discuss current techniques used to explore thermo-photo catalytic mechanisms, (6) highlight the broad applications of thermo-photo catalysis, (7) propose energy-related considerations and strategies for scaling up thermo-photo catalytic processes, and finally (8) outline current challenges and potential future research directions associated with thermo-photo catalysis.

## 2. What is thermo-photo catalysis?

Despite the booming development and wide application of thermo-photo catalysis, some key questions remain to be answered, such as "*What is thermo-photo catalysis?*" and "*What are the advantages of thermo-photo catalysis?*". In this section, the confusing term of thermo-photo catalysis will be defined together with a clear classification based on the catalytic principles. Furthermore, the superiority of thermo-photo catalysis over individual thermal catalysis and photocatalysis will be revealed.

### 2.1. Definition of thermo-photo catalysis

Here, we provide a broad and clear definition for thermo-photo catalysis. Namely, it is the catalysis with the participation of both thermal and photo energies in which thermal energy promotes photocatalysis and/or photo energy accelerates thermal catalysis. Thermal energy that elevates the temperature of catalyst surface above room temperature (~25 °C) can be either supplied by external heat sources or induced by light irradiation, while photo energy is generally provided by lamps on laboratory scale but expected for the direct utilization of sunlight. Moreover, it should be clarified that thermo-photo catalysis is distinct from the generally claimed photo-thermal catalysis that relies on light-induced temperature rise to realize desirable thermal catalytic performance.[15, 60] In other words, photo-thermal catalysis is just a small part of the thermo-photo catalysis that covers all aspects associated with the synergies of thermal and photo energies in catalysis.

### 2.2. Classification of thermo-photo catalysis

After elucidating the concept of thermo-photo catalysis, it is even more important to classify thermo-photo catalysis accurately and reasonably. Herein, based on catalytic principles, thermo-photo catalysis is classified into three categories, namely, thermo-assisted photocatalysis, photo-promoted thermal catalysis, and thermo-photo co-catalysis, which will be discussed in detail in the following parts.

#### 2.2.1. Thermo-assisted photocatalysis

Thermo-assisted photocatalysis represents the catalytic process mainly driven by photo-generated charge carriers over the (photo)catalyst with thermal energy playing certain stimulative roles. In this case, the supply of thermal energy alone to reach the same reaction temperature results in a negligible catalytic efficiency. The basic steps of thermo-assisted photocatalysis are identical to those of traditional photocatalysis (Fig. 3a). Namely, when photons whose energies are equal to or larger than the band gap of the catalyst are absorbed, electrons located at the top of valence band are excited to conduction band, with holes left in valence band (step Ⅰ). As-generated electrons and holes are expected to migrate to catalyst surface (step Ⅱ) to drive the reduction and oxidation semi-reactions of adsorbed reactants, respectively (step Ⅲ), while the recombination of some electrons and holes is generally unavoidable.[9, 65] The effective separation and migration of charge carriers are the key for a highly efficient thermo-assisted photocatalytic process.

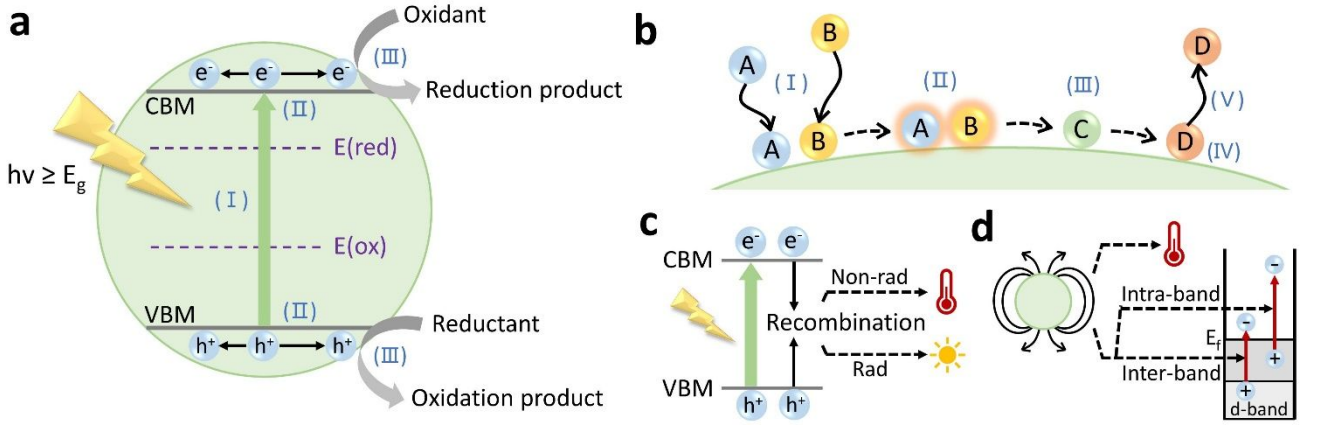


**Fig. 3** Catalytic principle and pathway of thermo-photo catalysis. (a) Thermo-assisted photocatalysis. (b) Photo-promoted thermal catalysis. (c) Photo-thermal effect induced by recombination of charge carriers over semiconductor catalysts. (d) Photo-thermal effect and hot carrier generation induced by the decay of plasmons over plasmonic metal catalysts.

The thermodynamic requirements for thermo-assisted photocatalysis are the same as those for traditional photocatalysis. Namely, the redox potential of reduction semi-reaction is below conduction band minimum, while the redox potential of oxidation semi-reaction is above valence band maximum.[66] Since there is no requirement on the relative positions of redox potentials of semi-reactions, both thermodynamically downhill (ΔG < 0) and uphill (ΔG > 0) reactions can proceed, showing its superiority over thermal catalytic processes.

The roles of thermal energy in thermo-assisted photocatalysis can be clearly outlined according to the above-discussed basic steps and thermodynamic requirements. On the one hand, from the perspective of basic steps, the introduction of thermal energy can facilitate the migration of charge carriers, accelerate mass transfer, enhance kinetic driving force, and promote the dissociation of reactant molecules.[21] On the other hand, in terms of thermodynamics, adjusting reaction temperature can help to tune the redox potentials of semi-reactions and broaden the application range for narrow-band-gap semiconductors.[33, 67] In addition, thermal input can contribute to the structural control of catalysts. These aspects will be thoroughly discussed in section 4.

### 2.2.2. Photo-promoted thermal catalysis

As the counterpart of thermo-assisted photocatalysis, photo-promoted thermal catalysis is predominantly driven by thermal energy or hot carriers with photons acting as a promoter (Fig. 4). In this case, the catalyst with light absorption characteristics shows an evident thermal catalytic efficiency for thermodynamically downhill (ΔG < 0) reactions. Similar to traditional thermal catalysis, photo-promoted thermal catalysis generally undergoes five steps (Fig. 3b), namely, adsorption of reactants (step Ⅰ), activation of chemical bonds (step Ⅱ), generation of intermediate species (step Ⅲ), transformation of intermediates to final products (step Ⅳ), and desorption of product molecules (step Ⅴ), among which the generation of intermediate species is typically the rate-limiting step which is directly related to the surface properties of catalysts.[11] As one of the promotion effects of photo energy, light irradiation can dynamically adjust the catalyst structure to retain adequate active sites.[24, 52]

The widely investigated photo-thermal catalysis and plasmonic catalysis are two subgroups of photo-promoted thermal catalysis. Photo-thermal catalysis depends on the light-induced temperature rise owing to the direct vibration absorption of far infrared (IR) light and indirect non-radiative relaxation.[68, 69] Non-radiative relaxation occurs via either Auger recombination or Shockley-Read-Hall recombination, leading to the dissipation of excessive energy in the form of lattice vibrations (namely, phonons), rendering it the main contributor to heat generation in semiconductor catalysts (Fig. 3c).[60] In this light, to allow favourable excitation and recombination of charge carriers, dark catalysts with narrow band gaps are desired.

While, for plasmonic metal catalysts with LSPR effect (induced by the consistent frequencies of photons with the natural oscillation of surface electrons), hot charge carriers are resulted under illumination along with local heat (Fig. 3d).[19] These hot charge carriers are generated via non-radiative decay through intra-band s-to-s transitions or inter-band d-to-s transitions under the intense electric field on metal surface.[19, 61, 70] As-generated hot electrons can promote both bond activation (step Ⅱ) and intermediate transformation (step Ⅳ) via transient electronic excitations with an evident decrease in activation energy and thus the lower requirement on reaction temperature (Fig. 4b).[19, 71] The promotion effects of photo energy on thermal catalysis will be further elucidated in section 5.

### 2.2.3. Thermo-photo co-catalysis

Thermo-photo co-catalysis is a unique synergetic process in which heat and light can respectively drive the thermal catalytic and photocatalytic reactions. In this case, both thermal catalysis and photocatalysis demonstrate decent catalytic efficiencies, while the co-catalytic efficiency is higher than the sum of individual thermal and photo catalytic efficiencies. Here, both the above catalytic pathways illustrated in Figs. 3a and 3b are

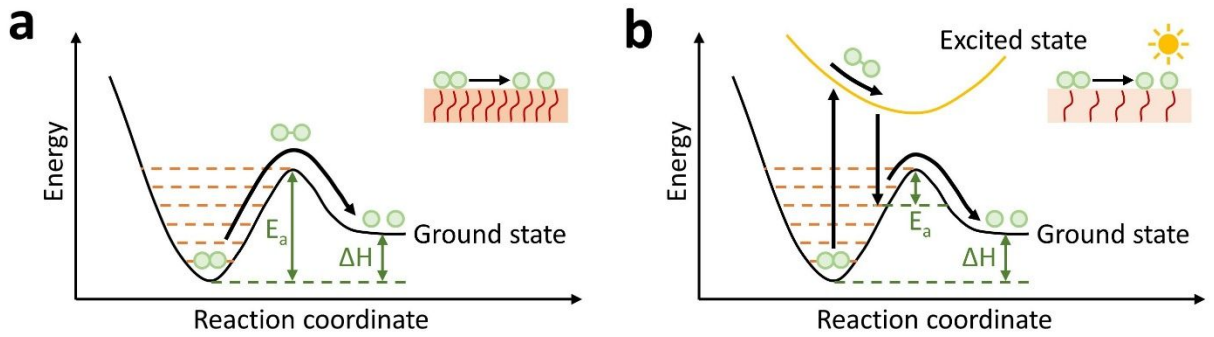


**Fig. 4** Energy diagram for (a) thermal catalysis and (b) thermo-photo catalysis over plasmonic metal catalysts. Here, an endothermic dissociation reaction is shown as an example, while the enthalpy change can be negative as well.

present. Moreover, the synergetic effects between thermal and photo energies are similar to those in thermo-assisted photocatalysis and photo-promoted thermal catalysis.

### 2.3. Superiority of thermo-photo catalysis over individual thermal catalysis and photocatalysis

Thermo-photo catalysis, as a whole greater than the sum of its parts (thermal catalysis and photocatalysis), has shown a number of advantages in terms of apparent catalytic performance such as improved activity, selectivity, and stability, as well as mild reaction condition and thus a low cost. In this subsection, the superiority of thermo-photo catalysis over individual thermal catalysis and photocatalysis will be revealed respectively.

#### 2.3.1. Compared with thermal catalysis

The most critical issue of thermal catalysis is the harsh reaction condition such as high temperature and high pressure which can cause noticeable energy consumption and some safety issues. Moreover, the generation of some byproducts such as coke that results in the loss of catalytic selectivity and the deterioration of catalyst lifetime is generally unavoidable in thermal catalytic processes.[32, 72] Furthermore, it is hard to retain active sites at high temperatures especially for the oxidation reactions (generally with $O_2$) over metal catalysts and reduction reactions (generally with $H_2$) over metal oxide catalysts.[52] The inclusion of photo energy which leads to a novel thermo-photo catalytic process can well address these issues.

Firstly, compared with thermal catalysis, thermo-photo catalysis demonstrates higher catalytic efficiencies at lower temperatures. For example, while dry reforming of $CH_4$ typically requires a high temperature of 800-900 °C, visible light irradiation over Pt/black $TiO_2$ catalyst realized highly efficient production of $H_2$ (71 mmol/h/g) at a low temperature down to 550 °C, in great contrast to those in dark (0 and 50 mmol/h/g at 550 °C and 700 °C, respectively).[33] Similar improvements have been demonstrated in a wide range of thermal catalytic reactions such as steam reforming of $CH_4$, partial oxidation of $CH_4$, $CO_2$ hydrogenation, water splitting, etc. as summarized in Table 1. Furthermore, the power required to shine the light is lower than that required to heat the reactor, so the overall energy consumption can be reduced by introducing photo energy and lowering thermal input for thermal catalytic systems.[34, 73, 74]

Secondly, the introduction of photo energy can tune the catalytic selectivity toward some products which cannot be attained in traditional thermal catalysis.[36, 56, 75, 76] Most representatively, while thermal catalytic alkyne hydroamination at 30-100 °C over Au-Co/$ZrO_2$ catalyst led to very low selectivities toward imine (below 10%), thermo-photo catalysis in the same temperature range showed high selectivities surpassing 90% owing to photo-induced intramolecular electronic transitions.[56] Similar phenomena have also been observed in preferential CO oxidation in $H_2$ streams,[36, 77] $CO_2$ hydrogenation,[76] propylene epoxidation,[52] etc.

Thirdly, catalytic stability is enhanced under light irradiation as the generation of some undesirable byproducts such as coke is avoided,[30, 32, 78-80] and the surface structure of catalyst is dynamically adjusted.[52, 81] For instance, while thermal catalytic dry reforming of $CH_4$ over MgO/Pt/Zn-$CeO_2$ catalyst showed a ~80% decay in 20 hours, thermo-photo catalysis demonstrated an excellent stability at higher conversions.[81]

Fourthly, thermo-photo catalysis can be freed from tedious pre-treatment processes for catalysts, thus being much more convenient and cost-effective. Since metals perform as active sites in many catalytic processes, a reduction pre-treatment with $H_2$ at high temperatures is generally required.[82-85] While, in-situ photo-induced reduction of catalysts with a fast start-up in a few seconds has been demonstrated in thermo-photo catalytic steam reforming of $CH_3OH$ over Cu-Zn-Ti oxide catalyst, which successfully eliminated the pre-reduction procedure.[82]

Fifthly, thermo-photo catalysis enables the instantaneous control of reactions. Typically, the highest catalytic efficiency can be obtained within a few minutes upon turning on the light and the efficiency can drop to zero right after turning off the light.[36, 73, 86] While, for traditional thermal reactors, the instantaneous temperature control is almost impossible especially for the cooling process which leads to a long tail of catalytic efficiency due to the residual heat.

#### 2.3.2. Compared with photocatalysis

Photocatalysis is a promising technology relying on the inexhaustible solar energy. However, it generally suffers from poor catalytic activity and limited utilization of visible light,

resulting in low energy conversion efficiencies which are much below the industrial requirement.[87, 88] Moreover, the catalyst might get deactivated due to the generation of some undesirable byproducts.[89] The introduction of thermal energy into photocatalytic systems is an effective strategy to enhance catalytic efficiency, promote the utilization of visible light, tune product selectivity, and extend catalyst lifetime.

Firstly, thermo-photo catalysis can lead to a significantly enhanced catalytic activity compared with room-temperature photocatalysis (Table 1) due to the improved reaction kinetics.[21, 28, 39, 40, 90] Impressively, both the $H_2$ evolution rate and apparent quantum efficiency were found to be enhanced by three orders of magnitude in thermo-photo catalytic water splitting over Rh/black $TiO_2$ catalyst.[40] Moreover, very recently, an unprecedentedly high $CH_3CH_2OOH$ yield of 5.6 mmol/h/g was achieved in visible-light driven thermo-photo catalytic partial oxidation of $C_2H_6$ over Au/$WO_3$ catalyst, which is 6 times higher than that at room temperature.[90]

Secondly, the introduction of thermal energy enables the effective utilization of visible light in photocatalytic processes.[21, 22, 28, 39, 40, 90] In 2015, Hu and co-workers first revealed the intrinsic issue in visible-light photocatalysis and demonstrated their design of thermo-photo catalysis for enhancing the contribution of visible light to $H_2$ production from 0 to ~85% of the entire solar spectrum.[21] Besides, the absolute $H_2$ yield under visible light was enhanced from 0 to 497 mmol/h/g. The underlying mechanism will be further discussed in section 4.1.

Thirdly, thermo-photo catalysis allows the regulation on product selectivity by tuning temperature.[91, 92] In thermo-photo catalytic water-free alcohol reforming, a low temperature was found favourable for oxidative coupling to form ester while a high temperature induced a high selectivity toward aldehyde since its fast desorption inhibited the further conversion.[91]

Fourthly, the catalytic durability of thermo-photo catalysis is much better than that of traditional photocatalysis due to the supressed formation or promoted conversion of poisonous byproducts. This is especially important for catalytic oxidation of aromatic compounds such as benzene and toluene, where the severe deposition of refractory carbonaceous intermediates on catalysts occurring during photocatalysis is inhibited in the thermo-photo catalytic process.[89, 93, 94]

Fifthly, the desorption of products from the catalyst surface is generally difficult in photocatalytic processes, which can be addressed by introducing thermal energy. This inhibits the over-reaction of reactants such as the over-oxidation of $CH_4$ into $CO_2$ due to the timely desorption of the desired mildly oxidized oxygenates.[28, 95] More importantly, this realizes the efficient refresh of active sites for subsequent adsorption of reactants.

**Table 1** Comparison of thermal, photo, and thermo-photo catalytic performances.

| Reaction | Catalyst | Light | Thermal catalysis | Photocatalysis (RT) | Thermo-photo catalysis | Ref. |
|---|---|---|---|---|---|---|
| Water splitting<br>$2H_2O \rightarrow 2H_2 + O_2$<br>(Or with sacrificial reagents) | Pt/black $TiO_2$ | λ > 420 nm | 280 °C: 117 mmol $H_2$/h/g | 0 | 280 °C: 614 mmol $H_2$/h/g | 21 |
| | $NiO_x$/black $TiO_2$ | λ > 420 nm | 260 °C: 21 mmol $H_2$/h/g | 0 | 260 °C: 48 mmol $H_2$/h/g | 39 |
| | Rh/black $TiO_2$ | λ > 420 nm | 260 °C: 49 mmol $H_2$/h/g | 0 | 260 °C: 79 mmol $H_2$/h/g | 40 |
| | $Ru/TiO_2$ | UV light | 240 °C: 8 mmol $H_2$/h/g | 0 | 240 °C: 11 mmol $H_2$/h/g | 96 |
| | Au/N-doped $TiO_2$/MgO | Vis light | 270 °C: 0 | 0 | 270 °C: 11 mmol $H_2$/h/g | 42 |
| | Ti@$TiO_2$ | λ < 850 nm | 60 °C: 0 | 0.3 mmol $H_2$/h/g | 60 °C: 0.5 mmol $H_2$/h/g | 97 |
| | SnSe/$ZnIn_2S_4$ | λ > 400 nm | NA | 5.1 mmol $H_2$/h/g (Vis light) | 73 °C: 5.7 mmol $H_2$/h/g (Vis + IR light) | 98 |
| | CoO | AM 1.5 G | 73 °C: 0 | 0.3 mmol $H_2$/h/g | 73 °C: 5.8 mmol $H_2$/h/g | 41 |
| Hydrogenation of carbon dioxide<br>$CO_2 + H_2 \rightarrow CO$ or $CH_4$ or… | Rh/$TiO_2$ | 365 nm | 250 °C: 0 | NA | 250 °C: 648 mmol $CH_4$/h/g | 99 |
| | Ru/black $TiO_2$ | AM 1.5 G | 150 °C: 0<br>250 °C: 7 mmol $CH_4$/h/g | 0 | 150 °C: 2 mmol $CH_4$/h/g<br>250 °C: 46 mmol $CH_4$/h/g | 22 |
| | $RuO_2$/$SrTiO_3$ | Full light | NA | 0 | 150 °C: 15 mmol $CH_4$/h/g | 100 |
| | $Ru/SiO_2$ | Full light | 150 °C: 1 mmol $CH_4$/h/g | NA | 150 °C: 22 mmol $CH_4$/h/g | 73 |
| | $Ru/Ni_2V_2O_7$ | Full light | 350 °C: 12 mmol $CH_4$/h/g | 17 mmol $CH_4$/h/g | 350 °C: 115 mmol $CH_4$/h/g | 101 |
| | $RuO_2$ | Full light | 170 °C: 0.5 mmol $CH_4$/h/g | NA | 170 °C: 4.4 mmol $CH_4$/h/g | 102 |
| | $NiO_x/La_2O_3$@ $TiO_2$ | λ > 420 nm | 200 °C: 2 mmol $CO_2$/h/g (Conversion) | 0 | 200 °C: 11 mmol $CO_2$/h/g (Conversion) | 23 |
| | $Cu_2O$/graphene | Full light | 250 °C: 0 | 0 | 250 °C: 15 mmol $CH_4$/h/g | 103 |
| | $Ni/SiO_2$ | Full light | 600 °C: 435 mmol $CO_2$/h/g (Conversion) | NA | 579 °C: 1796 mmol $CO_2$/h/g (Conversion) | 25 |
| | $Ni_{12}P_5/SiO_2$ | Full light | 320 °C: 8 mmol CO/h/g | NA | 320 °C: 26 mmol CO/h/g | 104 |
| | $Ni/ZrO_2$ | Full light | 121 °C: 0 | 0 | 121 °C: 1 mmol $CH_4$/h/g | 105 |
| | $Ag/ZrO_2$ | Full light | 90 °C: 0.2 μmol CO/h/g (λ > 320 nm) | NA | 90 °C: 0.6 μmol CO/h/g (Full light) | 106 |
| | $In_2O_{3-x}(OH)_y$ | Full light | 150 °C: 0 | NA | 150 °C: 22 μmol CO/h/g | 107 |
| | $In_2O_{3-x}(OH)_y$ | Full light | 250 °C: 54 μmol MeOH/h/g | NA | 250 °C: 98 μmol MeOH/h/g | 108 |
| | $In_2O_3$@$In_2O_{3-x}$ | Full light | 300 °C: 0.5 mmol CO/h/g | NA | 300 °C: 2.1 mmol CO/h/g | 109 |
| | $In_2O_{3-x}(OH)_y$/ $TiO_2$/TiN | Full light | 150 °C: 0 | NA | 150 °C: 68 mmol CO/h/g | 110 |

| | | | | | | |
|---|---|---|---|---|---|---|
| | Cu-Zn-Al oxide | 350 nm < λ < 800 nm | 225 °C: 5.9 mmol MeOH/h/g | NA | 225 °C: 7.9 mmol MeOH/h/g | 85 |
| | La/Cu-Zn-Al oxide | 350 nm < λ < 800 nm | 225 °C: 1.5 mg MeOH/$m^2$/g | NA | 225 °C: 2.5 mg MeOH/$m^2$/g | 111 |
| Carbon dioxide reduction by water<br>$CO_2 + H_2O \rightarrow CO$ or $CH_4$ or… | $Cu_2O$ | AM 1.5 G | NA | 18 μmol CO/h/g,<br>6 μmol $CH_4$/h/g | 56 °C: 63 μmol CO/h/g,<br>7 μmol $CH_4$/h/g | 112 |
| | $Ru/Al_2O_3$ | Full light | NA | NA | 370 °C: 18 mmol $CH_4$/h/g | 113 |
| | Bi-$H_x$/Ni foam | LED light | 180 °C: 0 | NA | 180 °C: 0.3 mmol CO/h/g | 26 |
| | Pt/g-$C_3N_4$ | 420 nm | 125 °C: 0 | 0 | 125 °C: 15 μmol $CH_4$/h/g | 114 |
| | $LaSrCoFeO_{6-\delta}$ | λ > 420 nm | 350 °C: 94 μmol $CH_4$/h/g | NA | 350 °C: 468 μmol $CH_4$/h/g | 115 |
| Dry reforming of methane<br>$CH_4 + CO_2 \rightarrow 2H_2 + 2CO$ | Pt/black $TiO_2$ | λ > 420 nm | 550 °C: 0<br>700 °C: 50 mmol $H_2$/h/g | 0 | 550 °C: 71 mmol $H_2$/h/g<br>700 °C: 237 mmol $H_2$/h/g | 33 |
| | $Rh/SrTiO_3$ | UV light | 150 °C: 0<br>470 °C: 32 mmol $H_2$/h/g | NA | 150 °C: 58 mmol $H_2$/h/g<br>470 °C: 82 mmol $H_2$/h/g | 30 |
| | Rh/TaON | λ > 400 nm | 316 °C: 1.5% ($H_2$ yield) | NA | 316 °C: 5.0% ($H_2$ yield) | 116 |
| | Pt/TaN | 400 nm < λ < 500 nm | 500 °C: 25 mmol $H_2$/h/g | NA | 500 °C: 34 mmol $H_2$/h/g | 117 |
| | $Pt/CeO_2$ | Full light | 750 °C: 174 mmol $H_2$/h/g | NA | 750 °C: 192 mmol $H_2$/h/g | 118 |
| | $Ni/CeO_2$ | 400 nm < λ < 700 nm | 362 °C: 0.1 mmol $CH_4$/h/g (Consumption) | NA | 362 °C: 1.6 mmol $CH_4$/h/g (Consumption) | 119 |
| | MgO/Pt/Zn-$CeO_2$ | Full light | 600 °C: 37 mmol $H_2$/h/g | NA | 600 °C: 356 mmol $H_2$/h/g | 81 |
| | Si-Ni/$SiO_2$ | Full light | 520 °C: 132 mmol $H_2$/h/g | NA | 520 °C: 200 mmol $H_2$/h/g | 120 |
| | Cu-Ru/MgO-$Al_2O_3$ | White light | 727 °C: 216 mmol $CH_4$/h/g (Consumption) | NA | 727 °C: 990 mmol $CH_4$/h/g (Consumption) | 32 |
| | $Co/Al_2O_3$ | Full light | 542 °C: 360 mmol $CH_4$/h/g (Consumption) | NA | 542 °C: 750 mmol $CH_4$/h/g (Consumption) | 78 |
| | Ni-$Co/Al_2O_3$ | Full light | 600 °C: 600 mmol $CH_4$/h/g (Consumption) | 0 | 600 °C: 1080 mmol $CH_4$/h/g (Consumption) | 121 |
| Steam reforming of methane<br>$CH_4 + 2H_2O \rightarrow 4H_2 + CO_2$ | Pt/black $TiO_2$ | λ > 420 nm | 500 °C: 0 | 0 | 500 °C: 185 mmol $H_2$/h/g | 27 |
| | $Rh/TiO_2$ | 420 nm < λ < 800 nm | 260 °C: 2.5 mmol $H_2$/h/g | NA | 260 °C: 6.3 mmol $H_2$/h/g | 122 |
| Oxidative coupling of methane<br>$4CH_4 + O_2 \rightarrow 2C_2H_6 + 2H_2O$ | Au/ZnO-$TiO_2$ | 300 nm < λ < 500 nm | 140 °C: 0 | NA | 140 °C: 5 mmol $C_2H_6$/h/g | 31 |
| Partial oxidation of methane<br>$CH_4 + O_2 \rightarrow$ oxygenates or $C_xH_y$ | $Pt/WO_3$ | λ > 420 nm | 150 °C: 0 | 0.3 mmol MeOH/h/g | 150 °C: 2.2 mmol MeOH/h/g | 28 |
| | Au-Pd/$TiO_2$ | AM 1.5 G | 52 °C: 0 | 6.2 mmol MeOH/h/g (UV light) | 52 °C: 8.6 mmol MeOH/h/g (Full light) | 95 |
| | $H_4SiMo_{12}O_{40}$/ $TiO_2$ | AM 1.5 G | 150 °C: 0 | NA | 150 °C: 0.7 mmol HCOOH/h/g, 0.7 mmol HCHO/h/g | 29 |
| Partial oxidation of ethane<br>$C_2H_6 + O_2 \rightarrow$ oxygenates | $Au/WO_3$ | λ > 420 nm | 100 °C: 0 | 0.9 mmol EtOOH/h/g | 100 °C: 5.6 mmol EtOOH/h/g | 90 |
| Partial oxidation of propylene<br>$C_3H_6 + O_2 \rightarrow$ oxygenates | $Cu/SiO_2$ | Vis light | 200 °C: 0 (Conversion) | NA | 200 °C: 171 mmol PE/h/g (Conversion) | 52 |
| | $Au/Cu_2O$ | Vis light | 150 °C: 0.1 mmol PE/h/g (Conversion) | NA | 150 °C: 1.2 mmol PE/h/g (Conversion) | 123 |
| Steam reforming of methanol<br>$CH_3OH + H_2O \rightarrow 3H_2 + CO_2$ | Cu-Zn-Ti oxide | AM 1.5 G | 200 °C: 0 | 0 | 200 °C: 51 mmol $H_2$/h/g | 82 |
| | Cu-Zn-Zr oxide | Full light | 200 °C: 76 mmol $H_2$/h/g | NA | 200 °C: 241 mmol $H_2$/h/g | 124 |
| | Cu-Zn | 420 nm < λ < 800 nm | 220 °C: 52 mmol $H_2$/h/g | NA | 220 °C: 172 mmol $H_2$/h/g | 125 |
| Decomposition of methanol<br>$CH_3OH \rightarrow CO + 2H_2$ | $Pt/SiO_2$ | 440 nm | 225 °C: 15 mmol CO/h/g | NA | 225 °C: 19 mmol CO/h/g | 126 |
| Dehydrogenation of ethanol<br>$CH_3CH_2OH \rightarrow CH_3CHO + H_2$ | Ni-Cu | 420 nm < λ < 800 nm | 210 °C: 72 mmol $H_2$/h/g | NA | 210 °C: 177 mmol $H_2$/h/g | 127 |
| Water-gas shift reaction<br>$CO + H_2O \rightarrow CO_2 + H_2$ | $CuO_x/Al_2O_3$ | Full light | 300 °C: 187 mmol $H_2$/h/g | NA | 285 °C: 439 mmol $H_2$/h/g | 35 |
| Hydrogenation of carbon monoxide<br>$CO + 2H_2 \rightarrow CH_3OH$ or … | Cu-Zn-Al oxide | AM 1.5 G | 350 °C: 3.0 mmol MeOH/h/g | 0 | 350 °C: 8.5 mmol MeOH /h/g | 34 |
| | $NiO_x/Al_2O_3$ | Full light | 150 °C: 5% (Conversion) | NA | 150 °C: 28% (Conversion) | 128 |
| Oxidation of carbon monoxide<br>$2CO + O_2 \rightarrow 2CO_2$ | Ag@Pt | NA | 130 °C: 36 mmol $CO_2$/h/g | NA | 130 °C: 58 mmol $CO_2$/h/g | 36 |
| | $PdO/CeO_2$ | Full light | 80 °C: 25% (Conversion) | 7% (Conversion) | 80 °C: 100% (Conversion) | 129 |
| | Au/MgO | 545 nm | 150 °C: 24% (Conversion) | NA | 150 °C: 32% (Conversion) | 130 |

| | | | | | | |
|---|---|---|---|---|---|---|
| Oxidation of volatile organic compounds<br>$C_xH_yO_z + O_2 \rightarrow CO_2 + H_2O$ | $Ag_3PO_4$/Ag/GdCrO$_3$ | 420 nm < λ < 780 nm | 90 °C: 6% (Conversion) | 24% (Conversion) | 90 °C: 100% (Conversion) | 47 |
| | Pt/$SrTiO_{3-x}$ | 420 nm < λ < 780 nm | 150 °C: 20% (Conversion) | 20% (Conversion) | 150 °C: 100% (Conversion) | 48 |
| | ε-$MnO_2$ | λ > 420 nm | 160 °C: 16% (Conversion) | 0 (Conversion) | 160 °C: 100% (Conversion) | 131 |
| | $TiO_2$ | UV light | 240 °C: 19 μmol $CO_2$/h/g | 46 μmol $CO_2$/h/g | 240 °C: 329 μmol $CO_2$/h/g | 93 |
| | Pt/$TiO_2$-$WO_3$ | UV + vis light | 200 °C: 4% (Conversion) | 5% (Conversion) | 200 °C: 43% (Conversion) | 132 |
| | PdO-$Mn_3O_4$-$CeO_2$ | λ > 420 nm | 250 °C: 4% (Conversion) | 0 (Conversion) | 250 °C: 60% (Conversion) | 133 |
| Degradation of aqueous pollutants<br>$C_xH_yO_z + O_2 \rightarrow CO_2 + H_2O$ | $CeO_2$-CeN | λ > 420 nm | 80 °C: 5% (Conversion) | 61% (Conversion) | 80 °C: 97% (Conversion) | 50 |
| | $Mn_3O_4$-$MnCO_3$ | λ > 420 nm | 80 °C: 5% (Conversion) | 16% (Conversion) | 80 °C: 89% (Conversion) | 51 |
| Reduction of nitrogen monoxide by carbon monoxide<br>$2NO + 2CO \rightarrow N_2 + 2CO_2$ | Pt/$CeO_2$-$TiO_2$ | UV light | 150 °C: 62% (Conversion) | 20% (Conversion) | 150 °C: 90% (Conversion) | 134 |
| | Pd/$LaFeO_3$ | 420 nm < λ < 760 nm | 80 °C: 5% (Conversion) | NA | 80 °C: 48% (Conversion) | 135 |
| | $NiCo_2O_4$ | 420 nm < λ < 760 nm | 120 °C: 32% (Conversion) | NA | 120 °C: 72% (Conversion) | 136 |
| Nitrogen fixation with hydrogen<br>$N_2 + 3H_2 \rightarrow 2NH_3$ | Ru-Cs/MgO | 455 nm | 333 °C: 1.5 mmol $NH_3$/h/g | NA | 333 °C: 4.5 mmol $NH_3$/h/g | 44 |
| | Fe/$TiO_{2-x}H_y$ | Full light | 495 °C: 560 ppm $NH_3$ | NA | 495 °C: 1939 ppm $NH_3$ | 43 |
| Nitrogen fixation with water<br>$2N_2 + 6H_2O \rightarrow 4NH_3 + 3O_2$ | Cu-Fe | Full light | 50 °C: 0 | NA | 42 °C: 0.3 mmol $NH_3$/h/g | 45 |
| | Fe/$MoS_2$ | Vis light | 270 °C: 0 | 0 | 270 °C: 2.1 mmol $NH_3$/h/g | 46 |
| Decomposition of ammonia<br>$2NH_3 \rightarrow N_2 + 3H_2$ | Cu-Ru/MgO-$Al_2O_3$ | 400 nm < λ < 900 nm | 482 °C: 324 mmol $H_2$/h/g | NA | 482 °C: 4320 mmol $H_2$/h/g | 86 |
| Suzuki coupling reaction<br>$R_1$-$BY_2 + R_2$-$X \rightarrow R_1$-$R_2$ | Au-Pd | 809 nm | 62 °C: 55% (Yield) | NA | 62 °C: 99% (Yield) | 53 |
| Alkyne hydroamination<br>$R_1$-C≡CH + $R_2$-$NH_2 \rightarrow R_1CH{=}NR_2$ | Au-Co/$ZrO_2$ | Vis light | 80 °C: 46% (Conversion) | 48% (Conversion) | 80 °C: 100% (Conversion) | 56 |

## 3. How to design a highly efficient thermo-photo catalytic system?

Thermo-photo catalysis has demonstrated its advantages in a wide range of reactions, whereas there are a few guidelines on the design of thermo-photo catalytic systems. The present section will elucidate the design principles and strategies for building a highly efficient thermo-photo catalytic system with an emphasis on energy utilization and mass transfer. The design of a catalyst is guided by its function and its rational placement can further enhance the catalytic efficiency. The reactor design is mainly based on the heat source, namely, either photo-converted heat or external heat. An elaborate design on the catalyst, catalyst placement, and catalytic reactor together leads to an excellent catalytic performance.

### 3.1. Catalyst design

Catalyst is the core of a thermo-photo catalytic system. In the following part, we will first reveal the general and specific principles for designing efficient thermo-photo catalysts, and then discuss the strategies to acquire the desirable properties of the designed semiconductor-based and metal-based catalysts. Furthermore, the up-to-date design of synergetic catalysts will be outlined, which is expected to open a new door to catalyst design and fabrication.

#### 3.1.1. Design principles

There are some general principles applicable to all categories of thermo-photo catalysis, while some catalytic processes may follow some specific principles. Generally, strong light absorption across the full solar light spectrum, sufficient accessible active sites, low cost, and high natural abundance are desired for an ideal catalyst for thermo-photo catalysis.

Firstly, strong light absorption across the entire solar irradiation spectrum is expected for efficient generation of charge carriers and/or local heat over the catalyst. In the solar irradiation spectrum, UV light accounts for only 3%, while visible and IR lights constitute 44% and 53%, respectively.[137, 138] However, most of the semiconductor-based catalysts exploited so far (such as $TiO_2$ and ZnO) only absorb UV light, which greatly limits their practical application.[139] Besides, the main light absorption of plasmonic catalysts is limited to certain wavelengths.[70] Therefore, broadening light absorption especially in the visible and IR regions deserves a high priority for catalyst design.

Secondly, the designed catalyst should possess sufficient catalytically active sites which are accessible for reactants. Generally, the catalytic efficiency is determined by the number of active sites and the activity of each site.[40] While the activity of each site depends on the structure and intrinsic properties of the catalytic material, the number of active sites can be tuned by adjusting the surface area of catalysts and the dispersion of active sites.[15, 40] Moreover, the active sites should properly interact with reactant molecules for the sequential adsorption, activation, and reaction.[73, 100] It is worth mentioning that ultra-strong interaction and excessive occupation are not desired and may even deteriorate the catalytic activity.[55, 77] Furthermore, the products should be quickly desorbed from the catalyst surface to avoid their further conversion and refresh active sites.

Thirdly, from the perspective of large-scale application, catalysts should have low cost and high natural abundance. Currently, however, most of excellent catalytic performances are attained with noble metals such as Pt, Au, Ag, Pd, Rh, and Ru.[21, 22, 40] These noble metals act as light absorber, electron trapper, or reactant adsorber, whereas their high cost and scarcity present huge obstacles to industrial application. Hence, it is crucial to exploit inexpensive noble-metal-free catalysts with Fe, Co, Ni, Cu, Al, etc. playing the similar roles.[16, 39, 140]

Besides above-discussed general principles for catalyst design, there are three important design principles applicable for specific catalysis types. For semiconductor-based photocatalysis, the thermodynamic requirements on the relative positions of catalyst energy bands to the redox potentials of desirable semi-reactions must be met (Fig. 3a).[66] Moreover, one can control catalytic selectivity by inhibiting the generation of undesirable products based on the thermodynamic design.[28, 90]

For charge-carrier-mediated catalysis involving either photo carriers or hot carriers, the efficient separation and transfer of charge carriers should be ensured.[63, 141] This principle is opposite to that of thermal-energy-driven (photo-thermal) catalysis. In this case, only when charge carriers are effectively separated and transferred to catalyst surface to contact reactant molecules can the reaction take place.[98] Moreover, for multi-component catalysts, energetically favourable band alignment and fast interfacial electron transfer are required.[125, 141]

For photo-thermal catalysis, efficient photo-to-thermal conversion and subsequent heat transfer are desired. After charge excitation by photons, the photon energy should be effectively converted into thermal energy via the recombination of charge carriers instead of being reflected or re-emitted radiatively.[60] Moreover, the catalyst should possess an appropriate thermal conductivity to ensure the efficient heat transfer from the catalyst to adsorbed reactant molecules, but limit the heat loss to surrounding environment.[25, 142]

#### 3.1.2. Semiconductor-based catalysts

Semiconductor-based catalysts are widely used for thermo-assisted photocatalysis and thermo-photo co-catalysis through photo-induced charge excitation across the band gap. Based on the design principles revealed above, defect engineering is considered as an effective strategy for fabricating a highly efficient semiconductor-based catalyst, which not only enhances light harvesting for the generation of charge carriers and/or efficient photo-to-thermal conversion,[109, 143-145] but also promotes the adsorption of reactants.[94, 144, 146] However, charge recombination at deep-level defects would hamper the catalytic activity, which can be addressed by creating some shallow-level defects and thermally activating the trapped electrons to migrate out of deep-level defects via shallow-level defects.[147] Furthermore, non-metal doping may play a synergetic role with defect engineering by extending light absorption and lowering the energy for defect formation.[148]

Moreover, semiconductors are usually loaded with some metal nanoparticles, to enhance light absorption, extend charge lifetime, and provide more active sites.[22, 39] While, when plasmonic metals are loaded onto the semiconductor, the electron transfer direction can be controlled by light irradiation.[149, 150] When photon energy is large enough to drive charge excitation in the semiconductor, electrons would be injected from the conduction band of the semiconductor to the loaded metal. In this case, the metal serves as a cocatalyst to promote the transfer and separation of charge carriers. While, if photon energy is below the band gap of semiconductor but is capable of exciting electrons in the metal to overcome the Schottky barrier, a plasmon-mediated electron transfer from the metal to the semiconductor occurs.

#### 3.1.3. Metal-based catalysts

Metal-based catalysts are generally applied for plasmonic catalysis. The size and morphology of metal nanostructures can affect the electromagnetic field enhancement, hot carrier generation, and catalyst surface temperature under light irradiation, thus influencing the thermo-photo catalytic performance.[151, 152] Compared with spherical nanoparticles, nanoparticles with sharp features (such as nanocubes and nanocones) typically show a stronger light absorption due to the lightning rod effect[153] and reduced radiative damping,[154] which further contributes to stronger local electromagnetic field enhancement and more favourable generation of hot carriers.[155, 156] While, the size effect is more complex, as a smaller size is beneficial to display high energies and maximize surface active sites but in the meantime causes a blue shift of the resonant frequency and a poor charge separation due to spatial confinement.[157, 158]

Thermal conductivity is another important consideration for designing metal-based catalysts. Decreasing the size of metals would create a high density of grain boundaries and enhance phonon scattering, thus reducing the thermal conductivity.[159] Besides, increasing the surface roughness of metals would decrease phonon velocity, which can also reduce the thermal conductivity.[160] However, there is a trade-off between efficient heat transfer to reactants and heat loss to surrounding, which is hard to be addressed by tuning the thermal conductivity of catalysts. Instead, heat insulation with a shell or framework material can effectively address this issue by reducing the heat loss to the surrounding.[25, 142] The design of core@shell structured catalysts is highlighted, where the shell not only performs as an insulation layer to slow heat conduction but also acts as a trapper of IR light radiated from the hot core via absorption and scattering.[25] Furthermore, the outer shell may also protect inner metal nanoparticles from thermal expansion and sintering at high temperatures, thus enhancing the catalytic stability.[25]

Moreover, it is noted that hydrogenating metal catalysts can promote the reactions involving protons such as $CO_2$ reduction by water.[26] This is because the hydrogenated metal (M-H) can perform as an electron-proton-transfer mediator, in which the electron and proton in M-H can be released under light irradiation (M-H $\rightarrow$ M + $H^+$ + $e^-$) and then induce the reduction reaction (e.g., $2H^+ + 2e^- + CO_2 \rightarrow CO + H_2O$). While, the re-hydrogenation of the catalyst is needed for its reuse.[26]

Furthermore, the formation of bimetallic antenna-reactor catalysts by coupling the plasmonic and catalytic functions in a hybrid material effectively extends plasmonic catalysis to materials other than noble metals.[161] Typically, in the hybrid material, a metal performs as the concentrator for photo energy (named as plasmonic metal or antenna) and then the energy is directed to the other more active metal (named as catalytic metal or reactor) via energetic charge carriers.[36, 53, 71, 162] Tuning the composition, size, and shape of the plasmonic antenna can realize an independent control on the optical property of the complex, while the composition and surface structure of the catalytic metal determine the affinity for adsorbates and affect the overall reactivity of the complex.[163] Nevertheless, there is a balance among the light absorption in plasmonic metal, local field enhancement at catalytic metal, and collective scattering of photons out of the complex, to reach the optimal catalytic performance.[164]

#### 3.1.4. Synergetic catalysts

Combing multiple components which play different roles is an effective approach to develop highly efficient thermo-photo catalysts. Firstly, a thermal catalyst can be coupled with a photocatalyst, in which the charge carriers generated in the photocatalyst under illumination can be transferred to the thermal catalyst to promote its thermal catalytic activity.[165, 166] In this case, the synergetic effect occurs at the interface between the thermal catalyst and photocatalyst.[167] Secondly, a photocatalyst which is responsible for photo-induced redox reactions can be coupled with a photo-thermal material for heat supply. This allows the effective utilization of full-spectrum solar light since the former mainly relies on high-energy photons while the latter is set apart for the utilization of low-energy photons.[95, 106, 110, 168] Thirdly, a thermal catalyst can be loaded on a photo-thermal support which shows an excellent light absorption property and thus increases the catalyst temperature for an improved catalytic performance.[32, 55, 169] The above-discussed bimetallic antenna-reactor catalyst is a representative of this type of synergetic catalysts.

### 3.2. How to place catalyst?

Though having received less attention, thermo-photo catalytic performance is highly dependent on the placement method of catalysts. In general, the catalyst can be suspended in a certain liquid, compacted into a catalyst bed, or coated on a substrate. In this subsection, we will present the placement principles and analyse each kind of placement method with an emphasis on the state-of-the-art substrates developed for coating catalysts.

#### 3.2.1. Placement principles

Firstly, a rational placement of catalysts should ensure the efficient adsorption of reactants and desorption of products. Namely, the surface active sites of the catalyst should be adequately exposed to reactants, and meanwhile the products can be fast desorbed from catalyst surface to regenerate the active sites.[95, 170] Only with the guaranteed mass transfer can the catalytic reaction proceed efficiently.

Secondly, all the catalyst particles can easily access thermal and photo energies with high energy absorption and conversion rates. To meet this requirement, the heat transfer distance and light penetration depth should be carefully considered.[44, 171, 172] Moreover, photons are expected to be absorbed to excite charge carriers instead of being scattered or reflected.[21, 107]

#### 3.2.2. Catalyst suspension

If the catalytic process involves liquid-phase substances at the operating condition (temperature and pressure), catalyst particles are generally suspended in liquid under continuous stirring.[21, 29, 173] The liquid substance can be either reactants or additional inert solvents, and continuous stirring is essential to achieve fast mass transfer as well as sufficient and uniform exposure of catalyst particles to thermal and photo energies.

The suitability of catalyst suspension for a catalytic reaction mainly depends on the phase of reactants. Namely, if all the reactants are in (mutually soluble) liquid phase such as water splitting (below 100 °C), the suspension system is favoured. While, if some reactants are in gas phase such as $CO_2$ reduction by water, the suspension system would limit the accessibility of the catalyst toward gas reactants unless these gas reactants possess high solubilities in the liquid.[170, 173, 174]

While, the influence of the product phase on catalytic efficiency is not significant since the stirred catalyst suspension is advantageous for cleaning active sites, especially for the removal of soluble products from catalyst surface to the liquid solvent.[28, 95, 173] For example, in partial oxidation of $CH_4$, water suppressed the accessibility of $CH_4$ but promoted the desorption of liquid oxygenates, leading to an overall enhancement in catalytic efficiency.[28, 173] This implies that the rate-limiting mass transfer step should be clarified before considering building a catalyst suspension system.

#### 3.2.3. Catalyst bed

For gas-phase reactions conducted in flow reactors, catalyst particles are generally compacted into a catalyst bed. The gas flow goes through the whole catalyst bed with light irradiation along or perpendicular to the gas flow direction.[30, 44, 175] The gas-phase catalyst-bed system generally demonstrates efficient molecular adsorption and desorption. However, it is noted that the penetration depth of incident photons is below 100 μm, so not all the catalyst particles share the same opportunity to access photons especially in thick catalyst beds.[44, 171, 172] Namely, the short penetration depth may cause the “waste” of catalysts. While, the combination with photo-thermal effect would result in temperature gradients throughout the catalyst bed, which might be favourable for the generation of unstable products (see section 5.1 for details).[44] Even putting photo-thermal effect aside, the temperature of catalyst beds may still be non-uniform as affected by the heating mode, position of thermocouples, and thermal conductivity of gases, which should be taken into account when analysing the relation between the temperature and catalytic activity.

#### 3.2.4. Catalyst coated on a substrate

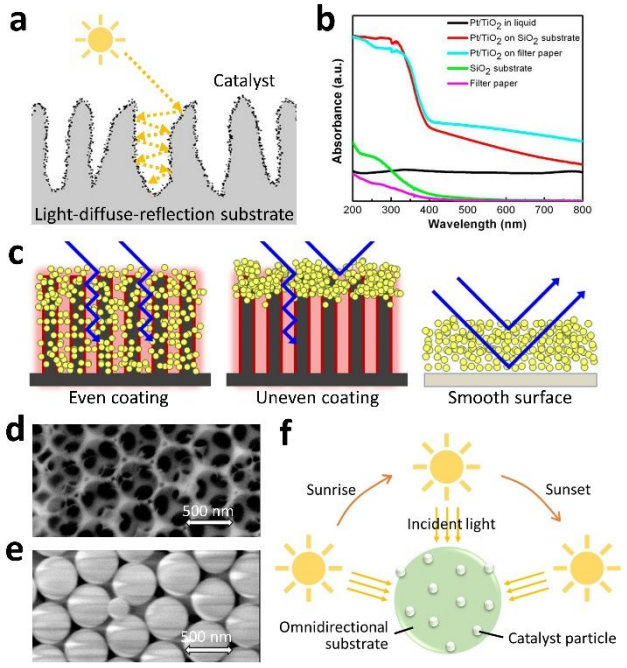


**Fig. 5** Novel substrates for thermo-photo catalysis. (a) Schematic illustration of light propagation over a light-diffuse-reflection substrate. (b) UV-visible spectra of Pt/black $TiO_2$ catalyst and light-diffuse-reflection substrates ($SiO_2$ or filter paper). Reproduced with permission from ref. 21. Copyright (2015) American Chemical Society. (c) Schematic illustration of the effect of nanostructures on light propagation. Reproduced with permission from ref. 107. Copyright (2016) American Chemical Society. SEM images of (d) inverted and (e) general silicon opal photonic crystals. Reproduced with permission from ref. 178. Copyright (2018) Royal Society of Chemistry. (f) Schematic illustration of the spherical omnidirectional substrate under sunrise and sunset. Reproduced with permission from ref. 112. Copyright (2021) John Wiley and Sons.

On top of the traditional catalyst suspension and catalyst bed, catalyst particles can be coated on a substrate. While general substrates just support and disperse catalyst particles, some novel substrates including light-absorption substrates, light-diffuse-reflection substrates, and omnidirectional substrates have been developed, which can increase catalyst temperature, enhance incident light utilization, and prepare thermo-photo catalysis for practical application, respectively. These substrates and their unique functions will be elucidated in the following part.

*3.2.4.1. General substrates*

General substrates refer to the substrates without specific functions except for supporting catalyst particles and suppressing their agglomeration, such as glass fibre, glass slide, etc.[169, 176, 177] Coating catalyst particles onto a general substrate allows the convenient collection and reuse of catalysts compared with catalyst suspensions, and moreover, enhances the dispersion and reduces the required amount of catalyst particles compared with catalyst beds. Substrates coated with catalysts can be applied for catalytic systems of all phases.

*3.2.4.2. Light-absorption (dark) substrates*

Light-absorption substrates are exploited to convert photo energy into thermal energy to heat loaded catalyst particles, so they can also be regarded as photo-thermal substrates. These substrates generally have a dark or even black appearance with a broad light absorption across the entire solar spectrum. The explored light-absorption substrates range from synthetic materials such as black silicon,[102, 107, 178] $Fe_3Si$ aerogel,[179] and Cr film,[180] to biomass such as surface-charred wood.[41, 181]

Furthermore, photo-thermal substrate can be coupled with a pyroelectric substrate, which allows the generation of pyroelectric field around the catalyst.[182] As-induced pyroelectric field can guide the migration direction of photo-generated charge carriers, thus promoting their separation, extending their lifetime, and achieving high catalytic efficiencies.[183]

*3.2.4.3. Light-diffuse-reflection substrates*

The employment of light-diffuse-reflection substrates contributes to the redirection of incident light, thus promoting light utilization (Fig. 5a).[21, 107] This concept was first demonstrated by Hu and co-workers by creating a light-diffuse-reflection $SiO_2$ substrate with a surface roughness of 0.078 μm and a light scattering coefficient of 385 $cm^2/g$, which enhanced the photocatalytic efficiency by 100 times compared with the catalyst suspension system.[21] Such improvement was owed to the remarkably increased light absorbance of the catalyst for surface-diffuse-reflected lights as supported by UV-visible spectra (Fig. 5b). Besides $SiO_2$, filter paper with rough surface also exhibits a strong light diffuse reflection, making it a cheap and convenient substrate for photocatalysis. While, filter paper can only be applied under mild conditions but $SiO_2$ with a high chemical and mechanical stability can be applied under harsher conditions.[21, 22, 27, 33, 39, 40, 82]

Besides, some well aligned architectures have been explored as light-diffuse-reflection substrates. The vertically aligned Si nanowires showed an enhanced light harvesting with reflectance below ~3% across the entire solar spectrum.[107, 184, 185] Here, the even distribution of catalyst particles on substrate plays a key role for efficient light scattering and internal reflections within the long nanowire arrays (Fig. 5c).[107] In addition, inverse opal photonic crystal (Fig. 5d) also acts as a promising substrate due to the coupling of incident light into resonant photonic modes which increases the light propagation length through the material.[102, 178] While, opaline photonic crystal support comprised of silica spheres (Fig. 5e) showed a much poorer light harvesting.[178]

*3.2.4.4. Omnidirectional (spherical) substrates*

Planar substrates are the most widely used so far, whereas they cannot absorb all rays as long as it is not at the perpendicular incidence. From the perspective of practical application based on sunlight irradiation, since the solar azimuth and elevation angles keep changing throughout the day, the photon density acquired by planar substrates from sun remains low.[186] In contrast, the development of spherical omnidirectional substrates can address this issue with a

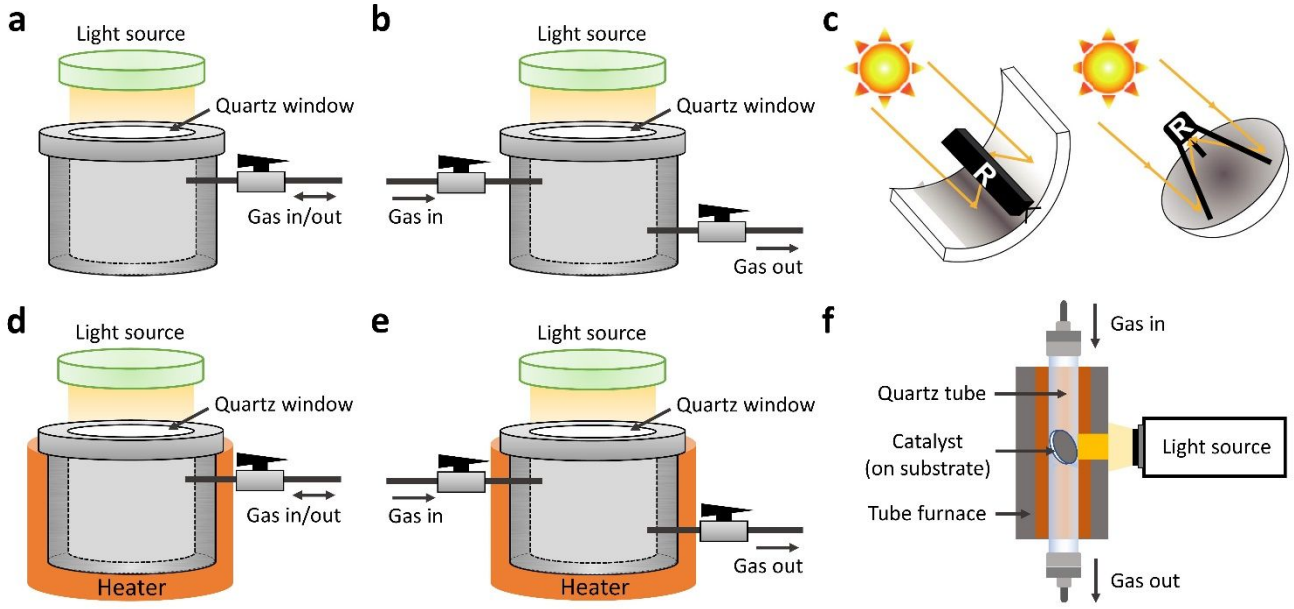


**Fig. 6** Schematic illustration of thermo-photo catalytic reactors. (a) Photo-thermal batch reactor. (b) Photo-thermal flow reactor. (c) Parabolic trough and parabolic dish solar concentrators. Reproduced with permission from ref. 192. Copyright (2017) Elsevier. (d) Externally heated batch reactor. (e) Externally heated flow reactor. (f) Externally heated flow reactor modified from traditional tube furnace. Reproduced with permission from ref. 40. Copyright (2020) Elsevier.

hemispherical surface facing sunlight all day long regardless of incident angles (Fig. 5f).[112]

### 3.3. Design of thermo-photo catalytic reactor

Designing and building an appropriate reactor for the target catalytic reaction is of vital importance to achieve a satisfying catalytic performance. Depending on the heat source, thermo-photo catalytic reactors can be divided into two groups, namely, reactors with light-induced local heating and reactors with external global heating. Here, the general design principles of thermo-photo catalytic reactors will be revealed first, followed by discussion on these two groups of reactors.

#### 3.3.1. Design principles

The first consideration for reactor design is the heat source, namely, either photo-converted heat or external heat, followed by consideration on the operation mode, namely, either batch mode or flow mode. While, no matter which type of thermo-photo catalytic reactor is needed, the following design principles should be complied.

Firstly, light can shine on all catalyst particles. This requires a rational design on the direction and intensity of incident light. Moreover, the window used for closed reaction systems should demonstrate a high light transmittance, and the quartz glass has been considered as an ideal window material.[21, 90] The reactants and products should not accumulate on the window to supress light transmission.

Secondly, an efficient thermal transfer inside the reactor and an excellent thermal insulation against outer environment are desired. These two aspects contribute to high energy utilization and conversion efficiencies, which reduce energy consumption and thereby the cost of running the system.[187, 188]

Thirdly, no safety issues exist when running the catalytic reactor. The safety issues might be resulted from the high temperature, high pressure, high-intensity illumination, gas leakage, mechanical damage, etc. Therefore, a prudent reactor design and safety precautions are indispensable.

#### 3.3.2. Reactors with light-induced local heating

Some of thermo-photo catalytic reactors rely on light-induced local heating over the catalyst and/or substrate without any external resistive heating sources. These reactors are also called photo-thermal reactors. For these reactors, the primary design considerations are the reactor geometry for maximizing incident light flux and the highly efficient internal heat deposition.[187, 189-191]

Typical photo-thermal batch reactor and flow reactor are illustrated in Fig. 6a and Fig. 6b, respectively. The inside catalyst placement is not shown, which can refer to section 3.2. The photo-thermal batch reactor only has one port for initial gas feeding and sampling at a certain time interval (Fig. 6a). While, in photo-thermal flow reactor, feed gases enter the reactor from one end and then pass through the catalyst under light irradiation to the other end (Fig. 6b). Moreover, for practical application, collectors can be designed to concentrate lights toward the reactor to amplify the heat intensity (Fig. 6c).[74, 192, 193]

#### 3.3.3. Reactors with external global heating

Distinct from above photo-thermal reactors, some thermo-photo catalytic reactors are equipped with external heating devices (such as electric furnaces). In contrast to the local heating in photo-thermal reactors which is only for the catalyst, the external heating devices typically provide the global heating for both catalyst and reactants, thus enhancing the catalytic

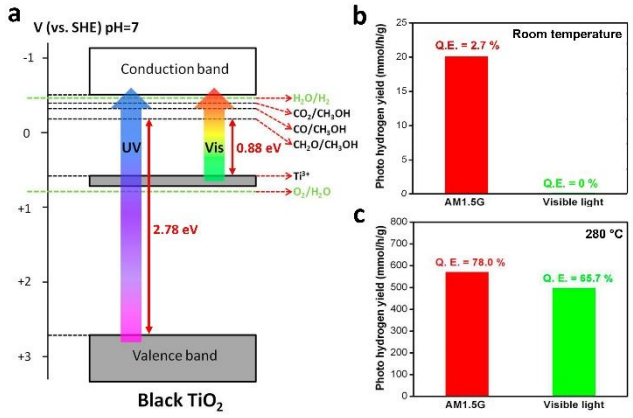


**Fig. 7** (a) Driving force for $CH_3OH$ oxidation illustrated based on the band structure of black $TiO_2$ and redox potentials of water splitting with sacrificial $CH_3OH$. $H_2$ production rate and quantum efficiency obtained at (b) room temperature and (c) 280 °C. Reproduced with permission from ref. 21. Copyright (2015) American Chemical Society.

activity.[34] While, a few devices provide single-plane heating, which may result in the temperature gradient for thick catalyst beds.[44, 175]

The typical externally heated batch reactor and flow reactor are illustrated in Fig. 6d and Fig. 6e, respectively. The only difference from above photo-thermal reactors is the outer electric heater.[30, 73] In addition, the externally heated thermo-photo catalytic flow reactor can be easily built by modifying a traditional tube furnace.[21, 40] As shown in Fig. 6f, this is achieved by creating a hole in the furnace wall and using a quartz tube to allow light transmission.

## 4. How does thermal energy promote photocatalysis?

While a number of efforts have been made to get excellent thermo-photo catalytic performance, the synergetic effects of thermal and photo energies remain confusing, and a systematic analysis and evaluation of current works is still lacking. To make it clear, the following two sections will be respectively focused on "*How does thermal energy promote photocatalysis?*" and "*How does light irradiation accelerate thermal catalysis?*" to reveal the synergetic roles of thermal and photo energies.

In the present section, a deep and comprehensive understanding on the approaches that introducing thermal energy promotes the photocatalytic process will be provided based on principles and some specific examples of thermo-assisted photocatalysis and thermo-photo co-catalysis. This will cover the enhancement in kinetic driving force for effective utilization of visible light, controllable redox potentials, facilitated migration of charge carriers, accelerated mass transfer, promoted dissociation of reactants, as well as adjustable catalyst structure.

### 4.1. Enhancing the kinetic driving force of reactants

How to effectively utilize visible and IR lights for photocatalytic processes has been a puzzle for almost half a century. A great number of research efforts have been made in developing photocatalysts with visible light absorption,[12, 194, 195] whereas it was found that light absorption cannot guarantee its effective utilization for catalytic conversion.[12, 39, 40] Groundbreakingly, in 2015, Hu's group revealed the intrinsic conflict of visible-light photocatalysis and introduced thermal energy to enhance the kinetic driving force of reactants to effectively address this issue, realizing highly efficient visible-light driven $H_2$ production from water.[21]

As shown in Fig. 7a, when UV light is absorbed, electrons would be excited from the valence band to the conduction band of black $TiO_2$ catalyst to reduce protons into $H_2$, and meanwhile, sacrificial $CH_3OH$ is oxidized. In this case, the driving force for electron donation from $CH_3OH$ (energy difference between the redox potential of $CH_2O/CH_3OH$ and valence band maximum) is 2.78 eV. In contrast, when visible or near-IR light is absorbed, electrons can only be excited from the $Ti^{3+}$ mid-gap state due to the low photon energy, to drive the same reaction. Here, the driving force of $CH_3OH$ oxidation (energy difference between the redox potential of $CH_2O/CH_3OH$ and $Ti^{3+}$ level) is just 0.88 eV, much smaller than that under UV light. The insufficient oxidation driving force is the main cause of the negligible $H_2$ production rate and quantum efficiency under visible light irradiation (Fig. 7b). This reflects the intrinsic conflict in photocatalysis which cannot be addressed by tuning the band structure of photocatalysts. Namely, while a narrow band gap is beneficial for visible light absorption, a wide band gap is desired to provide sufficient driving force.

Instead of adjusting the band structure, Hu and co-workers introduced thermal energy into the photocatalytic system to increase the kinetic energy of $CH_3OH$ molecules.[21] This, as kinetic driving force, compensates the insufficient potential driving force, allowing electron donation from $CH_3OH$ to $Ti^{3+}$ level and thus stimulating the whole reaction. Consequently, photo-induced $H_2$ production rate and quantum efficiency in visible range were enhanced by several orders of magnitude (Fig. 7c). Although black $TiO_2$ with a mid-gap state is used as an example here, the compensation effect of kinetic driving force of reactants to the potential driving force of corresponding semi-reactions is applicable for all semiconductor-based catalysts with narrow band gaps such as $WO_3$.[28, 90] The effective utilization of visible light for highly efficient photocatalysis with thermal input has been demonstrated in a series of reactions over varied catalysts.[22, 27, 28, 33, 39, 40, 90]

On top of effectively utilizing visible light, elevating temperature shows a universal advantage for activating reactant molecules. This is due to the increased population of adsorbates in excited vibrational states based on Bose-Einstein distribution, which generally leads to an enhanced reaction rate.[26, 95, 196] Moreover, since heat can be provided via photo-to-thermal conversion with visible and IR lights, the full-spectrum light utilization for different functions can be achieved. Namely, heat resulted from visible and IR light absorption on metals or defective metal oxides activates reactants and thus promotes the photocatalytic process driven by charge excitation with UV light absorption over the semiconductor.[95, 106, 145, 168, 197]

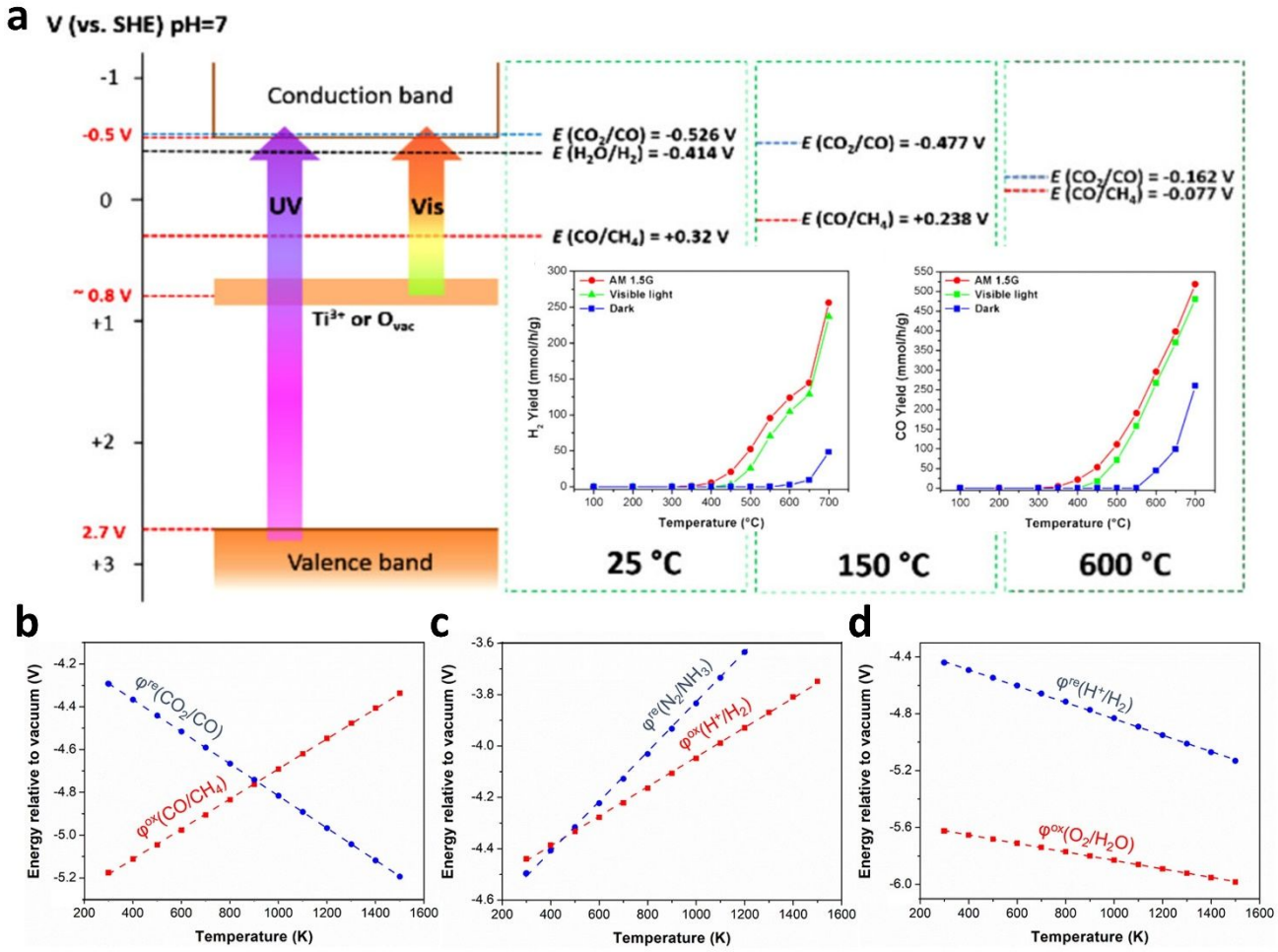


**Fig. 8** (a) Relative position of redox potentials of dry reforming of $CH_4$ to band structure of black $TiO_2$ and catalytic activities at varied temperatures (inset). Reproduced with permission from ref. 33. Copyright (2016) American Chemical Society. Temperature dependence of redox potentials of semi-reactions in (b) dry reforming of $CH_4$, (c) $NH_3$ synthesis, and (d) water splitting. Reproduced with permission from ref. 67. Copyright (2021) Elsevier.

### 4.2. Tuning the redox potential of semi-reactions

Photocatalysis requires a favourable band alignment for both thermodynamics and kinetics, namely, appropriate relative positions of redox potentials for semi-reactions to the energy bands of catalyst.[21, 33, 39, 40] The redox potential of semi-reactions is dependent on temperature, whereas in most cases the temperature effect is neglected. According to Nernst equation and thermochemical (Born-Haber) cycle, the redox potential of $H^+/H_2$ at temperature T can be calculated via eqn 1.[33, 67]

$$\varphi\left(\frac{H^+}{H_2},T\right) = \varphi\left(\frac{H^+}{H_2},298.15\ K\right) - \frac{\Delta G_f(H,\ T)}{nF} \quad (1)$$

where $\Delta G_f$, n, and F represent Gibbs free energy change of formation, number of electron equivalents, and Faraday constant, respectively. Then, the redox potential of the semi-reaction of interest can be calculated according to Gibbs free energy change of reaction $\Delta G_r(T)$ (eqn 2).

$$\varphi(T) = \varphi\left(\frac{H^+}{H_2},T\right) + \frac{\Delta G_r(T)}{nF} \quad (2)$$

For example, to obtain the redox potential of $O_2/H_2O$, $\Delta G_r(T)$ for the reaction between $H_2$ and $O_2$ to form $H_2O$ needs to be calculated.

The temperature control on redox potentials was first utilized by Hu and co-workers for dry reforming of $CH_4$, owing to which the favourable thermodynamics and kinetics were achieved.[33] As shown in Fig. 8a, at room temperature, the redox potential of $CO_2/CO$ (-0.526 V vs. SHE) is more negative than conduction band minimum (-0.500 V vs. SHE), indicating that the reduction of $CO_2$ into CO is thermodynamically impossible. While, elevating temperature can shift this redox potential to more positive values as -0.477 V at 150 °C and -0.162 V at 600 °C. This not only enables a thermodynamically favourable reaction, but also enhances the driving force (defined in section 4.1) for $CO_2$ reduction to 0.338 V at 600 °C. In the meantime, the driving force for $CH_4$ oxidation through electron donation to $Ti^{3+}$ mid-gap state is enhanced from 0.480 V at room temperature to 0.877 V at 600 °C. Owing to the favourable redox potentials and enhanced kinetic energy of reactants, $H_2$ and CO yields were significantly increased at high temperatures above 300 °C under both simulated sunlight and visible light irradiation (inset of Fig. 8a).

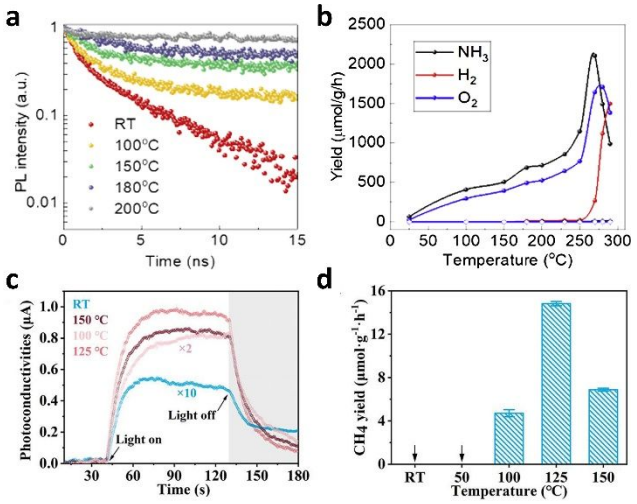


**Fig. 9** (a) Time-resolved photoluminescence intensity of Fe/$MoS_2$ catalyst as a function of temperature and (b) its thermo-photo catalytic performance for $N_2$ fixation at varied temperatures (empty symbols represent the results in dark). Reproduced with permission from ref. 46. Copyright (2021) Elsevier. (c) In-situ photoconductivity measurement of Pt/g-$C_3N_4$ catalyst and (d) its thermo-photo catalytic performance for $CO_2$ reduction into $CH_4$ at varied temperatures. Reproduced with permission from ref. 114. Copyright (2021) Elsevier.

In addition to dry reforming of $CH_4$ (Fig. 8b), redox potentials of $NH_3$ synthesis (Fig. 8c) and water splitting (Fig. 8d) have also been calculated.[67] It is clear that all the redox potentials are highly dependent on temperature, with variations up to ~1 V from room temperature to 1200 °C. Moreover, the reversal of thermodynamic favourability occurs at a certain temperature for dry reforming of $CH_4$ and $NH_3$ synthesis.

Furthermore, it is noted that elevating temperature would lead to a slight decrease in the band gap of semiconductors due to the increased interatomic spacings, while such an effect is not as noticeable as that on redox potentials.[27] The thermal contribution to band gap reduction is believed proportional to temperature change (ΔT) multiplied by the Boltzmann constant ($k = 8.617 \times 10^{-5}$ eV/K) (eqn 3).

$$\Delta E_{gap} = k \times \Delta T \quad (3)$$

Therefore, even a 1000 K temperature rise can only reduce the band gap by ~0.086 eV. While, reactants may induce more intense chemical alteration of catalysts at high temperatures such as catalyst reduction by $H_2$, which may further narrow the band gap.[119]

### 4.3. Facilitating the migration of charge carriers

By gaining energy from heating, the energy level of charge carriers is further raised, thus being more active than those only excited by illumination.[196, 198] Meanwhile, the migration of charge carriers toward either charge separation or charge recombination is facilitated.[147, 199] The facilitated charge separation promotes charge-carrier-mediated catalytic processes, while the facilitated charge recombination is beneficial for thermal-energy-driven catalytic processes. The overall effect, which is generally determined by the structure and properties of catalysts as well as the specific temperature, can be evaluated by collecting time-resolved photoluminescence spectra at elevated temperatures[46] or carrying out transient photovoltage measurements or in-situ photoconductivity tests.[114, 200, 201]

Fig. 9a shows that increased temperature prolonged the exciton lifetime of Fe/$MoS_2$ catalyst, which can be directly correlated to its catalytic activity for $N_2$ fixation (Fig. 9b).[46] Transient photovoltage measurement is another technology to reveal the carrier lifetime, based on which a higher temperature was found to increase the lifetime of photo-generated carriers over $TiO_2$, thus enhancing $H_2$ production.[201] Furthermore, a significant increase in photoconductivity upon elevating temperature to 125 °C revealed the increased number of active charge carriers by heating Pt/g-$C_3N_4$ catalyst, while further heating to 150 °C would promote charge recombination and thus lowering photoconductivity (Fig. 9c). The order of photocurrents at different temperatures ($I_{125\,°C} > I_{150\,°C} > I_{100\,°C} > I_{RT}$) is consistent with the $CH_4$ yields in thermo-photo catalytic $CO_2$ reduction (Fig. 9d).[114]

The current-voltage (I-V) curve obtained from current atomic force microscopy (c-AFM) and the contact potential difference between tip and sample measured by Kelvin probe force microscopy (KPFM) could illustrate the mobility of charge carriers.[202] While the former is based on conductivity, the latter implies electron transfer toward catalyst surface for reactions.[98] As an example, KPFM measurements revealed the facilitated escape of electrons from the surface of SnSe/$ZnIn_2S_4$ catalyst by 808 nm light irradiation to elevate temperature by 9.5 °C, which was responsible for the enhanced photocatalytic performance.[98]

### 4.4. Accelerating mass transfer

Mass transfer rate is directly correlated to temperature, namely, a higher temperature generally leads to a faster mass transfer. For thermo-photo catalysis, three aspects of mass transfer are involved, including the diffusion of reactants and products through liquid or gas media, adsorption onto and desorption from catalyst surface, and transfer of intermediate species across catalyst surface.[28, 90, 170]

The diffusion coefficient in liquid phase ($D_L$) can be calculated via Stokes-Einstein equation (eqn 4).

$$D_L = 7.4 \times 10^{-8} \frac{T(\psi M)^{0.5}}{\mu V^{0.6}} \quad (4)$$

where T, ψ, M, μ, and V denote temperature, solute-solvent interaction factor, molecular weight of solvent, viscosity of solvent, and molar volume of solute at boiling point, respectively. It is noted that diffusion coefficient $D_L$ increases with temperature, indicating accelerated mass transfer. While, the diffusion coefficient in gas phase ($D_G$) is acquired based on Chapman-Enskog theory (eqn 5).

$$D_G = 1.86 \times 10^{-3} \frac{T^2 \sqrt[3]{\frac{1}{M_1} + \frac{1}{M_2}}}{P\sigma^2 \Omega} \quad (5)$$

in which T, $M_1$, $M_2$, P, σ, and Ω represent temperature, molecular weight of solute gas, molecular weight of solvent gas, pressure of the system, average collision diameter, and temperature-dependent collision integral, respectively. Here, diffusion coefficient $D_G$ also increases with temperature. The solute gas would experience friction resistance in adjacent

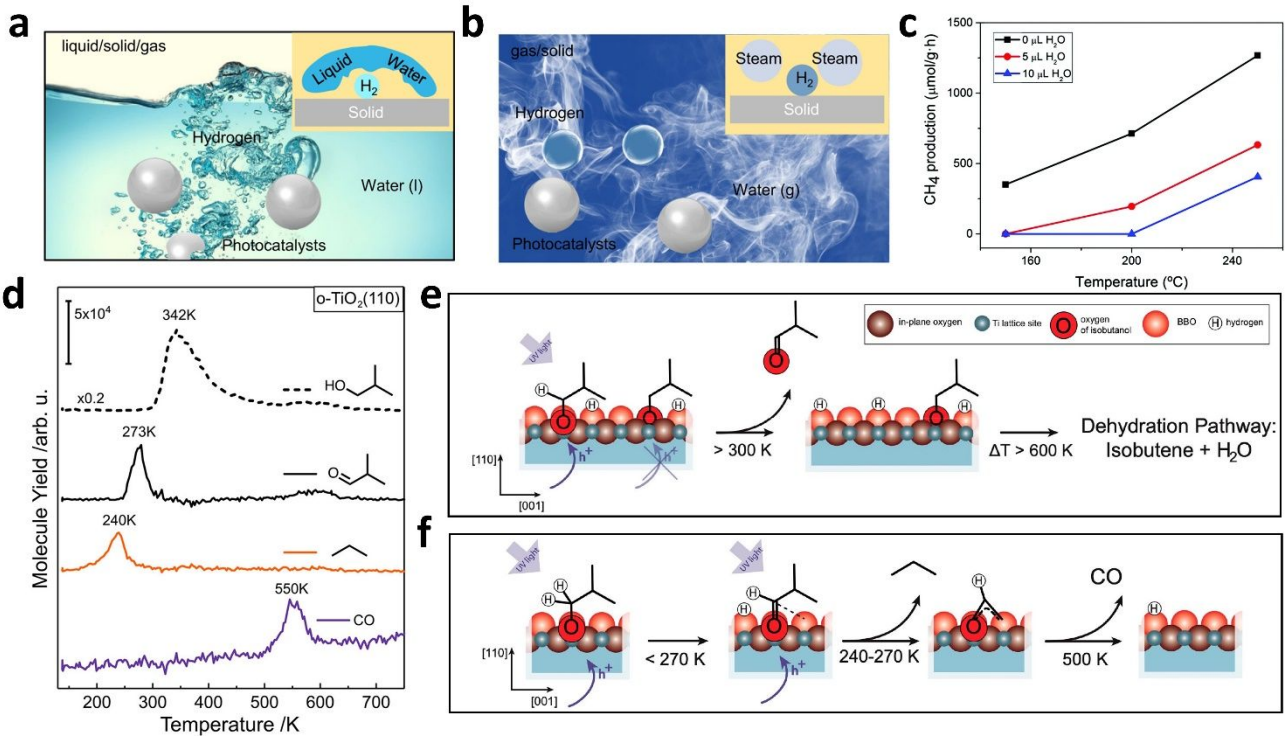


**Fig. 10** Schematic illustration for $H_2$ diffusion in (a) solid-liquid-gas three-phase system and (b) solid-gas two-phase system. Reproduced with permission from ref. 41. Copyright (2021) Springer Nature. (c) Temperature-dependent $CH_4$ production rate upon addition of water aliquots in thermo-photo catalytic $CO_2$ hydrogenation over $Cu_2O$/graphene catalyst. Reproduced with permission from ref. 103. Copyright (2017) Royal Society of Chemistry. (d) Temperature-dependent catalytic products generated in photo-oxidation of isobutanol over $TiO_2$(110) and (e) and (f) corresponding schemes of reactions. Reproduced with permission from ref. 92. Copyright (2020) American Chemical Society.

interlayers due to its relative motion with environmental particles.[203]

When the temperature is sufficient to drive the liquid-to-gas phase transition, the diffusion coefficient can undergo a significant change as the result of different interfacial friction resistances. Taking the diffusion of $H_2$ in water as an example, the liquid-phase diffusion coefficient $D_L$ at 100 °C is $5.03 \times 10^{-5}$, while in steam phase, the diffusion coefficient $D_G$ is as large as $2.65 \times 10^{-3}$ at the same temperature.[41] The 53-time enhancement in diffusion coefficient implies the facilitated mass transfer by converting traditional solid-liquid-gas three-phase catalytic system (Fig. 10a) to a solid-gas two-phase one (Fig. 10b) by raising temperature.[41, 181] Such effect is very important for the transfer of insoluble gaseous reactants toward catalyst surface, such as the diffusion of $CH_4$ through water to catalyst for its partial oxidation.[28, 29, 95]

In addition to the diffusion in liquid or gas media, the transfer of species on catalyst surface is another key factor determining catalytic efficiency.[97, 146, 204] The transferred species is typically the mediator for oxidation and reduction semi-reactions, such as proton transfer in $CO_2$ reduction by water.[26, 146, 205] Namely, protons produced in the oxidation semi-reaction ($2H_2O \rightarrow 4e^- + 4H^+ + O_2$) can be transferred to electron-rich reduction sites to be reduced ($2H^+ + 2e^- + CO_2 \rightarrow CO + H_2O$). It is clear that electron transfer and proton transfer are synchronous while proton transfer is the rate-limiting step with a time scale of hundreds of microseconds, in contrast to a few picoseconds for electron transfer.[146] The introduction of thermal energy is an effective strategy to promote proton transfer, which benefits multiple proton/electron coupling, thus enhancing the overall reaction rate.[205]

Besides, the desorption of products would also be facilitated by temperature rise. The timely removal of products allows the refresh of active sites, thus promoting catalytic activity and stability.[101, 197, 206] This has been demonstrated in a probe reaction of $CO_2$ hydrogenation with water as a byproduct.[103, 206] As shown in Fig. 10c, a small amount of water (5 or 10 μL, much below that of ~1.4 mL formed in $CO_2$ hydrogenation) could significantly decrease $CH_4$ production rate at all temperatures, indicating that water formed during reaction would inhibit subsequent $CO_2$ hydrogenation due to its strong adsorption on catalyst.[103] Nevertheless, it is evident that an increase in temperature, especially after surpassing the threshold temperature of 100 °C (boiling point of water), favoured water desorption, and therefore, enhanced $CH_4$ evolution.[103, 207] Moreover, it is worth mentioning that the heat that drives product desorption can be provided not only via electric furnaces or photo-to-thermal conversion but also through the exothermic reaction itself.[163] As an example, the heat generated by dissociative adsorption of $N_2O$ is larger than the desorption energy of $O_2$, leading to promoted $O_2$ desorption and self-sustained thermo-photo catalytic $N_2O$ decomposition.[163]

Furthermore, the temperature adjustment enables selectivity control based on the competition between thermal desorption of primary product and secondary photochemical reaction.[91, 92] As shown in Fig. 10d, the selectivity of

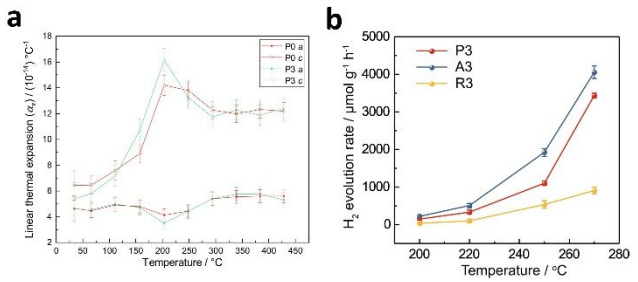


**Fig. 11** (a) Linear thermal expansion coefficient for a-axis and c-axis of the anatase phase in pristine P25 $TiO_2$ (P0) and N-doped P25 $TiO_2$ (P3). (b) Thermo-photo catalytic water splitting activity over P3, N-doped anatase $TiO_2$ (A3), and N-doped rutile (R3) at different temperatures under visible light irradiation. Reproduced with permission from ref. 211. Copyright (2021) Springer Nature.

photocatalytic reforming of isobutanol over $TiO_2$(110) highly depended on surface temperature.[92] Isobutanal was the primary product formed with the assistance of photo-generated holes and dominated at room temperature where its thermal desorption was fast (Fig. 10e). While, propane was formed at a lower temperature of 240 K due to the slow thermal desorption of isobutanal that allowed its subsequential photo-oxidation (Fig. 10f). Similar phenomenon has also been observed in photocatalytic reforming of $CH_3OH$ into HCHO and $HCOOCH_3$.[91] These works highlight the capability of tuning temperature to regulate photocatalytic selectivity.

### 4.5. Promoting the dissociation of reactants

Elevating temperature is an effective strategy to promote the dissociation of reactant molecules such as $H_2$,[101, 106, 208] CO,[105] and $H_2O$[42] on catalyst surface, allowing a much easier initiation of reactions.[26, 42] This is especially important for overall water splitting that relies on the ionic dissociation of $H_2O$ into $H^+$ and $OH^-$ for $H_2$ evolution and $O_2$ evolution, respectively. While the water ionization constant ($K_w$) at room temperature is as small as $1 \times 10^{-14}$, it can be enhanced by three orders of magnitude by raising temperature, showing a peak at ~270 °C.[209] Such trend is consistent with the temperature-dependent thermo-photo catalytic water splitting efficiency over Au/N-doped $TiO_2$/MgO catalyst, where the highest $H_2$ production rate was obtained at 270 °C.[42] Here, the increased $H^+$ and $OH^-$ ions not only promoted the reaction by providing more reacting species, but also created a local electric field on catalyst surface that can attract counter-charged carriers so as to suppress their recombination.

### 4.6. Adjusting catalyst structure

Catalyst structure can be adjusted by thermal input, in which thermal expansion is the most commonly observed. Besides, the change in crystal phase and size distribution of supported nanoparticles may occur upon temperature rise.[189] Moreover, reactants may induce more intense chemical change of catalysts at high temperatures.[119, 210] However, so far, only a few efforts have been made to correlate the catalyst structure at high temperatures to thermo-photo catalytic activity, which requires the use of advanced in-situ structure characterization equipment. Very recently, by means of variable-temperature synchrotron X-ray powder diffraction, an anisotropic linear thermal expansion was observed in pristine P25 $TiO_2$ (denoted as P0) and N-doped P25 $TiO_2$ (denoted as P3) at high temperatures.[211] Namely, as shown in Fig. 11a, linear thermal expansion coefficients for both a-axis and c-axis of the anatase phase in P0 and P3 showed abnormal extremums at 200 °C. This anisotropic linear thermal expansion was ascribed to the structural reorganization of $TiO_2$ resulted by the formation of oxygen vacancies above 200 °C, which could be correlated to catalytic activities with a clear onset at 200 °C for P3, N-doped anatase $TiO_2$ (A3), and N-doped rutile (R3) (Fig. 11b).

## 5. How does light irradiation accelerate thermal catalysis?

As the counterpart of last section, this section will reveal the approaches that light irradiation accelerates thermal catalysis, including elevating temperature, generating photo carriers and hot carriers, directly exciting adsorbates or adsorbate-catalyst bonds, dynamically controlling elementary step energetics, and modifying active sites. Some important examples for each aspect will be discussed with insights.

### 5.1. Elevating temperature

Light irradiation can induce the direct local heating on dark semiconductors and plasmonic metals, elevating temperature up to hundreds of degrees Celsius.[38, 140, 169, 212-215] For semiconductors, the heating effect is owed to direct vibration absorption of far IR light and indirect non-radiative relaxation of electron-hole pairs (Fig. 3c),[68, 69, 145] and the latter makes the dominant contribution by dissipating excessive energy through lattice vibrations.[60, 105, 106] For plasmonic metals, the non-radiative decay of surface plasmons would induce the local heating of metal lattice due to electron-phonon scattering (Fig. 3d).[15, 19, 123, 216] In addition, thermal vibration of molecules may also lead to photo-to-thermal conversion, which is applicable for carbonaceous and polymeric catalysts owing to their abundant conjugated π bonds.[63, 217]

The heat resulted from light irradiation is desired to be efficiently transferred from catalyst to adsorbates to drive catalytic reactions. The thermal equilibrium between the catalyst and adsorbates can be reached within a few picoseconds as evidenced by transient absorption spectroscopy.[218] While, the heat loss to surrounding caused by black-body radiation, thermal conduction, and thermal convection should be supressed.[25] The effect of light irradiation on catalyst temperature is generally evaluated using thermocouple or IR thermal imager, while the existence of local hot spots cannot be excluded due to the limited resolution of these techniques.[219] To identify if such temperature rise contributes to improved catalytic performance, further comparison with that at the same temperature in dark is needed.[16, 34, 172]

Herein, it is worth mentioning that local heating induced by light irradiation is different from global heating provided by electric furnace.[34, 219] Namely, in global heating, the

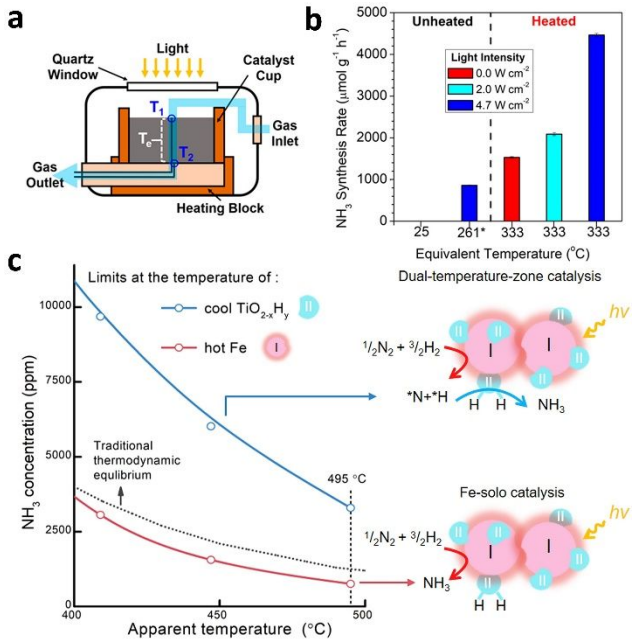


**Fig. 12** (a) Schematic illustration of set-up for in-situ measurements of the top and bottom temperatures of the catalyst bed. (b) $NH_3$ synthesis rate under varied test conditions. Reproduced with permission from ref. 44. Copyright (2019) American Chemical Society. (c) Equilibrium limit at the temperature of hot Fe and cool $TiO_{2-x}H_y$ for thermo-photo catalytic $NH_3$ synthesis in comparison with traditional thermodynamic equilibrium. Reproduced with permission from ref. 43. Copyright (2019) Elsevier.

temperatures of reactants and catalyst are almost the same, while in photo-induced local heating, the temperature of reactants is much lower than that of catalyst before their contact.[34] Based on the collision theory, thermal catalytic process strongly depends on the effective collision between reactants and catalyst surface, which is directly related to temperature.[220] Therefore, the temperature of reactants plays an important role for overall catalytic performance. This was demonstrated in thermo-photo catalytic synthesis of $CH_3OH$ from syngas, with a 3.3-time enhancement in $CH_3OH$ yield by elevating reactant temperature from 93 to 260 °C at a fixed catalyst temperature of 350 °C.[34]

Furthermore, while global heating results in a relatively uniform temperature for entire catalysts (the temperature of catalyst surface may be lower due to the cooling effect of gas flow), light irradiation leads to an evident vertical temperature gradient throughout catalysts especially for thick catalyst beds at high light intensities, since the penetration depth of incident photons is below 100 μm.[44, 171, 172] A new parameter named equivalent temperature ($T_e$) can describe the overall reactivity of thermal reactions in both thermal catalysis and thermo-photo catalysis, which is defined as[99]

$$e^{-E_a/RT_e} = \frac{1}{T_2 - T_1}\int_{T_1}^{T_2} e^{-E_a/RT} dT \quad (6)$$

in which $E_a$, R, $T_1$, and $T_2$ are apparent activation barrier, universal gas constant, and temperatures of the top and bottom of the catalyst bed (Fig. 12a), respectively. $E_a$ is obtained from temperature-dependent thermal catalytic activities. The derived $T_e$ is correlated to the effective thermal reaction rate contributed by the heater, lamp, and the exothermic reaction itself.

More importantly, the negative temperature gradient induced by light irradiation can perform as a thermodynamic pump to modulate the global equilibrium and resolve the conflicts in catalysis.[44] In the presence of temperature gradient, molecules tend to move from high-temperature zones to low-temperature zones due to thermophoretic force.[221] Therefore, under light irradiation, molecules would penetrate from catalyst surface to inner parts. As long as the thermophoretic force aligns with the direction of gas flow (such as that in Fig. 12a), the yield can be enhanced since the product is effectively drawn away from hot region to avoid its decomposition. Namely, a greater top temperature ($T_1$) ensures a high reaction rate, while a smaller bottom temperature ($T_2$) helps to maintain a high yield. This has been demonstrated for $NH_3$ synthesis over Ru-Cs/MgO catalyst, in which the $NH_3$ synthesis rate at the same $T_e$ of 333 °C was enhanced by 36% and 192% under light irradiation at 2.0 W/cm² (ΔT = -39 °C) and 4.7 W/cm² (ΔT = -184 °C), respectively, in comparison with that in dark (ΔT = +58 °C) (Fig. 12b).[44] In this case, the rate-limiting step of $N_2$ dissociation is favoured in the irradiated hotter region while as-produced $NH_3$ is preserved in the dark cooler region.

In addition to controlling the vertical temperature gradient, light irradiation may also induce lateral temperature variations on catalyst surface with an elaborate design on catalyst composition, which can break the theoretical thermal equilibrium limit.[43] The most common strategy is to couple a LSPR metal and a substance with a poor thermal conductivity which provide the heating zone and cooling zone, respectively. The local temperature difference in nanostructured catalysts can be measured by temperature-programmed Fourier-transform infrared (TP-FTIR) spectroscopy and surface-enhanced Raman spectroscopy (SERS) mapping with certain molecular temperature probes such as adonitol and phenyl isocyanide.[43, 222, 223] Extended X-ray absorption fine structure (EXAFS) spectroscopy is another powerful tool for local temperature monitoring based on thermal vibration of atoms illustrated by the Debye-Waller factor change.[105, 106, 224]

Again, using $NH_3$ synthesis as an example, a local temperature difference of 137 °C between hotter Fe and cooler hydrogenated $TiO_2$ ($TiO_{2-x}H_y$) under light irradiation contributed to a high $NH_3$ yield (1939 ppm) which is 3.5 times of the thermal catalytic result at the same apparent temperature of 495 °C (560 ppm).[43] Furthermore, Fig. 12c illustrates a surpassed thermodynamic equilibrium limit at 495 °C (1249 ppm < 1939 ppm). Taking local temperature differences into account, two new thermodynamic equilibriums at the temperatures of Fe and $TiO_{2-x}H_y$ can be plotted. The Fe-solo catalysis showed a reduced thermodynamic limit, while a new working-in-tandem pathway prominently enhanced the limit to 3294 ppm, by which the experimental result (1939 ppm) can be regarded thermodynamically favourable.

### 5.2. Forming photo carriers

When semiconductor-based catalysts (such as $TiO_2$, $SrTiO_3$, and $CeO_2$) are applied for thermal catalysis, introducing light

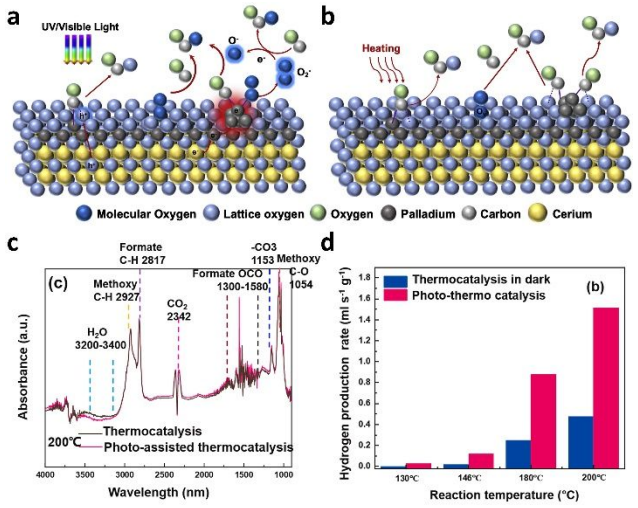


**Fig. 13** Schematic illustration of reaction mechanisms of (a) thermo-photo and (b) thermal catalytic oxidation of CO over $PdO_x/CeO_2$ catalyst. Reproduced with permission from ref. 129. Copyright (2021) Elsevier. (c) In-situ DRIFTS spectra collected at 200 °C and (d) $H_2$ production rate in steam reforming of $CH_3OH$ over Cu-Zn-Zr oxide catalyst with and without illumination. Reproduced with permission from ref. 124. Copyright (2021) Elsevier.

irradiation can induce the generation of photo carriers as long as the photon energy is not smaller than the catalyst band gap. As-generated photo carriers can activate reactant molecules either directly or indirectly. Direct activation represents the direct reaction between photo carriers (either holes or electrons) and reactants, which has been demonstrated for $H_2$,[22] $O_2$,[132, 133] CO,[35, 129] $CO_2$,[75, 225] $CH_4$,[31, 119] $H_2O$,[226] NO,[134-136] etc.

As a typical example for direct activation, $O_2$ adsorbed on Pd sites of $PdO_x/CeO_2$ catalyst could accept photo-generated electrons to form active $\bullet O_2^-$ under illumination (eqn 7), which then oxidized CO with $CO_2$ and $O^-$ as byproducts (Fig. 13a).[129] Meanwhile, photo-generated holes would be transferred to PdO and activate the adsorbed CO which then consumed $O^-$ or active lattice O atom to produce $CO_2$. Such a mechanism was supported by active species scavenging experiments and electron paramagnetic resonance (EPR) measurements. However, in dark, the only pathway was through the reaction between CO adsorbed on PdO and lattice O atoms (Fig. 13b). As a result, CO conversion at 80 °C was greatly enhanced from 25% to 100% by light irradiation. Similar activation has also been demonstrated in $CH_4$ oxidation,[133] $C_3H_8$ oxidation,[132] oxidation of benzyl alcohol to benzaldehyde,[227] etc.

$$O_2 + e^- \rightarrow \cdot O_2^- \quad (7)$$

$$H_2O + h^+ \rightarrow \cdot OH + H^+ \quad (8)$$

$$CH_4 + \cdot OH \rightarrow \cdot CH_3 + H_2O \quad (9)$$

Moreover, photo carriers may activate molecules indirectly via the production of free radicals such as •OH (eqn 8) and $\bullet O_2^-$ (eqn 7).[28, 90, 228] •OH and $\bullet O_2^-$, as the typical reactive oxygen species (ROS), are more active and oxidative than the precursory $H_2O$ and $O_2$.[93, 229] Here, just as traditional photocatalysis, thermodynamic requirement on the relative band position to redox potential must be satisfied for forming free radicals.[28, 90, 93] As-generated free radicals may react with inert molecules to achieve their activation and dissociation. Most importantly, the electrophilic •OH is able to abstract H atoms from $CH_4$ (eqn 9), which significantly reduces the required thermal input for the dissociation of C-H bonds.[28]

Besides, photo carriers may accelerate the formation of some intermediate species, thus promoting overall reaction.[124, 175, 210] This is generally demonstrated using in-situ diffuse reflectance infrared Fourier transform spectroscopy (DRIFTS) to compare two cases with and without illumination. As shown in Fig. 13c, the generation of formate with characteristic DRIFTS peaks at 1300-1580 $cm^{-1}$ was promoted by light irradiation over Cu-Zn-Zr oxide catalyst in steam reforming of $CH_3OH$ at 200 °C.[124] The promoted production of intermediate formate was believed as the main contributor to the 3.2-time enhancement in $H_2$ production shown in Fig. 13d.

Furthermore, photo carriers could enable the conversion of some poisonous species adsorbed on catalyst, which eliminates their negative effects or even makes them active species.[48, 132, 230] For example, water, as both the product and inhibiter of thermal catalytic decomposition of volatile organic compounds (VOCs) due to its competitive adsorption with $O_2$ on active sites, can combine with photo-generated holes to generate •OH (eqn 8) for accelerating VOC decomposition under illumination.[48] Via this way, an efficient catalytic loop with positive feedback is built.

### 5.3. Generating hot carriers

When photons resonantly oscillate with free electrons in metal nanoparticles, LSPR is established, which confines photo energy near metal surface in the form of elevated electric fields.[231] The stored energy in LSPR field is dissipated via either non-radiative decay or radiative photon scattering within a few femtoseconds.[19] The non-radiative decay leads to the generation of hot carriers through intra-band s-to-s transitions or inter-band d-to-s transitions accompanied with a (phonon) temperature increase of metal nanoparticles (Fig. 3d).[61, 70, 232] To identify the contribution of hot carriers from photo-thermal effect, a control experiment at the same temperature in dark is required.[32, 53] More details about the fundamental aspects of LSPR have been clearly presented in previous reviews,[19, 20, 61, 233-236] and here we will mainly focus on the catalysis-related principles and discoveries.

Hot carriers generated via the decay of localized surface plasmons are typically more energetic than the carriers produced via direct photoexcitation (photo carriers).[237, 238] Moreover, the photo-electronic current induced by hot carriers tracks the surface plasmon resonance absorption spectrum and shows a super-linear dependence on light intensity, which can be directly correlated to catalytic activity.[239, 240] Namely, as-generated hot carriers may undergo multiplication, leading to an apparent quantum efficiency exceeding 100% at large light intensities.[238] Moreover, it should be noted that besides metal itself, adsorbed reactants also affect light absorption and thereby generation of hot carriers, which has been evidenced by comparing the in-situ UV-visible spectrum of metal after adsorption and quantum efficiencies at varied wavelengths.[73]

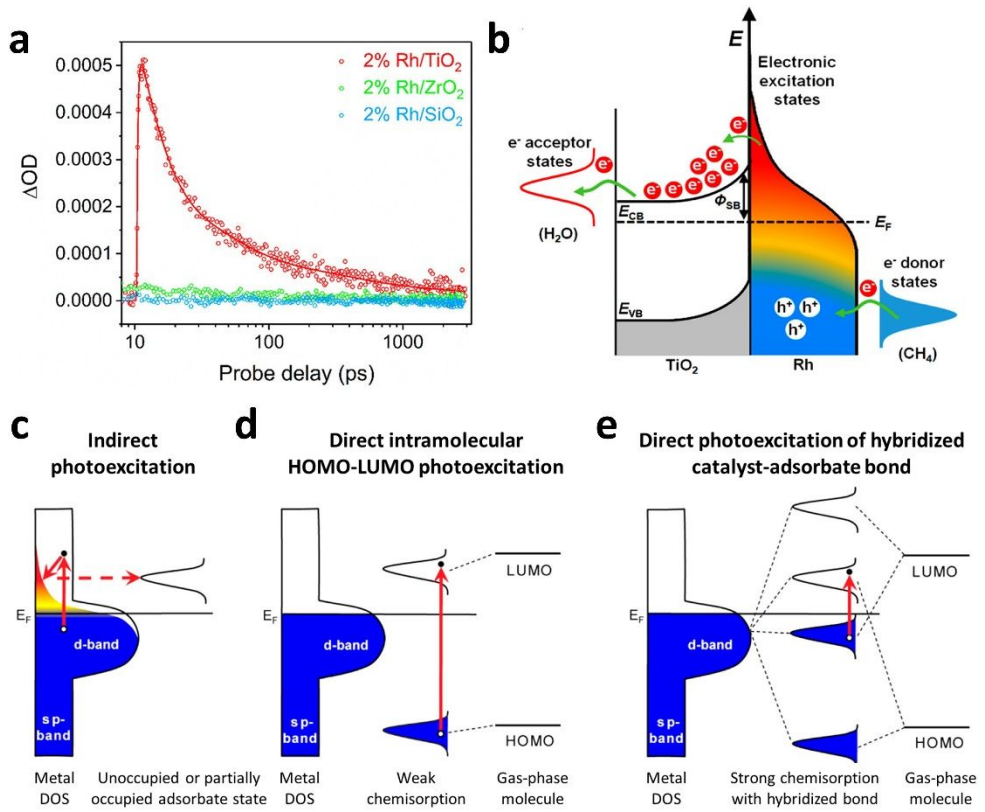


**Fig. 14** (a) Transient absorption spectra at 5000 nm for $Rh/TiO_2$, $Rh/ZrO_2$, and $Rh/SiO_2$ catalysts under photoexcitation at 450 nm. (b) Schematic illustration of electron transfer in steam reforming of $CH_4$ over $Rh/TiO_2$ catalyst under visible light irradiation. Reproduced with permission from ref. 122. Copyright (2018) American Chemical Society. Schematic illustration of photoexcitation on metal: (c) indirect photoexcitation via hot carriers, (d) direct photoexcitation with intramolecular HOMO-LUMO transitions in weakly chemisorbed systems, and (e) direct photoexcitation of hybridized catalyst-adsorbate bonds in strongly chemisorbed systems. Reproduced with permission from ref. 77. Copyright (2014) American Chemical Society.

As-generated hot carriers possess certain mobility due to their high energies.[237, 241] The transfer proceeds in an ultrafast timescale (< 50 fs) right after Landau damping and before electron thermalization.[242] Adsorbed reactant molecules can significantly change the charge flow within the excited plasmonic system, as a high-rate direct resonant flow from metal to adsorbate which bypasses the conventional charge excitation and thermalization occurring in metal nanoparticles and leads to a greater yield of extracted hot carriers.[243] Hot carriers would be injected into the unoccupied or partially occupied molecular orbitals of adsorbate molecule, forming a transient negative ion that subsequently undergoes bond breaking.[18, 163, 244] This mechanism can well describe the activation and dissociation of small molecules such as $H_2$,[162, 245, 246] $O_2$,[18] $N_2$,[45, 247] $CH_4$,[248] and $CO_2$.[171, 177, 249] This addresses the issue of difficult activation of nonpolar molecules in thermal catalysis.[70, 250] Moreover, the presence of hole scavengers such as ethanol would promote multiple electron harvesting, thus enabling reactions involving multi-electron and multi-proton transformation.[251] Nevertheless, since photon absorption mainly stimulates electronic transitions within bulk metal, wavelength dependences of competing reactions are similar, so the catalytic selectivity is hard to be controlled by varying excitation wavelength.[77]

Moreover, hot carriers can be transferred between metals or from metal to support. The electron transfer between metals relies on the d bands at Fermi level that enable the direct momentum-conserved inter-band excitation in visible range,[36] while the electron transfer from metal to support occurs as long as the conduction band of support is lower than the electronic excitation state in metal, which leads to the formation of a Schottky junction.[234, 252, 253] The electron transfer direction is opposite to that of traditional photocatalysis over metal-semiconductor composites.[175, 254, 255] As a result, an electron-deficient state is left at metal surface, which is promising to promote bond activation at low temperatures.[122] This could be elucidated in thermo-photo catalytic $CH_4$ steam reforming system. Namely, according to the transient absorption spectra (Fig. 14a), electron injection from Rh into $TiO_2$ in $Rh/TiO_2$ catalyst occurred within 250 fs, while such an injection was inhibited in $Rh/SiO_2$ and $Rh/ZrO_2$ catalysts due to the high conduction bands of $SiO_2$ and $ZrO_2$.[122] As shown in Fig. 14b, the resulting electron-deficient $Rh^{\delta+}$ site at Rh surface showed a great advantage to accept σ electrons of $CH_4$ and facilitated the cleavage of C-H bonds, while the electrons transferred to $TiO_2$ could deposit their energy into the antibonding orbital of water and induced its reduction into $H_2$.[122, 256]

Furthermore, as-generated hot carriers may change the rate-limiting step in the whole reaction, promote the

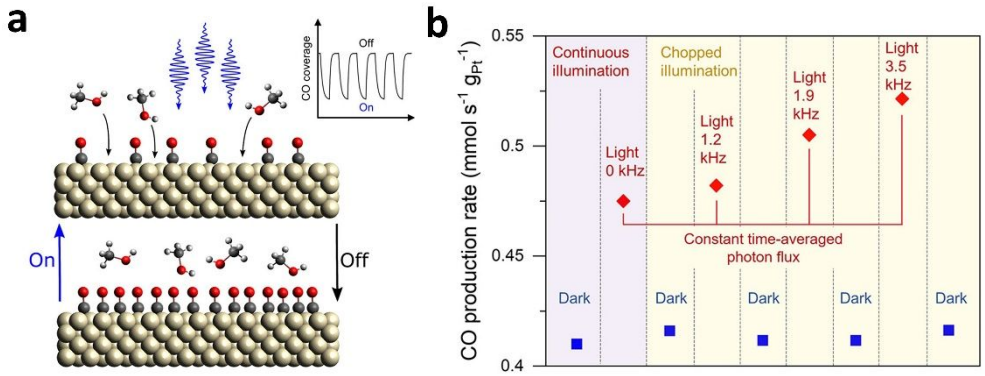


**Fig. 15** (a) Schematic illustration and (b) catalytic activity for $CH_3OH$ decomposition over $Pt/SiO_2$ under pulsed illumination. Reproduced with permission from ref. 126. Copyright (2020) American Chemical Society.

conversion of intermediate species, and accelerate the desorption of final products (by electronically exciting adsorbed species).[23, 32, 76, 86, 125, 257-259] It is highlighted that the surface coverage of catalyst can be dynamically controlled by hot carriers. Though the adsorption of reactants is necessary, their excessive occupation of active sites is undesirable, which affects reaction energetics.[55, 77] The generation of hot carriers can mitigate the energy penalty for cleaning active sites, thus reducing apparent activation barrier in comparison to that of thermal catalysis.[55] Besides catalytic activity, hot carriers may enhance catalytic selectivity and stability as well, by adjusting the kinetics for bond activation and product desorption from catalyst surface.[32, 76, 130, 248]

### 5.4. Directly exciting adsorbates or adsorbate-catalyst bonds

Besides the catalyst-mediated photoexcitation of charge carriers which then react with reactants (Fig. 14c) as discussed in the last two sections, there are two more direct photoexcitation mechanisms, which are the direct photoexcitation with intramolecular HOMO-LUMO transitions in weakly chemisorbed systems (Fig. 14d) and the direct photoexcitation of hybridized catalyst-adsorbate bonds in strongly chemisorbed systems (Fig. 14e).[56, 77, 260-262] The direct and indirect mechanisms can be distinguished by comparing the measured wavelength-resolved quantum efficiencies with the simulated characteristics of metals based on finite-difference time-domain simulations.[263] Simulated characteristics include surface electric field enhancement for direct photoexcitation and hot carrier density for indirect photoexcitation. Here, mechanistic distinction is essential for developing highly efficient plasmon-mediated catalytic processes due to the different optimization considerations on electromagnetic field strength either at the surface (direct) or inside (indirect) the nanostructure.[263, 264]

The intramolecular HOMO-LUMO transition of reactant molecule leads to an increased polarizability and thereby its response to plasmonic field gradient, which enhances its adsorption on catalyst and may further tune catalytic selectivity.[56, 262, 265] Namely, species with a stronger light absorption to transform into excited state may experience a stronger plasmon-based force of attraction, which adds up to general van-der-Waals force to overcome its Brownian motion, showing a greater coverage on catalyst surface and thus being converted more favourably.

More attention has been paid to the direct photoexcitation of catalyst-adsorbate bonds since a strong chemisorption is required for most chemical reactions. In this case, the electronic transition occurs between the hybridized bonding and antibonding states which are formed via charge donation from adsorbate or back-donation from the d states of metal.[266] This allows a much more efficient utilization of photons with low energies, extending light response from UV to visible and even near-IR regions.[260] More importantly, such a direct adsorbate-specific mechanism enables the selectivity control of catalytic reactions. This has been demonstrated for preferential CO oxidation in a $H_2$-rich atmosphere. Namely, the selective photon-induced activation of Pt-CO bonds on $Pt/SiO_2$ catalyst could significantly enhance $CO_2$ selectivity from 44% to 81% at 170 °C.[77] While, further increasing the temperature would lower the selectivity due to the favoured production of thermodynamically stable products. Therefore, the selectivity control by direct excitation of adsorbate-catalyst bonds suffers a balance between providing a high temperature for low-intensity photon fluxes to show a significant impact on activity and maintaining a low temperature to keep the kinetic control of selectivity.

### 5.5. Dynamically controlling elementary step energetics

Periodic oscillation of elementary step energetics on catalysts is promising to realize higher activity and selectivity than those with static energetics.[267, 268] Thanks to the capability of light to modify the energetics of elementary steps, pulsed illumination enables surface oscillation between two adsorbate binding energies and thereby two rate-limiting steps at frequencies in resonance with reaction kinetics, which leads to an enhancement in catalytic performance.[126, 269] Using $CH_3OH$ decomposition over $Pt/SiO_2$ as a probe reaction, the oscillation between a reactive surface limited by active site availability in dark (due to the strong bonding of CO to Pt) and a clean surface limited by activation of reactants ($CH_3OH$) under light irradiation (Fig. 15a) contributed to a steady-state rate surpassing either static conditions (Fig. 15b).[126]

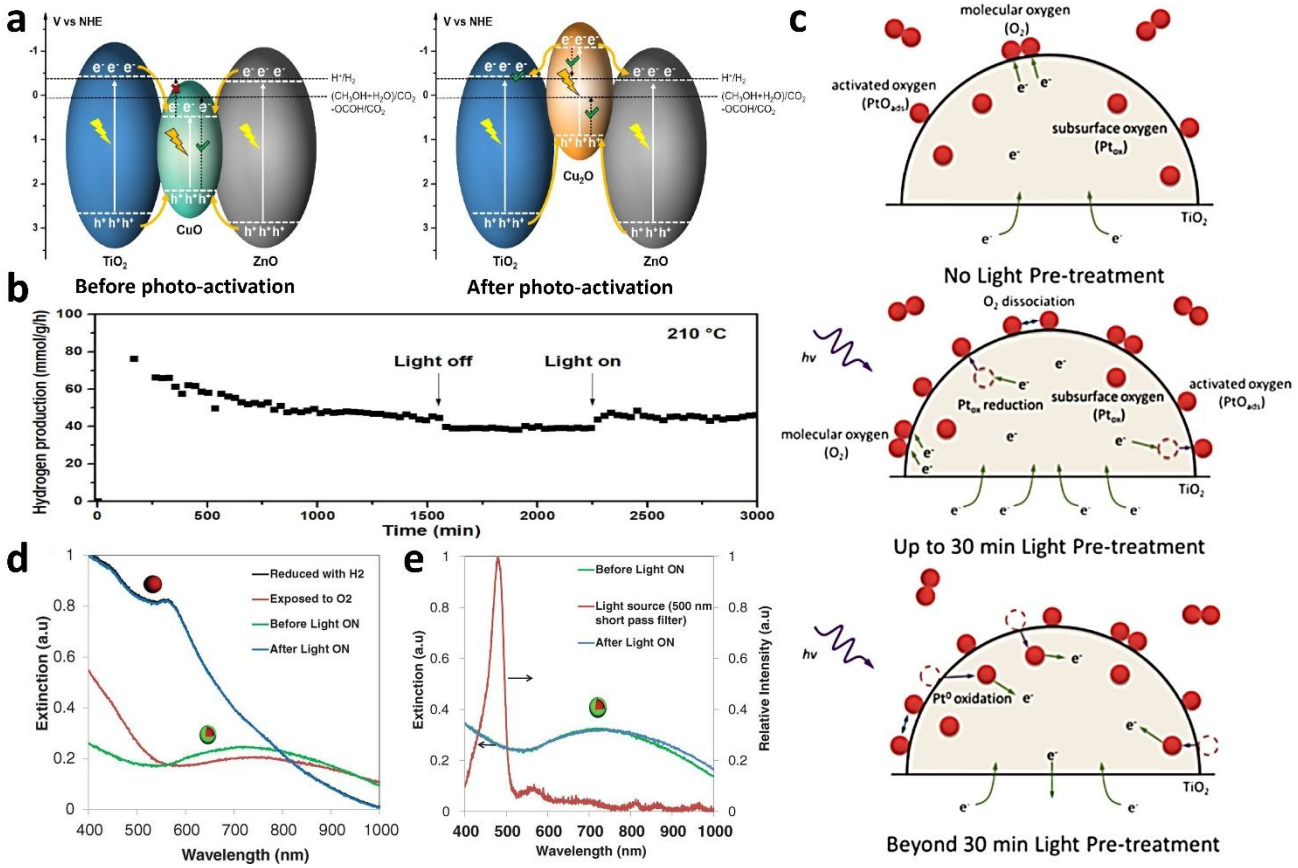


**Fig. 16** (a) Schematic illustration of in-situ photo-activation of Cu-Zn-Ti oxide catalyst in stem reforming of $CH_3OH$ and (b) thermo-photo catalytic $H_2$ production rate at 210 °C. Reproduced with permission from ref. 82. Copyright (2019) Elsevier. (c) Schematic illustration of the effect of light pre-treatment on oxygen activation in $Pt/TiO_2$ catalyst. Reproduced with permission from ref. 149. Copyright (2017) American Chemical Society. In-situ UV-visible spectra of $Cu/SiO_2$ catalyst at 200 °C under (d) full-spectrum and (e) $\lambda < 500$ nm light irradiation. Reproduced with permission from ref. 52. Copyright (2013) American Association for the Advancement of Science.

### 5.6. Modifying active sites

Light irradiation can modify active sites for thermal catalysis via either persistent adjustment or transient induction.[52, 82] In the former case, light irradiation is regarded as a pre-treatment or regeneration technique for catalysts, while in the latter case, photo energy must be provided all the time during reaction to maintain catalytically active sites, which will be respectively discussed in the following part.

The pre-treatment and regeneration of catalysts to provide sufficient active sites by light irradiation are mainly dependent on the redox abilities of photo-generated electrons and holes over semiconductor-based catalysts.[82, 230, 270] When metals or low-valence metal oxides (especially for non-noble metals with multiple valence states) act as active sites, a reduction pre-treatment process with $H_2$ is generally required.[83, 84] As long as the reduction potential of metal oxide is below its conduction band minimum, the in-situ photo-reduction of metal oxide by photo-generated electrons would occur.[40, 82, 85] This has been demonstrated on Cu-Zn-Ti oxide catalyst for steam reforming of $CH_3OH$.[82] Namely, photo-generated electrons in ZnO and $TiO_2$ tended to accumulate on the conduction band of CuO to induce its reduction into $Cu_2O$ (Fig. 16a). After in-situ photo-activation of the catalyst, light can be turned off with only a slight decrease in $H_2$ production rate (Fig. 16b) due to the contribution of photo carriers to the redox reaction (Fig. 16a).

In contrast, in some cases, high-valence metal ions are responsible for high catalytic activities, so in-situ photo-oxidation by holes plays an important role.[230] For example, thermal catalytic oxidation that benefits from high-valence metal oxide catalysts with sufficient lattice oxygen may lose activity due to the reduction of surface metal ions such as $Mn^{4+}/Mn^{3+}$ to $Mn^{2+}$ and $Ce^{4+}$ to $Ce^{3+}$, while the deactivated catalyst can be regenerated (re-oxidized) by light irradiation.[230]

The duration of illumination treatment would affect catalyst structure and thereby catalytic activity. As shown in Fig. 16c, pre-treatment of $Pt/TiO_2$ catalyst with UV light up to 30 min led to the injection of photo-generated electrons from $TiO_2$ to Pt, which facilitated the migration of subsurface oxygen and dissociation of $O_2$ molecule, thus increasing activated oxygen on catalyst surface.[149] However, light irradiation beyond 30 min resulted in partial oxidation of Pt because the overcrowded activated oxygen on Pt surface was forced into subsurface sites. Consequently, the optimal catalytic performance for HCOOH oxidation was obtained with 30 min illumination pre-treatment. This is also applicable for other noble metal deposits such as Au and Pd. Moreover, a pre-treatment (or post-treatment before next cycle) by illumination was also reported to be able to create defects (such as oxygen vacancies) in catalyst[271] and remove carbon-containing species from catalyst surface,[270]

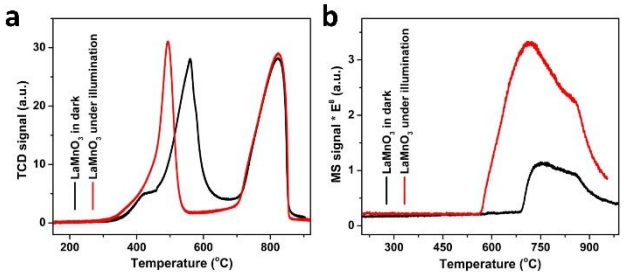


**Fig. 17** (a) $H_2$-TPR and (b) $O_2$-TPD of $LaMnO_3$ catalyst in dark and under illumination. Reproduced with permission from ref. 283. Copyright (2021) Elsevier.

which enhance the accessibility of active sites to reactant molecules, thus promoting catalytic activity up to 7 times.

In addition to persistent adjustment, the real-time control of catalytically active sites (transient induction) by light irradiation is even more attractive, which enables some impossible thermal catalytic reactions. Most importantly, light irradiation is able to maintain metallic active sites under an oxidative atmosphere for oxidation reactions.[52, 132] As reported by Linic's group, visible-light driven photoexcitation of LSPR of Cu contributed to the reduction of surface $Cu_2O$ into metallic Cu, thus realizing highly efficient and selective epoxidation of propylene.[52] This was demonstrated by the in-situ UV-visible spectra collected at 200 °C, where the illuminated catalyst showed an evident excitation corresponding to metallic Cu, in great contrast to that of the catalyst in dark (Fig. 16d). Besides, the spectrum under illumination of < 500 nm light showed no excitation for metallic Cu (Fig. 16e), suggesting the key role of LSPR of Cu with a characteristic absorption at ~565 nm.

Another role of light irradiation is to dynamically control the redox properties of metal oxide catalysts (such as $CeO_2$ and $Cu_2O$).[24, 81, 213, 272] Namely, photo-generated electrons can induce the reduction of metal ions to form lower-valence metal ions and oxygen vacancies, which is beneficial for reactions with oxygen vacancies as adsorption and catalytically active sites (such as $CO_2$ conversion), ensuring an excellent catalytic stability in long-term operation.[81, 135, 136, 225, 273] Moreover, in recent studies, it was found that light irradiation could help to reinstate the balance among Cu, $Cu^+$, and $Cu^{2+}$ in Cu-based catalysts, thus maintaining a high catalytic efficiency for $CO_2$ hydrogenation.[24, 274] On top of metal oxides, the controllable decoration of oxygen on the surface of metal carbide and metal nitride catalysts by light irradiation can also improve catalytic activity and selectivity.[37, 275]

Moreover, photo-activation of surface lattice oxygen in metal oxide catalysts can significantly promote thermal catalytic oxidation reactions that follow Mars-van Krevelen (MvK) pathway: adsorbed molecules are oxidized by surface lattice oxygen, and then the remaining oxygen vacancies are replenished by $O_2$.[89, 276-280] The former step is the rate-limiting one, which indicates the vital importance of activating lattice oxygen.[281, 282] The combination of temperature-programmed reduction (TPR, with $H_2$ or CO) and temperature-programmed desorption (TPD, with $O_2$) techniques in dark and under illumination can demonstrate the effect of light on lattice oxygen of catalysts.[131, 283, 284] As shown in Fig. 17a, the first $H_2$ reduction peak of $LaMnO_3$ catalyst showed an evident shift to low temperature with an increased $H_2$ consumption upon illumination, indicating improved lattice oxygen reducibility and

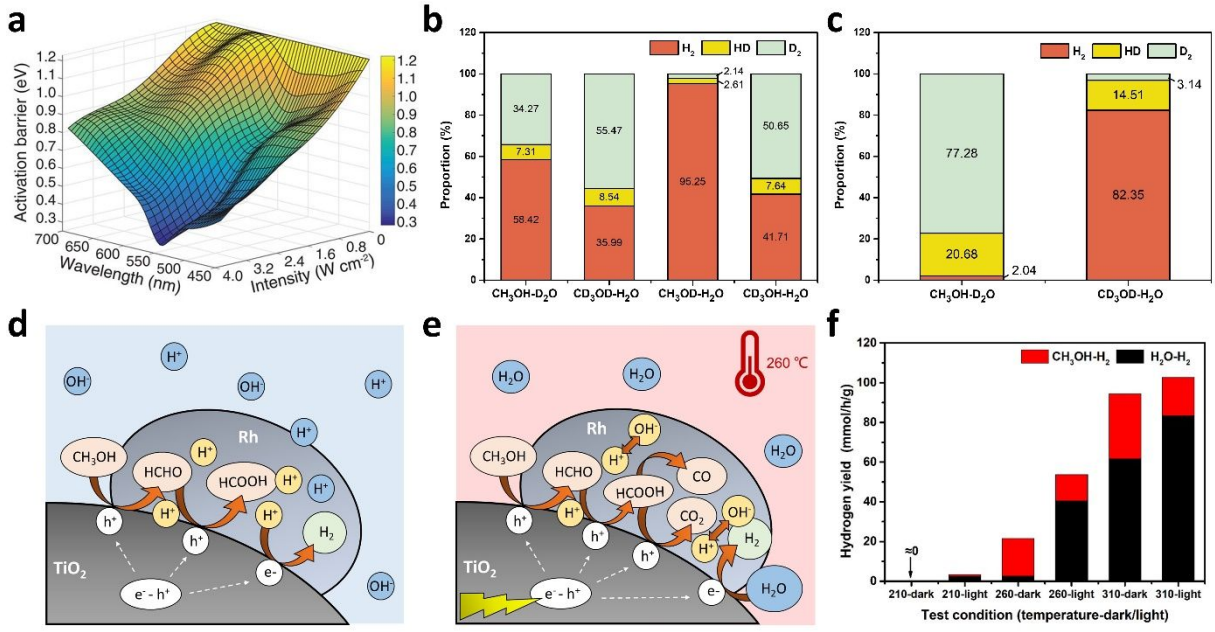


**Fig. 18** (a) 3D contour map of activation barriers for different light wavelengths and intensities for $NH_3$ decomposition over Cu-Ru/MgO-$Al_2O_3$ catalyst. Reproduced with permission from ref. 86. Copyright (2018) American Association for the Advancement of Science. Proportions of $H_2$, HD, and $D_2$ obtained in isotope labelling experiments of (b) photocatalytic and (c) thermo-photo catalytic water splitting with sacrificial methanol over Rh/black $TiO_2$ catalyst. Schematic illustration of (d) photocatalytic and (e) thermo-photo catalytic reactions over Rh/black $TiO_2$. Reproduced with permission from ref. 40. Copyright (2020) Elsevier. (f) $H_2$ production from water and methanol obtained in isotope labelling experiments of thermal and thermo-photo catalytic water splitting with sacrificial methanol over $NiO_x$/black $TiO_2$ catalyst. Reproduced with permission from ref. 39. Copyright (2019) American Chemical Society.

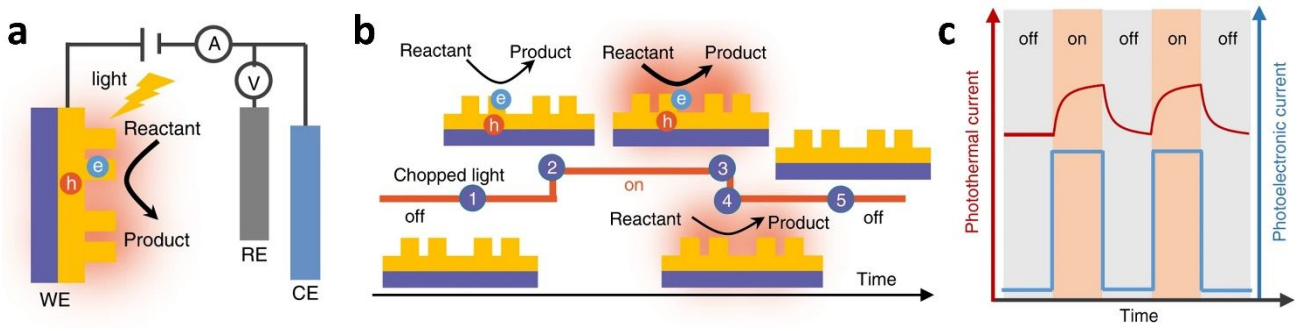


**Fig. 19** Schematic illustration of (a) three-electrode electrochemical cell with a plasmonic working electrode, (b) photoelectrochemical characterization under chopped light, and (c) photo-electronic current and photo-thermal current. Reproduced with permission from ref. 239. Copyright (2019) Springer Nature.

increased amount of active lattice oxygen.[283] $O_2$-TPD measurements (Fig. 17b) further confirmed the light-promoted generation of active oxygen according to the considerable increase in desorbed oxygen amount under illumination. Such photo-activation has been widely observed with a positive effect on thermo-photo catalytic decomposition of VOCs.[131, 276, 283]

## 6. How to explore thermo-photo catalytic mechanism?

The catalytic process involving both thermal and photo energies is rather complicated. The exploration of thermo-photo catalytic mechanism will provide more insights into reaction control. This section will comprehensively discuss the state-of-the-art approaches used to explore catalytic mechanisms of thermo-photo catalytic processes, including activation barrier determination, isotope labelling experiments, photoelectrochemical measurements, some advanced in-situ or operando characterization technologies, and emerging embedded correlated wavefunction calculations.

### 6.1. Activation barrier determination

Activation barrier for a reaction is recognized as the sum of activation barrier of the rate-limiting step, enthalpy of steps producing species involved in the rate-limiting step, and enthalpy for the desorption of reaction intermediates from active sites.[285] By measuring reaction rates at a range of temperatures and preparing Arrhenius (lnk-1/T) plot, apparent activation barrier ($E_a$) can be obtained based on Arrhenius equation (eqn 10 and eqn 11).

$$k = Ae^{-\frac{E_a}{RT}} \quad (10)$$

$$lnk = -\frac{E_a}{RT} + lnA \quad (11)$$

in which k, R, T, and A are rate constant, universal gas constant, surface temperature of catalyst, and a constant. The comparison of activation barriers from thermal catalytic process and thermo-photo catalytic process reveals the primary reaction enhancement mechanism. Namely, if two activation barriers are almost the same, the primary reaction enhancement is due to photo-thermal heating.[163] The determination of reaction orders in these two cases can further confirm this mechanism since the identical reaction orders indicate the same rate-limiting step.[55]

While, the difference in thermal catalytic activation barrier and thermo-photo catalytic activation barrier implies a more complex reaction enhancement mechanism due to the mediation of charge carriers, modification of active sites, etc.[40, 55, 86, 122, 132] For plasmonic catalysis, a concept of light-dependent activation barrier was introduced by Halas and co-workers, which enabled the quantification of hot carrier and thermal contributions in a unified picture.[86] Firstly, the reaction rates over a range of catalyst surface temperatures at certain light wavelengths (λ) and intensities (I) were measured. Subsequently, based on photo-induced reaction rates (by subtracting thermal catalytic reaction rates), activation barrier $E_a$(λ, I) was obtained according to Arrhenius equation. As shown in Fig. 18a, the 3D contour map of $E_a$(λ, I) for $NH_3$ decomposition over Cu-Ru/MgO-$Al_2O_3$ catalyst demonstrated that (1) the wavelength dependence was similar for all intensities and (2) the decreasing trend of $E_a$ with increasing intensity applied for all wavelengths. At 550 nm (corresponding to the LSPR frequency) and 4 W/cm$^2$, $E_a$ reached the minimum of ~0.27 eV.[86] Here, since $E_a$(λ, I) was determined by measuring catalyst surface temperature, the contribution of hot carriers could be clearly distinguished from that of photo-thermal heating. Moreover, this allowed us to predict the catalytic performance under varied conditions.

### 6.2. Isotope labelling experiments

Using isotope-labelled reactants to conduct catalytic experiments and analysing products via mass spectrometry is an effective approach to identify origins of products, which further implies reaction pathway.[28, 29, 39, 40, 90] Hu's group first used deuterated water ($D_2O$) and methanol ($CD_3OD$, $CH_3OD$, and $CD_3OH$) to explore the pathways of photocatalytic and thermo-photo catalytic water splitting in the presence of sacrificial methanol over Rh/black $TiO_2$ catalyst.[40] It was surprisingly found that ~60% of $H_2$ was generated from methanol rather than water in room-temperature photocatalytic reaction (Fig. 18b), in great contrast to the "true" water splitting with ~90% of evolved $H_2$ originated from water in thermo-photo catalysis (Fig. 18c). This is because protons produced in methanol oxidation could be reduced to $H_2$ by photo-generated electrons at room temperature (Fig. 18d),

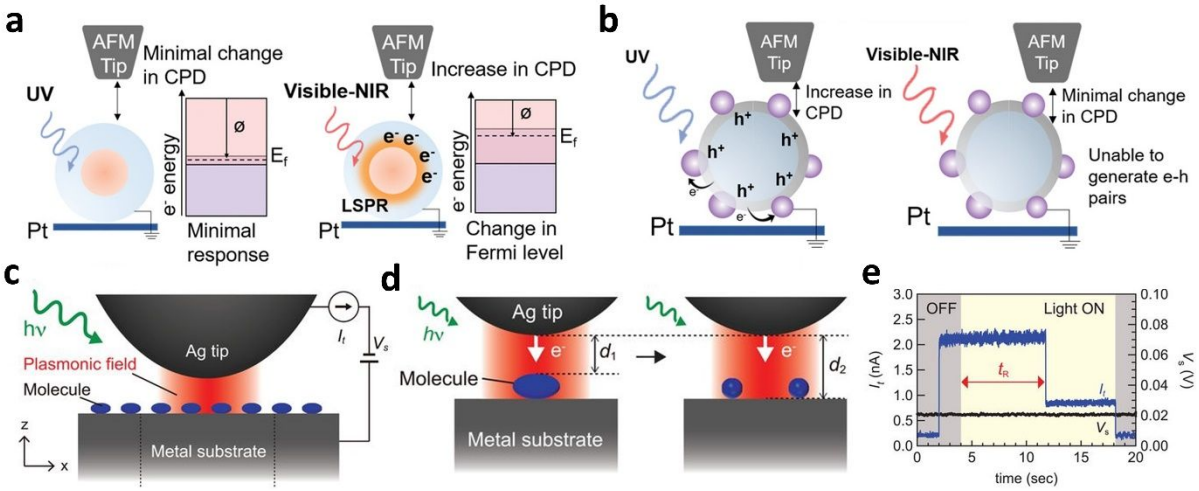


**Fig. 20** Schematic illustration of KPFM measurement and the effect of UV and visible-near IR light irradiation on the surface potential of (a) plasmonic and (b) semiconductor catalysts. Reproduced with permission from ref. 168. Copyright (2021) John Wiley and Sons. (c) and (d) Schematic illustration of STM measurement of surface reaction under illumination. (e) Current trace for detecting the molecular dissociation induced by light irradiation. Reproduced with permission from ref. 262. Copyright (2018) American Association for the Advancement of Science.

while at elevated temperatures, water molecules instead of protons became the dominant active species being reduced due to phase transition of water (Fig. 18e). Furthermore, solid isotope evidence revealed that while thermo-photo catalysis led to water splitting with methanol as the sacrificial electron donor, thermal catalysis resulted in methanol decomposition (Fig. 18f).[39] Besides, this methodology has also contributed to elucidating more complex reaction mechanisms such as partial oxidation of $CH_4$[28, 29] and $C_2H_6$.[90]

In addition to identifying origins of products to outline reaction pathway, analysing kinetic isotope effect (KIE) is another approach to clarify catalytic mechanism.[18, 240] KIE can be calculated via eqn 12.

$$KIE = \frac{r_{normal}}{r_{isotope-labelled}} \quad (12)$$

where $r_{normal}$ and $r_{isotope\text{-}labelled}$ are steady-state reaction rates with normal and isotope-labelled reactants, respectively. The electron-mediated process and thermal-energy-driven process can be distinguished as the former generally shows a higher KIE than the latter.[122, 125] This is ascribed to the larger acceleration and higher vibrational energy in the lighter isotope when an equivalent force is used, which contributes to a higher reaction rate.[286] Via comparing KIEs of thermal catalysis and thermo-photo catalysis, the role of light is implied.[18, 40]

Other than reactants, labelling catalyst with isotopes has also been exploited, which helps to reveal the function of catalyst.[30] For example, thermo-photo catalytic dry reforming of $CH_4$ over $^{18}O$-doped $Rh/SrTiO_3$ catalyst led to the generation of $C^{18}O$. Combined with the stoichiometric ratio of produced syngas, oxygen species in catalyst was proposed to perform as the mediator to react with carbon species from partial oxidation of $CH_4$ followed by being recovered with $CO_2$.

### 6.3. Photoelectrochemical measurements

In general, photocurrents obtained from photoelectrochemical measurements at varied temperatures with and without light irradiation could imply the amounts of active charge carriers under varied test conditions, which might be well correlated to catalytic activities.[114] On top of the traditional application, a new strategy has been developed to quantify the contributions of plasmon-induced temperature rise and energetic charge carriers to catalytic reactions.[239] As shown in Fig. 19a, the plasmonic working electrode in a three-electrode electrochemical cell was illuminated by chopped light. The hot-carrier-induced photocurrent responded immediately upon illumination and reached the peak in several milliseconds (2 in Fig. 19b), while the thermal diffusion equilibrium with surrounding took a few seconds (3 in Fig. 19b). When light was turned off, photo-electronic current disappeared rapidly while thermal energy dissipated much more slowly (4 in Fig. 19b). Thus, as shown in Fig. 19c, the photocurrent curve could be divided into a rapid-response photo-electronic current region (0.05 s) and a slow-response photo-thermal current region (10 s), realizing the quantitative disentanglement of photo-electronic and photo-thermal effects.

### 6.4. Optically coupled scanning probe microscopy

The optically coupled scanning probe microscopy, mainly referring to Kelvin probe force microscopy (KPFM) and scanning tunnelling microscopy (STM) here, can provide valuable information for charge transfer and reaction kinetics with a high spatial resolution.[98, 168, 262, 287] The contact potential difference (CPD) between tip and sample measured by KPFM illustrates the mobility of charge carriers toward catalyst surface.[98, 168, 202] As shown in Fig. 20a, over plasmonic catalysts, visible-near IR irradiation would cause a significant increase in CPD, while UV irradiation showed a little change compared with that in dark.[168] This is because hot electrons formed under visible-near IR light could increase the number of free electrons, which led to an upward shift of Fermi level and a decreased work function. In

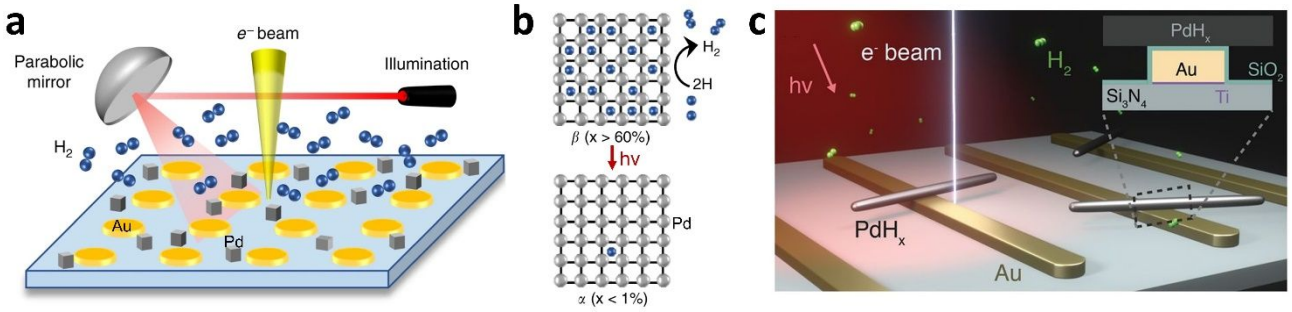


**Fig. 21** Schematic illustration of (a) optically coupled E-TEM and (b) dehydrogenation reaction via the β-to-α phase transformation of Pd. Reproduced with permission from ref. 258. Copyright (2018) Springer Nature. (c) Schematic illustration of optically coupled E-TEM measurement over Au-Pd crossed-bar nanostructure. Reproduced with permission from ref. 288. Copyright (2021) American Association for the Advancement of Science.

contrast, over semiconductor catalysts, UV irradiation resulted in an obvious CPD increase while visible-near IR irradiation showed a comparable value with that in dark (Fig. 20b). This is owed to the accumulation of photo-generated holes on catalyst surface with photo-generated electrons being grounded by Pt substrate.

Besides, synchronous illumination STM has also been exploited to induce and map out surface reactions.[262] As shown in Fig. 20c, the Ag tip could create localized plasmons under illumination, which drove the reaction. As-generated products were then analysed via topographic STM images. More attractively, such an advanced technology enabled the accurate quantification of single-molecule reaction rate since tunnelling current ($I_t$) is highly sensitive to the distance between tip and sample (Fig. 20d). Namely, a sudden drop in the time-dependent $I_t$ curve under illumination (Fig. 20e) reflected the change in d from $d_1$ to $d_2$ due to molecular dissociation as suggested in Fig. 20d. The dissociation rate could be further determined by the inverse of reaction time ($t_R$ in Fig. 20e).

### 6.5. Environmental transmission electron microscopy

The environmental transmission electron microscope (E-TEM) that allows for simultaneous optical excitation (Fig. 21a) enables real-time visualization of thermo-photo catalytic reactions and reveals the correlation of chemical activity to catalyst structure.[258, 288] Dionne and co-workers characterized the dehydrogenation reaction based on the phase transformation of Pd from H-rich β phase to H-poor α phase (Fig. 21b), which was accompanied with lattice constant contraction and plasmon resonance red shift captured by selected-area electron diffraction (SAED) and electron energy loss spectroscopy (EELS), respectively.[258, 288] As a result, light irradiation was found to enhance the reaction rate by 10 times, enable reaction nucleation at the edges rather than corners of Pd nanocubes, and open a new reaction pathway.[258] Furthermore, in a more recent work on crossed-bar Au-Pd antenna-reactor system (Fig. 21c), light irradiation was found to endow new catalytic sites on the flat middle faces of Pd nanorod besides its sharp tips.[288]

### 6.6. In-situ infrared and ultraviolet-visible spectroscopy

In-situ diffuse reflectance infrared Fourier transform spectroscopy (DRIFTS) is a widely applied technology to identify reaction intermediates based on molecular vibrations.[124, 132, 210, 289] Typically, the in-situ DRIFTS spectra of thermal catalysis and thermo-photo catalysis are comparatively analysed to depict the distinct reaction pathways. On top of traditional in-situ DRIFTS, a new technique coupling steady-state isotopic kinetic analysis (SSITKA) and DRIFTS was developed very recently.[23] This was achieved by collecting the DRIFTS spectrum under reacting atmosphere (such as $^{12}CO_2$) and then switching into an atmosphere containing isotope-labelled reactants (such as $^{13}CO_2$) and collecting another DRIFTS spectrum (Fig. 22a). The vibration frequencies of isotope-labelled species are typically lower than those of unlabelled ones. SSITKA-DRIFTS spectrum was obtained by subtracting the former general spectrum from the latter isotope-labelled spectrum. Such a technique demonstrates three advantages. Firstly, the interference from adsorbed spectator species and byproducts (such as water) on catalyst surface can be excluded. Secondly, the species that is actively exchanged or converted during reaction can be easily identified. Thirdly, the photo-enhancement effect can be captured based on the clearly resolved populations of intermediate species.

Though less applied than in-situ DRIFTS, operando ultraviolet-visible (UV-visible) spectroscopy is a powerful tool to characterize the optical properties of catalyst under reaction condition.[52, 73] On the one hand, it allows us to determine the band gap of catalyst in real space.[73] On the other hand, it helps to identify the catalytically active species as well as its behaviours under varied conditions (Figs. 16d and 16e).[52]

### 6.7. Synchronous illumination X-ray photoelectron spectroscopy

Synchronous illumination X-ray photoelectron spectroscopy (SI-XPS) is exploited to study the separation and transfer behaviours of photo-generated charge carriers which directly affect the thermo-photo catalytic efficiency.[290-292] As shown in Fig. 22b, XPS measurement under synchronous light irradiation can detect the peak shift caused by electron density change of elements in excited states. Since the valence band and conduction band of semiconductors are composed of spin orbits of various elements, charge excitation can be truly

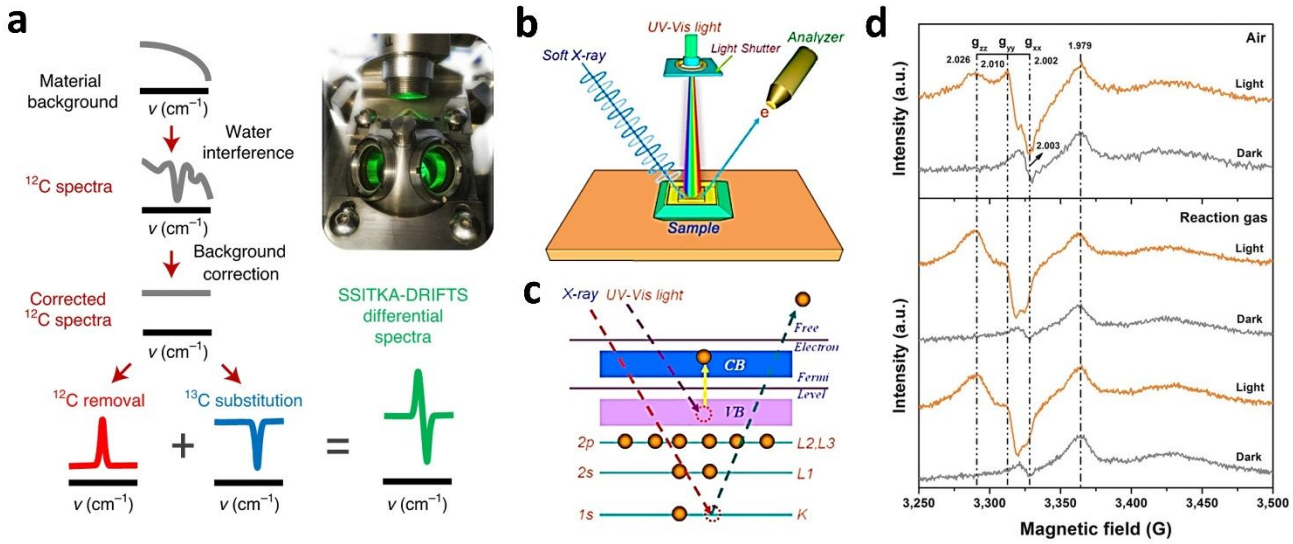


**Fig. 22** (a) Schematic illustration for the collection of SSITKA-DRIFTS spectrum with $^{12}CO_2$ and $^{13}CO_2$. Reproduced with permission from ref. 23. Copyright (2020) Springer Nature. (b) Schematic illustration of synchronous illumination XPS equipment and (c) corresponding electron density variations. Reproduced with permission from ref. 290. Copyright (2016) American Chemical Society. (d) EPR spectra of $Pt/TiO_2$-$WO_3$ catalyst in air and in reaction gas ($O_2$ + $C_3H_8$) with and without illumination. Reproduced with permission from ref. 132. Copyright (2020) John Wiley and Sons.

recorded in XPS spectra of multiple elements (Fig. 22c). Namely, an increased (or decreased) binding energy under illumination indicates that this element tends to lose (or accept) electrons, while unchanged binding energies for all elements reveal the rapid recombination of charge carriers.[290] When light is turned off, the recombination of charge carriers occurs, so all the binding energies should shift to their original positions.

### 6.8. Gas-adjustable electron paramagnetic resonance spectroscopy

Electron paramagnetic resonance (EPR) spectroscopy is a robust technology to detect unpaired electrons, suggesting the existence of electrons, holes, free radicals, etc.[146, 273] EPR spectra collected under reactant gases can further imply the identity and role of active species.[30, 132] Namely, if the EPR signal for the active species diminishes upon introducing a certain gas, the active species should actively react with this gas. As shown in Fig. 22d, light irradiation in air led to the generation of paramagnetic $\bullet O_2^-$ ($g_{xx}$ = 2.002, $g_{yy}$ = 2.010, $g_{zz}$ = 2.026), while the signals for $\bullet O_2^-$ were considerably weakened once $C_3H_8$ was introduced. Moreover, this process was reversible with and without illumination, further confirming the key role of $\bullet O_2^-$ for $C_3H_8$ oxidation.[132]

### 6.9. Embedded correlated wavefunction calculations

In spite of the wide application of plane-wave density functional theory (PW-DFT) for simulating heterogeneous catalytic reactions, it cannot yield accurate excited-state potential energy surfaces for metal nanostructures, thus unable to properly explain the kinetics of thermo-photo catalytic reactions.[293, 294] In contrast, embedded correlated wavefunction (ECW) theory, with the recovery of interactions between cluster and its extended environment with an optimized PW-DFT level embedding potential, enables the proper treatment of local excited states, providing quantitatively reliable predictions for both ground-state and excited-state reaction kinetics.[55, 293-295] The accuracy of ECW theory has been evidenced in various catalytic systems by comparing with experimentally obtained reaction barriers, reaction orders, and rate-limiting steps, so it is considered as the most robust calculation method for treating highly correlated local electronic structures by far.[294, 295]

## 7. Applications of thermo-photo catalysis

Thermo-photo catalysis has been applied in a wide range of chemical processes with excellent catalytic efficiencies, such as $CO_2$ reduction, $CH_4$ oxidation, CO conversion, $H_2$ production, $N_2$ fixation, pollutant degradation, and organic synthesis (Table 1). Here, instead of presenting the details of each catalytic process, we will make a brief discussion on these processes from a big picture and show some representative works.

### 7.1. $CO_2$ reduction

The reduction of the greenhouse gas $CO_2$ into value-added chemicals and fuels such as CO, $CH_4$, and $CH_3OH$ has been considered as one of the most attractive strategies for sustainable development.[63, 194] Due to the high energy of C=O bonds (750 kJ/mol), thermal catalytic $CO_2$ reduction suffers from high energy cost (up to ~1000 °C) and uncontrollable product selectivity, while photocatalytic $CO_2$ reduction typically shows low conversions.[11, 57] In recent years, thermo-photo catalysis has emerged as an effective solution for efficient $CO_2$ reduction with $H_2$,[22, 100, 107, 296] $H_2O$,[26, 112, 297] or $CH_4$.[30, 32, 33] These reactions are also known as $CO_2$ hydrogenation, artificial photosynthesis, and $CO_2$ reforming, respectively. Taking $CO_2$ hydrogenation as an example, a high $CH_4$ yield of 20 mmol/h/g was acquired over Ru/black $TiO_2$ catalyst at 200 °C under simulated sunlight irradiation at only 100 mW/cm², which is

several times larger than those obtained from individual thermal catalysis and photocatalysis.[22] Furthermore, photo-activation of formate adsorbate ($HCO_2$*) was demonstrated to contribute to an eight-fold enhancement in $CO_2$ hydrogenation to $CH_4$ over $NiO_x/La_2O_3@TiO_2$ catalyst at 200 °C and 390 mW/cm$^2$ illumination.[23]

### 7.2. $CH_4$ oxidation

$CH_4$ is another primary greenhouse gas and also the main constituent of natural gas with an ultra-high chemical stability due to its tetrahedral structure and strong C-H bonds (439 kJ/mol).[63] The activation and conversion of $CH_4$ into $H_2$, CO, C2+ hydrocarbons, high-value oxygenates, etc., are highly desired but remain as a huge challenge. While, thermo-photo catalysis, which can not only overcome the high dissociation barrier of $CH_4$ in traditional thermal catalysis but also increase the low activity in photocatalysis, has been demonstrated efficient for steam reforming of $CH_4$,[27, 122] oxidative coupling of $CH_4$,[31] partial oxidation of $CH_4$,[28, 29, 95] and dry reforming of $CH_4$,[30, 32, 33] under mild conditions. Among these reactions, thermo-photo catalytic partial oxidation of $CH_4$ into high-value oxygenates such as $CH_3OH$ and HCOOH is booming very recently, in which the photo-induced reactive oxygen species such as •OH and $•O_2^-$ play a crucial role for oxidation while thermal energy helps to activate reactants and promotes the desorption of oxygenates to regenerate active sites.[28, 29, 95, 298] Representatively, visible-light driven thermo-photo catalytic partial oxidation of $CH_4$ over $Pt/WO_3$ catalyst at 150 °C led to an enhancement in $CH_4$ conversion by 4.6 and 14.7 times with regards to photocatalysis and thermal catalysis, respectively.[28]

### 7.3. CO conversion

Besides $CO_2$ and $CH_4$, CO is also an important C1 molecule, whose conversion has been greatly enhanced by coupling thermal catalysis and photocatalysis.[141] Current applications of thermo-photo catalytic CO conversions range from CO oxidation by $O_2$,[36, 129, 130] $H_2O$,[35, 299] or NO,[134-136] to Fischer-Tropsch synthesis.[34, 37, 38, 300, 301] Thermo-photo catalytic CO oxidation by $O_2$ is developed to treat low-concentration CO in buildings and in $H_2$ streams for fuel cells, while CO oxidation by NO to form non-toxic $CO_2$ and $N_2$ realizes the concurrent removal of two primary pollutants from vehicles and stationary power plants.[141] Moreover, CO oxidation by $H_2O$, which is also named water-gas shift reaction, provides a sustainable approach for simultaneous CO removal and $H_2$ production.[35, 299] For instance, under focused sunlight irradiation, $CuO_x/Al_2O_3$ catalyst delivered an excellent thermo-photo catalytic activity with 95% CO conversion and 439 mmol/h/g $H_2$ production, owing to the synergetic photo-thermal catalysis and photocatalysis.[35] Furthermore, thermo-photo catalytic Fischer-Tropsch synthesis from CO and $H_2$ is even more intriguing toward efficient production of alkanes,[38, 300] alkenes,[37, 38, 300, 301] and oxygenates,[34] with controllable selectivities. While, most of these Fischer-Tropsch processes relied on photo-thermal effect and showed similar CO conversion and product distribution to those in dark reaction at the same temperature.[37, 38, 301]

### 7.4. $H_2$ production

$H_2$, with a high heating value of 286 kJ/mol, holds a great promise as the alternative to fossil fuels.[87] On top of above-mentioned dry/steam reforming of $CH_4$ and water-gas shift reaction, water splitting is believed as the cleanest route for $H_2$ production. However, photocatalytic water splitting shows a poor visible light utilization and a low energy conversion efficiency far below the industrial requirement (10%).[39, 87] In 2015, Hu and co-workers designed and demonstrated a thermo-photo co-catalytic process which could overcome these obstacles with a high $H_2$ evolution rate of 688 mmol/h/g over Pt/black $TiO_2$ catalyst at 280 °C under simulated sunlight irradiation.[21] Afterwards, a number of efforts have been made to broaden the range of catalysts applied for $H_2$ production from water.[39, 40, 62, 64, 96, 145, 302] In addition, $H_2$ may also be produced via thermo-photo catalytic $NH_3$ decomposition[86] and thermo-photo catalytic $NH_3BH_3$ dehydrogenation.[259, 303] The dehydrogenation of $NH_3BH_3$ is highlighted owing to its high gravimetric $H_2$ capacity (1 $NH_3BH_3 \rightarrow$ 3 $H_2$). Under concentrated sunlight irradiation (1000 mW/cm$^2$), the $H_2$ evolution rate from $NH_3BH_3$ dehydrogenation over Pt/TiN catalyst was enhanced by 11 times with a turnover frequency of 346 mol $H_2$/mol Pt/min due to the synergetic effects of collective heating and plasmonic hot electrons.[259]

### 7.5. $N_2$ fixation

$N_2$ fixation is another important application of thermo-photo catalysis, which can be conducted under mild conditions, in contrast to traditional operations at high temperatures (300-500 °C) and pressures (150-250 bar) due to the rate-limiting $N_2$ activation caused by the huge N≡N bond energy (945 kJ/mol).[204] In most cases, $N_2$ is fixed with $H_2$ as the well-known Haber-Bosch reaction,[43, 44, 204] while $N_2$ fixation with $H_2O$ has also been reported.[45, 46] The traditional $N_2$ fixation suffers a conflict between the reaction rate and $NH_3$ yield because a high temperature leads to a high reaction rate but causes the decomposition of $NH_3$. While, as discussed in section 5.1, the controllable temperature gradient in thermo-photo catalysis that provides both hot zones and cold zones allows the realization of high reaction rate and high $NH_3$ yield in the meantime (Fig. 12b).[43, 44] The utilization of $H_2O$ to fix $N_2$ is more promising due to the reduced energy consumption and carbon emission.[46] Representatively, a thermo-photo catalytic process over $Fe/MoS_2$ catalyst demonstrated an impressive $NH_3$ yield of 2.1 mmol/h/g at 270 °C under visible light irradiation, in great contrast to the negligible yields in individual thermal catalytic and photocatalytic processes (Fig. 9b).[46]

### 7.6. Pollutant degradation

Thermo-photo catalysis has also been applied in environmental remediation as a sustainably efficient technology to degrade organic pollutants, including VOCs in air and aqueous pollutants in water.[50, 281] The earliest work on thermo-photo catalytic VOC decomposition might be dated back to 2010 when Li and co-workers coated $TiO_2$ catalyst onto the UV lamp surface for simultaneous supplies of thermal and photo energies, realizing a much higher removal efficiency of

benzene (100%) than those of thermal catalysis (16%) and photocatalysis (48%).[49] Other VOCs having been decomposed via thermo-photo catalysis include formaldehyde,[47] ethyl acetate,[131] isopropanol,[167] n-hexane,[94] cyclohexane,[94] toluene,[47, 48, 283] xylene,[47, 48] styrene,[94] etc. For these gas pollutants, thermo-photo catalysis generally demonstrates a much more efficient mineralization toward $CO_2$ than individual thermal catalysis and photocatalysis. Besides, thermo-photo catalytic degradation of aqueous pollutants such as methyl blue,[50, 51] methyl orange,[304] rhodamine B,[305] 4-nitrophenol,[306, 307] tetracycline,[308] oxytetracycline,[309] and ciprofloxacin hydrochloride,[310] has been reported with high degradation efficiencies mainly attributed to the promoted photocatalysis by thermal energy. As an example, visible-light driven thermo-photo catalytic degradation of methyl blue over $Mn_3O_4/MnCO_3$ catalyst at 80 °C showed a high degradation efficiency of 89% in contrast to 5% in thermal catalysis and 16% in photocatalysis.[51]

### 7.7. Organic synthesis

Besides above applications in energy and environment, thermo-photo catalysis has also been utilized for organic synthesis. Most of organic reactions are basically thermal catalytic processes affected by reaction temperature, in which light irradiation plays some auxiliary roles.[311] The superiority of thermo-photo catalysis has been demonstrated in ethylene epoxidation,[18, 52] Suzuki coupling,[53, 54] alkyne hydroamination,[56] hydrodefluorination,[55] cyclocondensation,[312] etc. For instance, plasmon-driven Suzuki coupling reaction between bromobenzene and m-tolylboronic acid over Au-Pd catalyst was reported with joint contributions by hot carriers and photo-to-thermal conversion, giving a high yield of 99% under 809 nm laser illumination in just one hour, much larger than that of 55% in thermal catalysis at the same temperature (62 °C).[53] The introduced photo energy not only enhances the yield in a short period but also allows the selectivity control toward desirable products.[53, 54, 56, 262, 265] The selectivity control by light irradiation has been evidenced in alkyne hydroamination toward imine over Au-Co/$ZrO_2$ catalyst[56] and ethylene epoxidation over metallic Cu[52] as discussed in section 5.4 and section 5.6, respectively.

## 8. Energy management for scaling up thermo-photo catalytic processes

Currently, most of thermo-photo catalytic processes are still at the laboratory stage on relatively small scales except for a few processes such as pollutant degradation and dry reforming of $CH_4$.[313] Even so, since the ultimate goal of academic studies is to move toward industrial application, here we propose some important considerations for scaling up thermo-photo catalytic processes, including (1) solar energy utilization, (2) thermal energy supply, (3) energy conversion efficiency, (4) scalable production of equipment, (5) cost effectiveness, (6) system life span, and (7) carbon tax. Moreover, some non-technical factors such as supply chain partnership, labour force optimization, consumer behaviour, and public policy, are also important for commercial adoption.[314] Due to the close relationship between thermo-photo catalytic system and traditional thermal catalytic system, the scale-up technologies for thermal catalytic processes can be used for reference. The major difference between them is the incorporation of light, so in this section we will place an emphasis on energy management in thermo-photo catalytic processes.

### 8.1. Solar energy utilization

Although photo energy is generally provided by lamps at laboratory stage, the direct utilization of sunlight is expected for scalable application. However, the number of hours in a day during which natural sunlight can be utilized to drive reactions is limited and highly dependent on weather. Besides, solar azimuth and elevation angles are varying all the time, while the maximum light absorption is achieved only at perpendicular incidence.[186] Moreover, the intensity of natural sunlight (~100 mW/cm$^2$) is much lower than those employed in laboratories (up to 20000 mW/cm$^2$).[23, 25, 31, 32, 86] This reveals the urgency of boosting solar energy collection and utilization.

Concentrators can be used to collect solar energy and increase light intensity.[74, 192, 193] The concentration ratios of up-to-date concentrators range from 30-100 for parabolic trough concentrators to 5000-10000 corresponding to double-concentration systems.[192] Among these, parabolic trough concentrator (Fig. 6c) is considered as the most competitive one for scalable application of thermo-photo catalysis due to its easy construction as well as the high flexibility to expand light absorption area and thus the scale of systems.[180, 193, 313, 315]

Moreover, the development of omnidirectional reactors or substrates can enhance the utilization of solar energy by addressing the issue of changing solar azimuth and elevation angles.[112] Omnidirectional reactors or substrates generally exhibit a 3D spherical geometry, which not only guarantees solar absorption with one light-facing hemisphere but also keeps the other hemisphere to acquire energy from warmer environment by thermal convection and radiation (Fig. 5f). This outperforms the widely applied mechanical tracking infrastructures which require both high capital investment and large energy consumption to achieve accurate and continuous angle manipulation.[316]

Furthermore, since the continuous direct utilization of sunlight throughout a day for thermo-photo catalysis is impossible, the conversion of solar energy into electric energy in the daytime which is then used to power the lamp to provide illumination at night can be applied. The solar-to-electricity conversion can be achieved via three main technologies including thermal, photovoltaic, and hybrid thermal photovoltaic, all of which have been well established and can be directly employed.[317, 318]

### 8.2. Thermal energy supply

Thermal energy is typically supplied by electric furnaces, leading to a considerable energy consumption. Using renewable photo energy to supply both photons and required heat is considered as an effective solution. Photo-thermal effect has been widely applied for catalysts and substrates which results

in local heating,[34, 109, 163] while the recent development of "solar furnaces" enables the global heating just as electric furnaces do.[42, 46] In solar furnaces, highly concentrated solar radiation can heat the light-absorption reactor, which leads to a high temperature up to 2300 °C, thus showing a great promise for scalable application of solar-driven thermo-photo catalysis.[319] Distinctively, aiming at directly utilizing weak sunlight, IR light absorber may be coated on the reactor to avoid IR radiation and thus heat dissipation.[320]

Except utilizing solar power, coupling an endothermic process with an exothermic process can be an alternative solution, where the heat required for endothermic process can be provided by heat released in exothermic process. Water splitting is a representative endothermic reaction for $H_2$ production, which can be coupled with exothermic processes for $H_2$ utilization.[42] Coupling water splitting with $N_2$ fixation enables the transition from current natural-gas-based Haber-Bosch process to a carbon-free and energy-efficient practice for $NH_3$ synthesis. Furthermore, combining water spitting and $CO_2$ methanation sparks a novel carbon-recycle technology for energy and environment.[42]

## 9. Conclusions and outlook

In conclusion, the synergetic effects of thermal and photo energies render thermo-photo catalysis efficient to promote activity, control selectivity, and enhance stability of catalysts in a wide range of chemical processes under mild conditions. On the one hand, thermal energy promotes photocatalysis by (1) enhancing the kinetic driving force of reactants, (2) tuning the redox potentials of semi-reactions, (3) facilitating the migration of charge carriers, (4) accelerating mass transfer, (5) promoting the dissociation of reactants, and (6) adjusting catalyst structure. On the other hand, photo energy accelerates thermal catalysis via (1) elevating temperature, (2) forming photo carriers, (3) generating hot carriers, (4) directly exciting adsorbates or adsorbate-catalyst bonds, (5) dynamically controlling elementary step energetics, and (6) modifying active sites. These synergetic effects perform as a valuable guideline for designing, applying, and scaling up thermo-photo catalytic processes, in which the efficient energy conversion and mass transfer should always be primary considerations.

In spite of the exciting progress in last few years, there remains seven challenges and concerns that deserve more attention in future research. Firstly, it is hard to accurately measure catalyst temperature under light irradiation, which might be resulted from non-uniform illumination, emissivity of catalysts, placement of thermocouples, limited resolution of temperature detectors, etc.[219, 313] Without accurate temperature, one cannot discriminate photo-thermal and photo-electronic (via photo carriers or hot carriers) contributions in thermo-photo catalysis because photo-thermal contribution is derived from a control experiment at the "same" temperature in dark. While, typically, the "same" temperature is reached under external global heating, which is different from photo-thermal heating that exhibits a localized inhomogeneous temperature distribution. Namely, based on current techniques, we can hardly quantify the photo-thermal and photo-electronic contributions. This inspires the exploration of direct temperature measurement technologies at active sites.[321-323] It is also an opportunity since a precise thermal definition would allow the utilization of temperature gradients to achieve high reaction rate and high yield of unstable products in the meantime.[43, 44]

Secondly, so far, with most research attention paid to catalyst design and the resulting catalytic performance, the underlying reaction pathway and synergetic effects of thermal and photo energies in thermo-photo catalysis remain confusing. In many works, the mechanism was not discussed or was briefly mentioned without solid evidence, which severely limits subsequent improvement and development. Therefore, it is highly expected that every publication regarding thermo-photo catalysis can provide the answer to the question "*Why does thermo-photo catalysis outperform individual thermal catalysis and photocatalysis?*" for the specific case with strong experimental and/or theoretical evidence.

Thirdly, energy conversion efficiency should be further improved to push the industrialization process forward, especially for thermo-photo catalytic $CO_2$ reduction.[11, 63] It is worth noting that energy conversion efficiency is calculated based on Gibbs free energy change of reaction rather than enthalpy change as used in some reports. To promote energy conversion, the catalyst should demonstrate a strong light absorption across entire solar irradiation spectrum. Moreover, an efficient thermal transfer inside reactor and an excellent thermal insulation against outer environment should be ensured. It is also suggested that future works can present the power consumption in thermo-photo catalysis and compare it with that in thermal catalysis at the same productivity.[34, 73]

Fourthly, the investigation in long-term stability of catalysts under thermo-photo catalytic conditions is lacking. Currently, most stability tests are carried out within several hours, which cannot prove the robustness of catalysts and is not sufficient for scale-up toward practical application. Moreover, the spent catalysts are poorly characterized, so the recyclability of catalysts cannot be evaluated. Therefore, long-term test for hundreds of hours and comprehensive characterizations of the catalysts after test are desired in the forthcoming work. Besides, the development of in-situ synchronous illumination characterization technologies should be boosted to reveal the structural change of catalysts in real time which allows a thorough analysis of the relationship among catalyst structure, chemical activity, and reaction pathway.

Fifthly, although the use of noble-metal-based catalysts contributes to excellent thermo-photo catalytic performance, their high cost and scarcity hamper their industrial application. The exploitation of low-cost naturally-abundant catalysts (such as Fe-, Co-, Ni-, Cu-, and Al-based catalysts) that can replace noble metals to serve as light absorber, electron trapper, and/or molecular adsorber, is a matter of urgency. In addition to widely employed metal and metal oxide catalysts, carbides, nitrides, chalcogenides, and pnictogenides might be promising alternatives for thermo-photo catalysis owing to their broad light absorption.[37, 169, 289, 324, 325]

Sixthly, the transient behaviours of catalysts and reactants upon introducing or removing light irradiation are less investigated. One of the advantages of thermo-photo catalysis is the instantaneous control of reactions that cannot be achieved in traditional thermal catalysis. After identifying light-induced transient behaviours, novel thermo-photo catalytic processes under controlled periodic illumination can be designed, which can realize the dynamic control of elementary step energetics on catalyst surface for improved catalytic activity and selectivity.[126, 269]

Last but not the least, the standardized experimental design and data presentation are lacking. Setting standards not only benefits the reproduction of reported experimental results but also contributes to a fair comparison among the catalytic performances from different laboratories. Currently, thermo-photo catalytic efficiencies are reported in a variety of ways, while it is recommended to be presented in the unit of $\mu mol/h/g_{cat}$ or $mmol/h/g_{cat}$ with light intensity for rational comparison.

Although thermo-photo catalysis is currently at the laboratory stage, its bright future for practical application is ahead with a clear mechanism understanding and an elaborate system design. Furthermore, this review which focuses on the synergetic roles of thermal and photo energies in catalysis should inspire more efforts into other synergetic catalytic processes in the presence of two or more energies such as thermal, photo, electric, magnetic, ultrasonic, microwave, and mechanical energies.

## Conflicts of interest

There are no conflicts to declare

## Acknowledgements

This work was supported by National Science Foundation (CMMI-1661699) and ACS Petroleum Research Fund (PRF-60329-ND10).

## References

1. G. A. Somorjai and Y. Li, *Introduction to surface chemistry and catalysis*, John Wiley & Sons, 2010.
2. G. Ertl, H. Knözinger and J. Weitkamp, *Handbook of heterogeneous catalysis*, VCH Weinheim, 1997.
3. B. Elvers, *Ullmann's encyclopedia of industrial chemistry*, Verlag Chemie, 1991.
4. A. Eibner, *Chem-Ztg*, 1911, **35**, 753-755.
5. J. M. Coronado, *Design of advanced photocatalytic materials for energy and environmental applications*, Springer, 2013.
6. A. Fujishima and K. Honda, *Nature*, 1972, **238**, 37-38.
7. T.-H. Yang, J. Ahn, S. Shi, P. Wang, R. Gao and D. Qin, *Chem. Rev.*, 2021, **121**, 796-833.
8. C. Perego and R. Millini, *Chem. Soc. Rev.*, 2013, **42**, 3956-3976.
9. C. Xu, P. Ravi Anusuyadevi, C. Aymonier, R. Luque and S. Marre, *Chem. Soc. Rev.*, 2019, **48**, 3868-3902.
10. X. Lang, X. Chen and J. Zhao, *Chem. Soc. Rev.*, 2014, **43**, 473-486.
11. Z.-j. Wang, H. Song, H. Liu and J. Ye, *Angew. Chem. Int. Ed.*, 2020, **59**, 8016-8035.
12. X. Chen, L. Liu, P. Y. Yu and S. S. Mao, *Science*, 2011, **331**, 746-750.
13. J. Melsheimer, W. Guo, D. Ziegler, M. Wesemann and R. Schlögl, *Catal. Lett.*, 1991, **11**, 157-168.
14. V. I. Anikeev, V. N. Parmon, V. A. Kirillov and K. I. Zamaraev, *Int. J. Hydrogen Energy,* 1990, **15**, 275-286.
15. D. Mateo, J. L. Cerrillo, S. Durini and J. Gascon, *Chem. Soc. Rev.*, 2021, **50**, 2173-2210.
16. G. Chen, R. Gao, Y. Zhao, Z. Li, G. I. N. Waterhouse, R. Shi, J. Zhao, M. Zhang, L. Shang, G. Sheng, X. Zhang, X. Wen, L.-Z. Wu, C.-H. Tung and T. Zhang, *Adv. Mater.*, 2018, **30**, 1704663.
17. S. Zhou, L. Shang, Y. Zhao, R. Shi, G. I. N. Waterhouse, Y.-C. Huang, L. Zheng and T. Zhang, *Adv. Mater.*, 2019, **31**, 1900509.
18. P. Christopher, H. Xin and S. Linic, *Nat. Chem.*, 2011, **3**, 467-472.
19. U. Aslam, V. G. Rao, S. Chavez and S. Linic, *Nat. Catal.*, 2018, **1**, 656-665.
20. A. Gellé, T. Jin, L. de la Garza, G. D. Price, L. V. Besteiro and A. Moores, *Chem. Rev.*, 2020, **120**, 986-1041.
21. B. Han and Y. H. Hu, *J. Phys. Chem. C*, 2015, **119**, 18927-18934.
22. C. Wang, S. Fang, S. Xie, Y. Zheng and Y. H. Hu, *J. Mater. Chem. A*, 2020, **8**, 7390-7394.
23. T. H. Tan, B. Xie, Y. H. Ng, S. F. B. Abdullah, H. Y. M. Tang, N. Bedford, R. A. Taylor, K.-F. Aguey-Zinsou, R. Amal and J. Scott, *Nat. Catal.*, 2020, **3**, 1034-1043.
24. L. Wan, Q. Zhou, X. Wang, T. E. Wood, L. Wang, P. N. Duchesne, J. Guo, X. Yan, M. Xia, Y. F. Li, A. A. Jelle, U. Ulmer, J. Jia, T. Li, W. Sun and G. A. Ozin, *Nat. Catal.*, 2019, **2**, 889-898.
25. M. Cai, Z. Wu, Z. Li, L. Wang, W. Sun, A. A. Tountas, C. Li, S. Wang, K. Feng, A.-B. Xu, S. Tang, A. Tavasoli, M. Peng, W. Liu, A. S. Helmy, L. He, G. A. Ozin and X. Zhang, *Nat. Energy*, 2021, **6**, 807-814.
26. Y. Li, D. Hui, Y. Sun, Y. Wang, Z. Wu, C. Wang and J. Zhao, *Nat. Comm.*, 2021, **12**, 123.
27. B. Han, W. Wei, M. Li, K. Sun and Y. H. Hu, *Chem. Commun.*, 2019, **55**, 7816-7819.
28. Y. Zhu, S. Chen, S. Fang, Z. Li, C. Wang and Y. H. Hu, *J. Phys. Chem. Lett.*, 2021, **12**, 7459-7465.
29. Z. Sun, C. Wang and Y. H. Hu, *J. Mater. Chem. A*, 2021, **9**, 1713-1719.
30. S. Shoji, X. Peng, A. Yamaguchi, R. Watanabe, C. Fukuhara, Y. Cho, T. Yamamoto, S. Matsumura, M.-W. Yu, S. Ishii, T. Fujita, H. Abe and M. Miyauchi, *Nat. Catal.*, 2020, **3**, 148-153.
31. S. Song, H. Song, L. Li, S. Wang, W. Chu, K. Peng, X. Meng, Q. Wang, B. Deng, Q. Liu, Z. Wang, Y. Weng, H. Hu, H. Lin, T. Kako and J. Ye, *Nat. Catal.*, 2021, **4**, 1032-1042.
32. L. Zhou, J. M. P. Martirez, J. Finzel, C. Zhang, D. F. Swearer, S. Tian, H. Robatjazi, M. Lou, L. Dong, L. Henderson, P. Christopher, E. A. Carter, P. Nordlander and N. J. Halas, *Nat. Energy*, 2020, **5**, 61-70.
33. B. Han, W. Wei, L. Chang, P. Cheng and Y. H. Hu, *ACS Catal.*, 2016, **6**, 494-497.
34. X. Wu, J. Lang, Y. Jiang, Y. Lin and Y. H. Hu, *ACS Sustain.*

*Chem. Eng.*, 2019, **7**, 19277-19285.
35. L. Zhao, Y. Qi, L. Song, S. Ning, S. Ouyang, H. Xu and J. Ye, *Angew. Chem. Int. Ed.*, 2019, **58**, 7708-7712.
36. U. Aslam, S. Chavez and S. Linic, *Nat. Nanotechnol.*, 2017, **12**, 1000-1005.
37. W. Gao, R. Gao, Y. Zhao, M. Peng, C. Song, M. Li, S. Li, J. Liu, W. Li, Y. Deng, M. Zhang, J. Xie, G. Hu, Z. Zhang, R. Long, X.-D. Wen and D. Ma, *Chem*, 2018, **4**, 2917-2928.
38. Z. Li, J. Liu, Y. Zhao, G. I. N. Waterhouse, G. Chen, R. Shi, X. Zhang, X. Liu, Y. Wei, X.-D. Wen, L.-Z. Wu, C.-H. Tung and T. Zhang, *Adv. Mater.*, 2018, **30**, 1800527.
39. S. Fang, Z. Sun and Y. H. Hu, *ACS Catal.*, 2019, **9**, 5047-5056.
40. S. Fang, Y. Liu, Z. Sun, J. Lang, C. Bao and Y. H. Hu, *Appl. Catal., B* 2020, **278**, 119316.
41. S. Guo, X. Li, J. Li and B. Wei, *Nat. Comm.*, 2021, **12**, 1343.
42. Y. Li, Y.-K. Peng, L. Hu, J. Zheng, D. Prabhakaran, S. Wu, T. J. Puchtler, M. Li, K.-Y. Wong, R. A. Taylor and S. C. E. Tsang, *Nat. Comm.*, 2019, **10**, 4421.
43. C. Mao, H. Li, H. Gu, J. Wang, Y. Zou, G. Qi, J. Xu, F. Deng, W. Shen, J. Li, S. Liu, J. Zhao and L. Zhang, *Chem*, 2019, **5**, 2702-2717.
44. X. Li, X. Zhang, H. O. Everitt and J. Liu, *Nano Lett.*, 2019, **19**, 1706-1711.
45. T. Hou, L. Chen, Y. Xin, W. Zhu, C. Zhang, W. Zhang, S. Liang and L. Wang, *ACS Energy Lett.*, 2020, **5**, 2444-2451.
46. J. Zheng, L. Lu, K. Lebedev, S. Wu, P. Zhao, I. J. McPherson, T.-S. Wu, R. Kato, Y. Li, P.-L. Ho, G. Li, L. Bai, J. Sun, D. Prabhakaran, R. A. Taylor, Y.-L. Soo, K. Suenaga and S. C. E. Tsang, *Chem Catal.*, 2021, **1**, 162-182.
47. J. Li, X. Yang, C. Ma, Y. Lei, Z. Cheng and Z. Rui, *Appl. Catal., B* 2021, **291**, 120053.
48. J. Kong, C. Jiang, Z. Rui, S. Liu, F. Xian, W. Ji and H. Ji, *Chem. Eng. J.*, 2020, **397**, 125485.
49. Y. Li, J. Huang, T. Peng, J. Xu and X. Zhao, *ChemCatChem* 2010, **2**, 1082-1087.
50. Y. Huang, Y. Lu, Y. Lin, Y. Mao, G. Ouyang, H. Liu, S. Zhang and Y. Tong, *J. Mater. Chem. A*, 2018, **6**, 24740-24747.
51. G. Wang, B. Huang, Z. Lou, Z. Wang, X. Qin, X. Zhang and Y. Dai, *Appl. Catal., B* 2016, **180**, 6-12.
52. A. Marimuthu, J. Zhang and S. Linic, *Science*, 2013, **339**, 1590.
53. F. Wang, C. Li, H. Chen, R. Jiang, L.-D. Sun, Q. Li, J. Wang, J. C. Yu and C.-H. Yan, *J. Am. Chem. Soc.*, 2013, **135**, 5588-5601.
54. Z. Lou, Q. Gu, Y. Liao, S. Yu and C. Xue, *Appl. Catal., B* 2016, **184**, 258-263.
55. H. Robatjazi, J. L. Bao, M. Zhang, L. Zhou, P. Christopher, E. A. Carter, P. Nordlander and N. J. Halas, *Nat. Catal.*, 2020, **3**, 564-573.
56. E. Peiris, S. Sarina, E. R. Waclawik, G. A. Ayoko, P. Han, J. Jia and H.-Y. Zhu, *Angew. Chem. Int. Ed.*, 2019, **58**, 12032-12036.
57. F. Zhang, Y.-H. Li, M.-Y. Qi, Y. M. A. Yamada, M. Anpo, Z.-R. Tang and Y.-J. Xu, *Chem Catal.*, 2021, **1**, 272-297.
58. Z. Zhu, W. Guo, Y. Zhang, C. Pan, J. Xu, Y. Zhu and Y. Lou, *Carbon Energy*, 2021, **3**, 519-540.
59. V. Nair, M. J. Muñoz-Batista, M. Fernández-García, R. Luque and J. C. Colmenares, *ChemSusChem* 2019, **12**, 2098-2116.
60. M. Ghoussoub, M. Xia, P. N. Duchesne, D. Segal and G. Ozin, *Energy Environ. Sci.*, 2019, **12**, 1122-1142.
61. Z. Zhang, C. Zhang, H. Zheng and H. Xu, *Acc. Chem. Res.*, 2019, **52**, 2506-2515.
62. K. Czelej, J. C. Colmenares, K. Jabłczyńska, K. Ćwieka, Ł. Werner and L. Gradoń, *Catal. Today* 2021, **380**, 156-186.
63. M. Li, Z. Sun and Y. H. Hu, *Chem. Eng. J.*, 2022, **428**, 131222.
64. K. Ćwieka, K. Czelej, J. C. Colmenares, K. Jabłczyńska, Ł. Werner and L. Gradoń, *ChemCatChem* 2021, **13**, 4458-4496.
65. I. F. Teixeira, E. C. M. Barbosa, S. C. E. Tsang and P. H. C. Camargo, *Chem. Soc. Rev.*, 2018, **47**, 7783-7817.
66. X. Chen, S. Shen, L. Guo and S. S. Mao, *Chem. Rev.*, 2010, **110**, 6503-6570.
67. Z. Ma, W. Liu, W. Yang, W. Li and B. Han, *Fuel*, 2021, **286**, 119490.
68. D. J. Martin, G. Liu, S. J. A. Moniz, Y. Bi, A. M. Beale, J. Ye and J. Tang, *Chem. Soc. Rev.*, 2015, **44**, 7808-7828.
69. M. Sun, B. Zhao, F. Chen, C. Liu, S. Lu, Y. Yu and B. Zhang, *Chem. Eng. J.*, 2021, **408**, 127280.
70. X. Meng, L. Liu, S. Ouyang, H. Xu, D. Wang, N. Zhao and J. Ye, *Adv. Mater.*, 2016, **28**, 6781-6803.
71. S. Linic, U. Aslam, C. Boerigter and M. Morabito, *Nat. Mater.*, 2015, **14**, 567-576.
72. W.-C. Chung and M.-B. Chang, *Renew. Sustain. Energy Rev.*, 2016, **62**, 13-31.
73. C. Kim, S. Hyeon, J. Lee, W. D. Kim, D. C. Lee, J. Kim and H. Lee, *Nat. Comm.*, 2018, **9**, 3027.
74. A. Mohan, U. Ulmer, L. Hurtado, J. Loh, Y. F. Li, A. A. Tountas, C. Krevert, C. Chan, Y. Liang, P. Brodersen, M. M. Sain and G. A. Ozin, *ACS Appl. Mater. Interfaces,* 2020, **12**, 33613-33620.
75. L. Liu, A. V. Puga, J. Cored, P. Concepción, V. Pérez-Dieste, H. García and A. Corma, *Appl. Catal., B* 2018, **235**, 186-196.
76. X. Zhang, X. Li, D. Zhang, N. Q. Su, W. Yang, H. O. Everitt and J. Liu, *Nat. Comm.*, 2017, **8**, 14542.
77. M. J. Kale, T. Avanesian, H. Xin, J. Yan and P. Christopher, *Nano Lett.*, 2014, **14**, 5405-5412.
78. S. Wu, Y. Li, Q. Zhang, Z. Jiang, Y. Yang, J. Wu and X. Zhao, *Energy Environ. Sci.*, 2019, **12**, 2581-2590.
79. G. Zhang, S. Wu, Y. Li and Q. Zhang, *Appl. Catal., B* 2020, **264**, 118544.
80. H. Liu, X. Meng, T. D. Dao, L. Liu, P. Li, G. Zhao, T. Nagao, L. Yang and J. Ye, *J. Mater. Chem. A*, 2017, **5**, 10567-10573.
81. F. Pan, X. Xiang, Z. Du, E. Sarnello, T. Li and Y. Li, *Appl. Catal., B* 2020, **260**, 118189.
82. Z. Sun, S. Fang, Y. Lin and Y. H. Hu, *Chem. Eng. J.*, 2019, **375**, 121909.
83. S. Kattel, J. Ramírez Pedro, G. Chen Jingguang, A. Rodriguez José and P. Liu, *Science*, 2017, **355**, 1296-1299.
84. Y. H. Hu and E. Ruckenstein, *Science*, 2020, **368**, eabb5459.
85. B. Xie, R. J. Wong, T. H. Tan, M. Higham, E. K. Gibson, D. Decarolis, J. Callison, K.-F. Aguey-Zinsou, M. Bowker, C. R. A. Catlow, J. Scott and R. Amal, *Nat. Comm.*, 2020, **11**, 1615.
86. L. Zhou, D. F. Swearer, C. Zhang, H. Robatjazi, H. Zhao, L. Henderson, L. Dong, P. Christopher, E. A. Carter, P. Nordlander and N. J. Halas, *Science*, 2018, **362**, 69.
87. S. Fang and Y. H. Hu, *Int. J. Energy Res.*, 2019, **43**, 1082-1098.
88. G. Zhang, G. Liu, L. Wang and J. T. S. Irvine, *Chem. Soc. Rev.*, 2016, **45**, 5951-5984.
89. Z. Shi, L. Lan, Y. Li, Y. Yang, Q. Zhang, J. Wu, G. Zhang and X. Zhao, *ACS Sustain. Chem. Eng.*, 2018, **6**, 16503-16514.
90. Y. Zhu, S. Fang, S. Chen, Y. Tong, C. Wang and Y. H. Hu,

*Chem. Sci.*, 2021, **12**, 5825-5833.
91. S. L. Kollmannsberger, C. A. Walenta, C. Courtois, M. Tschurl and U. Heiz, *ACS Catal.*, 2018, **8**, 11076-11084.
92. C. Courtois, C. A. Walenta, M. Tschurl, U. Heiz and C. M. Friend, *J. Am. Chem. Soc.*, 2020, **142**, 13072-13080.
93. L. Ren, M. Mao, Y. Li, L. Lan, Z. Zhang and X. Zhao, *Appl. Catal., B* 2016, **198**, 303-310.
94. J. Kong, Z. Xiang, G. Li and T. An, *Appl. Catal., B* 2020, **269**, 118755.
95. X. Cai, S. Fang and Y. H. Hu, *J. Mater. Chem. A*, 2021, **9**, 10796-10802.
96. U. Caudillo-Flores, G. Agostini, C. Marini, A. Kubacka and M. Fernández-García, *Appl. Catal., B* 2019, **256**, 117790.
97. S. I. Nikitenko, T. Chave, C. Cau, H.-P. Brau and V. Flaud, *ACS Catal.*, 2015, **5**, 4790-4795.
98. C. Du, B. Yan and G. Yang, *Chem. Eng. J.*, 2021, **404**, 126477.
99. X. Zhang, X. Li, M. E. Reish, D. Zhang, N. Q. Su, Y. Gutiérrez, F. Moreno, W. Yang, H. O. Everitt and J. Liu, *Nano Lett.*, 2018, **18**, 1714-1723.
100. D. Mateo, J. Albero and H. García, *Joule*, 2019, **3**, 1949-1962.
101. Y. Chen, Y. Zhang, G. Fan, L. Song, G. Jia, H. Huang, S. Ouyang, J. Ye, Z. Li and Z. Zou, *Joule*, 2021, **5**, 3235-3251.
102. A. A. Jelle, K. K. Ghuman, P. G. O'Brien, M. Hmadeh, A. Sandhel, D. D. Perovic, C. V. Singh, C. A. Mims and G. A. Ozin, *Adv. Energy Mater.*, 2018, **8**, 1702277.
103. D. Mateo, J. Albero and H. García, *Energy Environ. Sci.*, 2017, **10**, 2392-2400.
104. Y.-F. Xu, P. N. Duchesne, L. Wang, A. Tavasoli, A. A. Jelle, M. Xia, J.-F. Liao, D.-B. Kuang and G. A. Ozin, *Nat. Comm.*, 2020, **11**, 5149.
105. H. Zhang, T. Itoi, T. Konishi and Y. Izumi, *Angew. Chem. Int. Ed.*, 2021, **60**, 9045-9054.
106. H. Zhang, T. Itoi, T. Konishi and Y. Izumi, *J. Am. Chem. Soc.*, 2019, **141**, 6292-6301.
107. L. B. Hoch, P. G. O'Brien, A. Jelle, A. Sandhel, D. D. Perovic, C. A. Mims and G. A. Ozin, *ACS Nano*, 2016, **10**, 9017-9025.
108. L. Wang, M. Ghoussoub, H. Wang, Y. Shao, W. Sun, A. A. Tountas, T. E. Wood, H. Li, J. Y. Y. Loh, Y. Dong, M. Xia, Y. Li, S. Wang, J. Jia, C. Qiu, C. Qian, N. P. Kherani, L. He, X. Zhang and G. A. Ozin, *Joule*, 2018, **2**, 1369-1381.
109. L. Wang, Y. Dong, T. Yan, Z. Hu, A. A. Jelle, D. M. Meira, P. N. Duchesne, J. Y. Y. Loh, C. Qiu, E. E. Storey, Y. Xu, W. Sun, M. Ghoussoub, N. P. Kherani, A. S. Helmy and G. A. Ozin, *Nat. Comm.*, 2020, **11**, 2432.
110. N. T. Nguyen, M. Xia, P. N. Duchesne, L. Wang, C. Mao, A. A. Jelle, T. Yan, P. Li, Z.-H. Lu and G. A. Ozin, *Nano Lett.*, 2021, **21**, 1311-1319.
111. B. Xie, P. Kumar, T. H. Tan, A. A. Esmailpour, K.-F. Aguey-Zinsou, J. Scott and R. Amal, *ACS Catal.*, 2021, **11**, 5818-5828.
112. H. Liu, H.-G. Ye, M. Gao, Q. Li, Z. Liu, A.-Q. Xie, L. Zhu, G. W. Ho and S. Chen, *Adv. Sci.*, 2021, **8**, 2101232.
113. X. Meng, T. Wang, L. Liu, S. Ouyang, P. Li, H. Hu, T. Kako, H. Iwai, A. Tanaka and J. Ye, *Angew. Chem. Int. Ed.*, 2014, **53**, 11478-11482.
114. N. Sun, Y. Zhu, M. Li, J. Zhang, J. Qin, Y. Li and C. Wang, *Appl. Catal., B* 2021, **298**, 120565.
115. M. N. Ha, G. Lu, Z. Liu, L. Wang and Z. Zhao, *J. Mater. Chem. A*, 2016, **4**, 13155-13165.
116. Y. Cho, S. Shoji, A. Yamaguchi, T. Hoshina, T. Fujita, H. Abe and M. Miyauchi, *Chem. Commun.*, 2020, **56**, 4611-4614.
117. H. Liu, H. Song, W. Zhou, X. Meng and J. Ye, *Angew. Chem. Int. Ed.*, 2018, **57**, 16781-16784.
118. M. Mao, Q. Zhang, Y. Yang, Y. Li, H. Huang, Z. Jiang, Q. Hu and X. Zhao, *Green Chem.*, 2018, **20**, 2857-2869.
119. K. Lorber, J. Zavašnik, J. Sancho-Parramon, M. Bubaš, M. Mazaj and P. Djinović, *Appl. Catal., B* 2022, **301**, 120745.
120. H. Huang, M. Mao, Q. Zhang, Y. Li, J. Bai, Y. Yang, M. Zeng and X. Zhao, *Adv. Energy Mater.*, 2018, **8**, 1702472.
121. S. Wu, Y. Li, Q. Zhang, Q. Hu, J. Wu, C. Zhou and X. Zhao, *Adv. Energy Mater.*, 2020, **10**, 2002602.
122. H. Song, X. Meng, Z.-j. Wang, Z. Wang, H. Chen, Y. Weng, F. Ichihara, M. Oshikiri, T. Kako and J. Ye, *ACS Catal.*, 2018, **8**, 7556-7565.
123. C. Zhan, Q.-X. Wang, J. Yi, L. Chen, D.-Y. Wu, Y. Wang, Z.-X. Xie, M. Moskovits and Z.-Q. Tian, *Sci. Adv.*, 2021, **7**, eabf0962.
124. X. Yu, L. Yang, Y. Xuan, X. L. Liu and K. Zhang, *Nano Energy*, 2021, **84**, 105953.
125. S. Luo, H. Lin, Q. Wang, X. Ren, D. Hernández-Pinilla, T. Nagao, Y. Xie, G. Yang, S. Li, H. Song, M. Oshikiri and J. Ye, *J. Am. Chem. Soc.*, 2021, **143**, 12145-12153.
126. J. Qi, J. Resasco, H. Robatjazi, I. B. Alvarez, O. Abdelrahman, P. Dauenhauer and P. Christopher, *ACS Energy Lett.*, 2020, **5**, 3518-3525.
127. S. Luo, H. Song, D. Philo, M. Oshikiri, T. Kako and J. Ye, *Appl. Catal., B* 2020, **272**, 118965.
128. Y. Zhao, B. Zhao, J. Liu, G. Chen, R. Gao, S. Yao, M. Li, Q. Zhang, L. Gu, J. Xie, X. Wen, L.-Z. Wu, C.-H. Tung, D. Ma and T. Zhang, *Angew. Chem. Int. Ed.*, 2016, **55**, 4215-4219.
129. C. Dong, X. Zong, Z. Liu, L. Niu, Z. Zhao, L. An, D. Qu, X. Wang and Z. Sun, *Cell Rep. Phys. Sci.*, 2021, **2**, 100678.
130. P. Novello, C. V. Varanasi and J. Liu, *ACS Catal.*, 2019, **9**, 578-586.
131. Y. Yang, Y. Li, Q. Zhang, M. Zeng, S. Wu, L. Lan and X. Zhao, *J. Mater. Chem. A*, 2018, **6**, 14195-14206.
132. L. Kang, X. Y. Liu, A. Wang, L. Li, Y. Ren, X. Li, X. Pan, Y. Li, X. Zong, H. Liu, A. I. Frenkel and T. Zhang, *Angew. Chem. Int. Ed.*, 2020, **59**, 12909-12916.
133. X. Feng, D. Liu, B. Yan, M. Shao, Z. Hao, G. Yuan, H. Yu and Y. Zhang, *Angew. Chem. Int. Ed.*, 2021, **60**, 18552-18556.
134. K. Huang, L. Lin, K. Yang, W. Dai, X. Chen and X. Fu, *Appl. Catal., B* 2015, **179**, 395-406.
135. G. Cheng, X. Tan, X. Song, X. Chen, W. Dai, R. Yuan and X. Fu, *Appl. Catal., B* 2019, **251**, 130-142.
136. G. Cheng, Z. Cai, X. Song, X. Chen, W. Dai and X. Fu, *Appl. Catal., B* 2022, **304**, 120988.
137. M. P. Thekaekara, *Sol. Energy*, 1976, **18**, 309-325.
138. D. M. Schultz and T. P. Yoon, *Science*, 2014, **343**, 1239176.
139. X. Chen, L. Liu and F. Huang, *Chem. Soc. Rev.*, 2015, **44**, 1861-1885.
140. Z. Li, J. Liu, R. Shi, G. I. N. Waterhouse, X.-D. Wen and T. Zhang, *Adv. Energy Mater.*, 2021, **11**, 2002783.
141. X. Wu, J. Lang, Z. Sun, F. Jin and Y. H. Hu, *Appl. Catal., B* 2021, **295**, 120312.
142. W. Zhang, L. Wang, K. Wang, M. U. Khan, M. Wang, H. Li and J. Zeng, *Small*, 2017, **13**, 1602583.
143. J. Li, Y. Ye, L. Ye, F. Su, Z. Ma, J. Huang, H. Xie, D. E. Doronkin, A. Zimina, J.-D. Grunwaldt and Y. Zhou, *J. Mater. Chem. A*, 2019, **7**, 2821-2830.
144. Y. Qi, L. Song, S. Ouyang, X. Liang, S. Ning, Q. Zhang and J. Ye, *Adv. Mater.*, 2020, **32**, 1903915.
145. M.-Q. Yang, L. Shen, Y. Lu, S. W. Chee, X. Lu, X. Chi, Z. Chen,

Q.-H. Xu, U. Mirsaidov and G. W. Ho, *Angew. Chem. Int. Ed.*, 2019, **58**, 3077-3081.
146. Y. Li, C. Wang, M. Song, D. Li, X. Zhang and Y. Liu, *Appl. Catal., B* 2019, **243**, 760-770.
147. F. Yu, C. Wang, Y. Li, H. Ma, R. Wang, Y. Liu, N. Suzuki, C. Terashima, B. Ohtani, T. Ochiai, A. Fujishima and X. Zhang, *Adv. Sci.*, 2020, **7**, 2000204.
148. Y. Qi, J. Jiang, X. Liang, S. Ouyang, W. Mi, S. Ning, L. Zhao and J. Ye, *Adv. Funct. Mater.*, 2021, **31**, 2100908.
149. W. H. Saputera, J. Scott, H. Tahini, G. K. C. Low, X. Tan, S. Smith, D.-W. Wang and R. Amal, *ACS Catal.*, 2017, **7**, 3644-3653.
150. T. H. Tan, J. Scott, Y. H. Ng, R. A. Taylor, K.-F. Aguey-Zinsou and R. Amal, *ACS Catal.*, 2016, **6**, 8021-8029.
151. L. Yuan, M. Lou, B. D. Clark, M. Lou, L. Zhou, S. Tian, C. R. Jacobson, P. Nordlander and N. J. Halas, *ACS Nano*, 2020, **14**, 12054-12063.
152. H. Robatjazi, M. Lou, B. D. Clark, C. R. Jacobson, D. F. Swearer, P. Nordlander and N. J. Halas, *Nano Lett.*, 2020, **20**, 4550-4557.
153. P. F. Liao and A. Wokaun, *J. Chem. Phys.*, 1982, **76**, 751-752.
154. M. Januar, B. Liu, J.-C. Cheng, K. Hatanaka, H. Misawa, H.-H. Hsiao and K.-C. Liu, *J. Phys. Chem. C*, 2020, **124**, 3250-3259.
155. B. D. Clark, C. R. Jacobson, M. Lou, D. Renard, G. Wu, L. Bursi, A. S. Ali, D. F. Swearer, A.-L. Tsai, P. Nordlander and N. J. Halas, *ACS Nano*, 2019, **13**, 9682-9691.
156. L. Yuan, C. Zhang, X. Zhang, M. Lou, F. Ye, C. R. Jacobson, L. Dong, L. Zhou, M. Lou, Z. Cheng, P. M. Ajayan, P. Nordlander and N. J. Halas, *Nano Lett.*, 2019, **19**, 4413-4419.
157. S. Dal Forno, L. Ranno and J. Lischner, *J. Phys. Chem. C*, 2018, **122**, 8517-8527.
158. Q. Zhang, W. Li, C. Moran, J. Zeng, J. Chen, L.-P. Wen and Y. Xia, *J. Am. Chem. Soc.*, 2010, **132**, 11372-11378.
159. H. Wu, J. Carrete, Z. Zhang, Y. Qu, X. Shen, Z. Wang, L.-D. Zhao and J. He, *NPG Asia Mater.*, 2014, **6**, e108-e108.
160. J. Lim, K. Hippalgaonkar, S. C. Andrews, A. Majumdar and P. Yang, *Nano Lett.*, 2012, **12**, 2475-2482.
161. D. F. Swearer, H. Zhao, L. Zhou, C. Zhang, H. Robatjazi, J. M. P. Martirez, C. M. Krauter, S. Yazdi, M. J. McClain, E. Ringe, E. A. Carter, P. Nordlander and N. J. Halas, *Proc. Nat. Acad. Sci.*, 2016, **113**, 8916-8920.
162. C. Zhang, H. Zhao, L. Zhou, A. E. Schlather, L. Dong, M. J. McClain, D. F. Swearer, P. Nordlander and N. J. Halas, *Nano Lett.*, 2016, **16**, 6677-6682.
163. D. F. Swearer, H. Robatjazi, J. M. P. Martirez, M. Zhang, L. Zhou, E. A. Carter, P. Nordlander and N. J. Halas, *ACS Nano*, 2019, **13**, 8076-8086.
164. K. Li, N. J. Hogan, M. J. Kale, N. J. Halas, P. Nordlander and P. Christopher, *Nano Lett.*, 2017, **17**, 3710-3717.
165. M. Zeng, Y. Li, M. Mao, J. Bai, L. Ren and X. Zhao, *ACS Catal.*, 2015, **5**, 3278-3286.
166. L. Lan, Y. Li, M. Zeng, M. Mao, L. Ren, Y. Yang, H. Liu, L. Yun and X. Zhao, *Appl. Catal., B* 2017, **203**, 494-504.
167. M. J. Muñoz-Batista, A. M. Eslava-Castillo, A. Kubacka and M. Fernández-García, *Appl. Catal., B* 2018, **225**, 298-306.
168. S. W. L. Ng, M. Gao, W. Lu, M. Hong and G. W. Ho, *Adv. Funct. Mater.*, 2021, **31**, 2104750.
169. Z. Wu, C. Li, Z. Li, K. Feng, M. Cai, D. Zhang, S. Wang, M. Chu, C. Zhang, J. Shen, Z. Huang, Y. Xiao, G. A. Ozin, X. Zhang and L. He, *ACS Nano*, 2021, **15**, 5696-5705.
170. S. Chen, S. Fang, Z. Sun, Z. Li, C. Wang and Y. H. Hu, *Chem. Commun.*, 2022, **58**, 787-790.
171. H. Robatjazi, H. Zhao, D. F. Swearer, N. J. Hogan, L. Zhou, A. Alabastri, M. J. McClain, P. Nordlander and N. J. Halas, *Nat. Comm.*, 2017, **8**, 27.
172. Y. Sivan, J. Baraban, W. Un Ieng and Y. Dubi, *Science*, 2019, **364**, eaaw9367.
173. L. Luo, J. Luo, H. Li, F. Ren, Y. Zhang, A. Liu, W.-X. Li and J. Zeng, *Nat. Comm.*, 2021, **12**, 1218.
174. R. Das, S. Chakraborty and S. C. Peter, *ACS Energy Lett.*, 2021, **6**, 3270-3274.
175. T. H. Tan, J. Scott, Y. H. Ng, R. A. Taylor, K.-F. Aguey-Zinsou and R. Amal, *ACS Catal.*, 2016, **6**, 1870-1879.
176. J.-J. Li, S.-C. Cai, E.-Q. Yu, B. Weng, X. Chen, J. Chen, H.-P. Jia and Y.-J. Xu, *Appl. Catal., B* 2018, **233**, 260-271.
177. H. Zhang, T. Wang, J. Wang, H. Liu, T. D. Dao, M. Li, G. Liu, X. Meng, K. Chang, L. Shi, T. Nagao and J. Ye, *Adv. Mater.*, 2016, **28**, 3703-3710.
178. P. G. O'Brien, K. K. Ghuman, A. A. Jelle, A. Sandhel, T. E. Wood, J. Y. Y. Loh, J. Jia, D. Perovic, C. V. Singh, N. P. Kherani, C. A. Mims and G. A. Ozin, *Energy Environ. Sci.*, 2018, **11**, 3443-3451.
179. Z. Lou, D. Yuan, F. Zhang, Y. Wang, Y. Li and L. Zhu, *Nano Energy*, 2019, **62**, 653-659.
180. C. Shi, D. Yuan, L. Ma, Y. Li, Y. Lu, L. Gao, X. San, S. Wang and G. Fu, *J. Mater. Chem. A*, 2020, **8**, 19467-19472.
181. Y. Wang, W. Huang, S. Guo, X. Xin, Y. Zhang, P. Guo, S. Tang and X. Li, *Adv. Energy Mater.*, 2021, **11**, 2102452.
182. B. Dai, J. Fang, Y. Yu, M. Sun, H. Huang, C. Lu, J. Kou, Y. Zhao and Z. Xu, *Adv. Mater.*, 2020, **32**, 1906361.
183. Y. Wang, L. Zhu, Y. Feng, Z. Wang and Z. L. Wang, *Adv. Funct. Mater.*, 2019, **29**, 1807111.
184. H.-C. Yuan, V. E. Yost, M. R. Page, P. Stradins, D. L. Meier and H. M. Branz, *Appl. Phys. Lett.*, 2009, **95**, 123501.
185. P. G. O'Brien, A. Sandhel, T. E. Wood, A. A. Jelle, L. B. Hoch, D. D. Perovic, C. A. Mims and G. A. Ozin, *Adv. Sci.*, 2014, **1**, 1400001.
186. Y. Wang, W. Liang, F. Liang, C. Wang, X. Song, M. Huang and H. Jiang, *Mater. Today Energy*, 2020, **16**, 100391.
187. D. Yadav and R. Banerjee, *Renew. Sustain. Energy Rev.*, 2016, **54**, 497-532.
188. W. K. Fan and M. Tahir, *Chem. Eng. J.*, 2022, **427**, 131617.
189. N. Keller, J. Ivanez, J. Highfield and A. M. Ruppert, *Appl. Catal., B* 2021, **296**, 120320.
190. X. E. Cao, Y. Kaminer, T. Hong, P. Schein, T. Liu, T. Hanrath and D. Erickson, *iScience*, 2020, **23**, 101856.
191. D. Marxer, P. Furler, M. Takacs and A. Steinfeld, *Energy Environ. Sci.*, 2017, **10**, 1142-1149.
192. E. T. Kho, T. H. Tan, E. Lovell, R. J. Wong, J. Scott and R. Amal, *Green Energy Environ.*, 2017, **2**, 204-217.
193. M. Gao, P. K. N. Connor and G. W. Ho, *Energy Environ. Sci.*, 2016, **9**, 3151-3160.
194. C. Wang, Z. Sun, Y. Zheng and Y. H. Hu, *J. Mater. Chem. A*, 2019, **7**, 865-887.
195. Y. H. Hu, *Angew. Chem. Int. Ed.*, 2012, **51**, 12410-12412.
196. Y. Li, M. Wen, Y. Wang, G. Tian, C. Wang and J. Zhao, *Angew. Chem. Int. Ed.*, 2021, **60**, 910-916.
197. D. Liu, Y. Xu, M. Sun, Y. Huang, Y. Yu and B. Zhang, *J. Mater. Chem. A*, 2020, **8**, 1077-1083.
198. S. Sarina, H.-Y. Zhu, Q. Xiao, E. Jaatinen, J. Jia, Y. Huang, Z. Zheng and H. Wu, *Angew. Chem. Int. Ed.*, 2014, **53**, 2935-2940.

199. L. Wang, Y. Wang, Y. Cheng, Z. Liu, Q. Guo, M. N. Ha and Z. Zhao, *J. Mater. Chem. A*, 2016, **4**, 5314-5322.
200. D. Li, Y. Huang, S. Li, C. Wang, Y. Li, X. Zhang and Y. Liu, *Chin. J. Catal.*, 2020, **41**, 154-160.
201. C. K. N. Peh, M. Gao and G. W. Ho, *J. Mater. Chem. A*, 2015, **3**, 19360-19367.
202. N. Zhou, R. Wang, X. Zhou, H. Song, X. Xiong, Y. Ding, J. Lü, L. Gan and T. Zhai, *Small*, 2018, **14**, 1702731.
203. D.-G. Xie, Z.-J. Wang, J. Sun, J. Li, E. Ma and Z.-W. Shan, *Nat. Mater.*, 2015, **14**, 899-903.
204. C. Mao, L. Yu, J. Li, J. Zhao and L. Zhang, *Appl. Catal., B* 2018, **224**, 612-620.
205. R. Fiorenza, M. Bellardita, S. A. Balsamo, L. Spitaleri, A. Gulino, M. Condorelli, L. D'Urso, S. Scirè and L. Palmisano, *Chem. Eng. J.*, 2022, **428**, 131249.
206. D. Mateo, J. Albero and H. García, *Appl. Catal., B* 2018, **224**, 563-571.
207. J. Barrio, D. Mateo, J. Albero, H. García and M. Shalom, *Adv. Energy Mater.*, 2019, **9**, 1902738.
208. F. Yu, C. Wang, H. Ma, M. Song, D. Li, Y. Li, S. Li, X. Zhang and Y. Liu, *Nanoscale*, 2020, **12**, 7000-7010.
209. A. V. Bandura and S. N. Lvov, *J. Phys. Chem. Ref. Data,* 2005, **35**, 15-30.
210. U. Caudillo-Flores, I. Barba-Nieto, M. J. Muñoz-Batista, D. Motta Meira, M. Fernández-García and A. Kubacka, *Chem. Eng. J.*, 2021, **425**, 130641.
211. C. Foo, Y. Li, K. Lebedev, T. Chen, S. Day, C. Tang and S. C. E. Tsang, *Nat. Comm.*, 2021, **12**, 661.
212. J. Guo, P. N. Duchesne, L. Wang, R. Song, M. Xia, U. Ulmer, W. Sun, Y. Dong, J. Y. Y. Loh, N. P. Kherani, J. Du, B. Zhu, W. Huang, S. Zhang and G. A. Ozin, *ACS Catal.*, 2020, **10**, 13668-13681.
213. J. Jia, P. G. O'Brien, L. He, Q. Qiao, T. Fei, L. M. Reyes, T. E. Burrow, Y. Dong, K. Liao, M. Varela, S. J. Pennycook, M. Hmadeh, A. S. Helmy, N. P. Kherani, D. D. Perovic and G. A. Ozin, *Adv. Sci.*, 2016, **3**, 1600189.
214. G. Fu, M. Jiang, J. Liu, K. Zhang, Y. Hu, Y. Xiong, A. Tao, Z. Tie and Z. Jin, *Nano Lett.*, 2021, **21**, 8824-8830.
215. X. Chen, G. Zhang, B. Li and L. Wu, *Sci. Adv.*, 2021, **7**, eabf8413.
216. K. Feng, S. Wang, D. Zhang, L. Wang, Y. Yu, K. Feng, Z. Li, Z. Zhu, C. Li, M. Cai, Z. Wu, N. Kong, B. Yan, J. Zhong, X. Zhang, G. A. Ozin and L. He, *Adv. Mater.*, 2020, **32**, 2000014.
217. C. Song, Z. Wang, Z. Yin, D. Xiao and D. Ma, *Chem Catal.*, 2022, **2**, 52-83.
218. W. Yang, Y. Liu, J. R. McBride and T. Lian, *Nano Lett.*, 2021, **21**, 453-461.
219. Y. Dubi, I. W. Un and Y. Sivan, *Chem. Sci.*, 2020, **11**, 5017-5027.
220. P. Schwach, X. Pan and X. Bao, *Chem. Rev.*, 2017, **117**, 8497-8520.
221. S. Duhr and D. Braun, *Proc. Nat. Acad. Sci.*, 2006, **103**, 19678.
222. S. Hu, B.-J. Liu, J.-M. Feng, C. Zong, K.-Q. Lin, X. Wang, D.-Y. Wu and B. Ren, *J. Am. Chem. Soc.*, 2018, **140**, 13680-13686.
223. H. Yang, L.-Q. He, Y.-W. Hu, X. Lu, G.-R. Li, B. Liu, B. Ren, Y. Tong and P.-P. Fang, *Angew. Chem. Int. Ed.*, 2015, **54**, 11462-11466.
224. D. Fukuhara, M. T. Joseph, T. Loumissi, C. Zhang, T. Itoi, H. Zhang and Y. Izumi, *J. Phys. Chem. C*, 2021, **125**, 14689-14701.
225. L. Lin, K. Wang, K. Yang, X. Chen, X. Fu and W. Dai, *Appl. Catal., B* 2017, **204**, 440-455.
226. Y. Tong, L. Song, S. Ning, S. Ouyang and J. Ye, *Appl. Catal., B* 2021, **298**, 120551.
227. Z. Yang, X. Xia, W. Yang, L. wang and Y. Liu, *Appl. Catal., B* 2021, **299**, 120675.
228. Y. Nosaka and A. Y. Nosaka, *Chem. Rev.*, 2017, **117**, 11302-11336.
229. Y. Xiao, Y. Huang, S. Xue and J. Zhao, *Appl. Catal., B* 2020, **265**, 118596.
230. D. Jiang, W. Wang, L. Zhang, R. Qiu, S. Sun and Y. Zheng, *Appl. Catal., B* 2015, **165**, 399-407.
231. N. J. Halas, S. Lal, W.-S. Chang, S. Link and P. Nordlander, *Chem. Rev.*, 2011, **111**, 3913-3961.
232. A. Manjavacas, J. G. Liu, V. Kulkarni and P. Nordlander, *ACS Nano*, 2014, **8**, 7630-7638.
233. Y. Xin, K. Yu, L. Zhang, Y. Yang, H. Yuan, H. Li, L. Wang and J. Zeng, *Adv. Mater.*, 2021, **33**, 2008145.
234. S. Linic, S. Chavez and R. Elias, *Nat. Mater.*, 2021, **20**, 916-924.
235. S. Linic, P. Christopher and D. B. Ingram, *Nat. Mater.*, 2011, **10**, 911-921.
236. C. Zhan, M. Moskovits and Z.-Q. Tian, *Matter*, 2020, **3**, 42-56.
237. B. Y. Zheng, H. Zhao, A. Manjavacas, M. McClain, P. Nordlander and N. J. Halas, *Nat. Comm.*, 2015, **6**, 7797.
238. L. Zhou, M. Lou, J. L. Bao, C. Zhang, J. G. Liu, J. M. P. Martirez, S. Tian, L. Yuan, D. F. Swearer, H. Robatjazi, E. A. Carter, P. Nordlander and N. J. Halas, *Proc. Nat. Acad. Sci.*, 2021, **118**, e2022109118.
239. C. Zhan, B.-W. Liu, Y.-F. Huang, S. Hu, B. Ren, M. Moskovits and Z.-Q. Tian, *Nat. Comm.*, 2019, **10**, 2671.
240. P. Christopher, H. Xin, A. Marimuthu and S. Linic, *Nat. Mater.*, 2012, **11**, 1044-1050.
241. S. W. Lee, W. Park, H. Lee, H. Chan Song, Y. Jung and J. Y. Park, *ACS Catal.*, 2019, **9**, 8424-8432.
242. D. Zhou, X. Li, Q. Zhou and H. Zhu, *Nat. Comm.*, 2020, **11**, 2944.
243. C. Boerigter, U. Aslam and S. Linic, *ACS Nano*, 2016, **10**, 6108-6115.
244. H. Jiang, X. Peng, A. Yamaguchi, T. Fujita, H. Abe and M. Miyauchi, *Chem. Commun.*, 2019, **55**, 13765-13768.
245. S. Mukherjee, F. Libisch, N. Large, O. Neumann, L. V. Brown, J. Cheng, J. B. Lassiter, E. A. Carter, P. Nordlander and N. J. Halas, *Nano Lett.*, 2013, **13**, 240-247.
246. Y. Xiong, H. Chen, Y. Hu, S. Yang, X. Xue, L. He, X. Liu, J. Ma and Z. Jin, *Nano Lett.*, 2021, **21**, 8693-8700.
247. L.-W. Chen, Y.-C. Hao, Y. Guo, Q. Zhang, J. Li, W.-Y. Gao, L. Ren, X. Su, L. Hu, N. Zhang, S. Li, X. Feng, L. Gu, Y.-W. Zhang, A.-X. Yin and B. Wang, *J. Am. Chem. Soc.*, 2021, **143**, 5727-5736.
248. Z. Rao, Y. Cao, Z. Huang, Z. Yin, W. Wan, M. Ma, Y. Wu, J. Wang, G. Yang, Y. Cui, Z. Gong and Y. Zhou, *ACS Catal.*, 2021, **11**, 4730-4738.
249. H. Liu, M. Li, T. D. Dao, Y. Liu, W. Zhou, L. Liu, X. Meng, T. Nagao and J. Ye, *Nano Energy*, 2016, **26**, 398-404.
250. H. Liu, X. Meng, T. D. Dao, H. Zhang, P. Li, K. Chang, T. Wang, M. Li, T. Nagao and J. Ye, *Angew. Chem. Int. Ed.*, 2015, **54**, 11545-11549.
251. Y. Kim, J. G. Smith and P. K. Jain, *Nat. Chem.*, 2018, **10**, 763-769.
252. C. Wang and D. Astruc, *Chem. Soc. Rev.*, 2014, **43**, 7188-7216.

253. K. Wu, J. Chen, J. R. McBride and T. Lian, *Science*, 2015, **349**, 632-635.
254. C. Xu, W. Huang, Z. Li, B. Deng, Y. Zhang, M. Ni and K. Cen, *ACS Catal.*, 2018, **8**, 6582-6593.
255. J. Liu, J. Feng, J. Gui, T. Chen, M. Xu, H. Wang, H. Dong, H. Chen, X. Li, L. Wang, Z. Chen, Z. Yang, J. Liu, W. Hao, Y. Yao, L. Gu, Y. Weng, Y. Huang, X. Duan, J. Zhang and Y. Li, *Nano Energy*, 2018, **48**, 44-52.
256. Y. Zhang, S. He, W. Guo, Y. Hu, J. Huang, J. R. Mulcahy and W. D. Wei, *Chem. Rev.*, 2018, **118**, 2927-2954.
257. V. A. Spata and E. A. Carter, *ACS Nano*, 2018, **12**, 3512-3522.
258. M. Vadai, D. K. Angell, F. Hayee, K. Sytwu and J. A. Dionne, *Nat. Comm.*, 2018, **9**, 4658.
259. S. Rej, L. Mascaretti, E. Y. Santiago, O. Tomanec, Š. Kment, Z. Wang, R. Zbořil, P. Fornasiero, A. O. Govorov and A. Naldoni, *ACS Catal.*, 2020, **10**, 5261-5271.
260. E. Kazuma, J. Jung, H. Ueba, M. Trenary and Y. Kim, *J. Am. Chem. Soc.*, 2017, **139**, 3115-3121.
261. P. V. Kumar, T. P. Rossi, D. Marti-Dafcik, D. Reichmuth, M. Kuisma, P. Erhart, M. J. Puska and D. J. Norris, *ACS Nano*, 2019, **13**, 3188-3195.
262. E. Kazuma, J. Jung, H. Ueba, M. Trenary and Y. Kim, *Science*, 2018, **360**, 521.
263. B. Seemala, A. J. Therrien, M. Lou, K. Li, J. P. Finzel, J. Qi, P. Nordlander and P. Christopher, *ACS Energy Lett.*, 2019, **4**, 1803-1809.
264. Y. Zhang, L. Yan, M. Guan, D. Chen, Z. Xu, H. Guo, S. Hu, S. Zhang, X. Liu, Z. Guo, S. Li and S. Meng, *Adv. Sci.*, **9**, 2102978.
265. Y. Zhou and J. Zhao, *Appl. Catal., B* 2022, **300**, 120721.
266. C. Boerigter, R. Campana, M. Morabito and S. Linic, *Nat. Comm.*, 2016, **7**, 10545.
267. M. A. Ardagh, M. Shetty, A. Kuznetsov, Q. Zhang, P. Christopher, D. G. Vlachos, O. A. Abdelrahman and P. J. Dauenhauer, *Chem. Sci.*, 2020, **11**, 3501-3510.
268. M. A. Ardagh, O. A. Abdelrahman and P. J. Dauenhauer, *ACS Catal.*, 2019, **9**, 6929-6937.
269. F. Sordello, F. Pellegrino, M. Prozzi, C. Minero and V. Maurino, *ACS Catal.*, 2021, **11**, 6484-6488.
270. J. Scott, W. Irawaty, G. Low and R. Amal, *Appl. Catal., B* 2015, **164**, 10-17.
271. W. H. Saputera, H. A. Tahini, M. Sabsabi, T. H. Tan, N. M. Bedford, E. Lovell, Y. Cui, J. N. Hart, D. Friedmann, S. C. Smith, R. Amal and J. Scott, *ACS Catal.*, 2019, **9**, 2674-2684.
272. T. Yan, L. Wang, Y. Liang, M. Makaremi, T. E. Wood, Y. Dai, B. Huang, A. A. Jelle, Y. Dong and G. A. Ozin, *Nat. Comm.*, 2019, **10**, 2521.
273. C. Xu, Y. Zhang, F. Pan, W. Huang, B. Deng, J. Liu, Z. Wang, M. Ni and K. Cen, *Nano Energy*, 2017, **41**, 308-319.
274. K. Wang, R. Jiang, T. Peng, X. Chen, W. Dai and X. Fu, *Appl. Catal., B* 2019, **256**, 117780.
275. P. Li, G. Xiao, Y. Zhao and H. Su, *ACS Catal.*, 2020, **10**, 3640-3649.
276. Y. Yang, Y. Li, M. Mao, M. Zeng and X. Zhao, *ACS Appl. Mater. Interfaces,* 2017, **9**, 2350-2357.
277. J. Chen, Y. Li, S. Fang, Y. Yang and X. Zhao, *Chem. Eng. J.*, 2018, **332**, 205-215.
278. E. Yu, J. Li, J. Chen, J. Chen, Z. Hong and H. Jia, *J. Hazard. Mater.*, 2020, **388**, 121800.
279. M. Zeng, Y. Li, F. Liu, Y. Yang, M. Mao and X. Zhao, *Appl. Catal., B* 2017, **200**, 521-529.
280. Y. Zhou, D. E. Doronkin, Z. Zhao, P. N. Plessow, J. Jelic, B. Detlefs, T. Pruessmann, F. Studt and J.-D. Grunwaldt, *ACS Catal.*, 2018, **8**, 11398-11406.
281. Y. Li, S. Wu, J. Wu, Q. Hu and C. Zhou, *J. Mater. Chem. A*, 2020, **8**, 8171-8194.
282. Y. Zeng, J. Zhong, H. Wang, M. Fu, D. Ye and Y. Hu, *Chem. Eng. J.*, 2021, **425**, 131658.
283. J. Li, M. Zhang, E. A. Elimian, X. Lv, J. Chen and H. Jia, *Chem. Eng. J.*, 2021, **412**, 128560.
284. F. Liu, M. Zeng, Y. Li, Y. Yang, M. Mao and X. Zhao, *Adv. Funct. Mater.*, 2016, **26**, 4518-4526.
285. H. Lynggaard, A. Andreasen, C. Stegelmann and P. Stoltze, *Prog. Surf. Sci.*, 2004, **77**, 71-137.
286. M. Bonn, S. Funk, C. Hess, D. N. Denzler, C. Stampfl, M. Scheffler, M. Wolf and G. Ertl, *Science*, 1999, **285**, 1042-1045.
287. S. Fang and Y. H. Hu, *Matter*, 2021, **4**, 1189-1223.
288. K. Sytwu, M. Vadai, F. Hayee, D. K. Angell, A. Dai, J. Dixon and J. A. Dionne, *Science*, 2021, **371**, 280-283.
289. C. Song, X. Liu, M. Xu, D. Masi, Y. Wang, Y. Deng, M. Zhang, X. Qin, K. Feng, J. Yan, J. Leng, Z. Wang, Y. Xu, B. Yan, S. Jin, D. Xu, Z. Yin, D. Xiao and D. Ma, *ACS Catal.*, 2020, **10**, 10364-10374.
290. X. Liu, G. Dong, S. Li, G. Lu and Y. Bi, *J. Am. Chem. Soc.*, 2016, **138**, 2917-2920.
291. L. Zhang, Y. Zhang, X. Huang, L. Tao and Y. Bi, *Appl. Catal., B* 2021, **283**, 119633.
292. L. Zhang, R. Long, Y. Zhang, D. Duan, Y. Xiong, Y. Zhang and Y. Bi, *Angew. Chem. Int. Ed.*, 2020, **59**, 6224-6229.
293. J. L. Bao and E. A. Carter, *J. Am. Chem. Soc.*, 2019, **141**, 13320-13323.
294. J. L. Bao and E. A. Carter, *ACS Nano*, 2019, **13**, 9944-9957.
295. P. Martirez John Mark and A. Carter Emily, *Sci. Adv.*, **3**, eaao4710.
296. B. Jin, X. Ye, H. Zhong, F. Jin and Y. H. Hu, *Chin. Chem. Lett.* , 2022, **33**, 812-816.
297. L. Wang, B. Zhao, C. Wang, M. Sun, Y. Yu and B. Zhang, *J. Mater. Chem. A*, 2020, **8**, 10175-10179.
298. L. Ming, C. Wang and Y. H. Hu, *Int. J. Energy Res.*, 2021, **45**, 12996-13006.
299. F. Liu, L. Song, S. Ouyang and H. Xu, *Catal. Sci. Technol.*, 2019, **9**, 2125-2131.
300. X.-N. Guo, Z.-F. Jiao, G.-Q. Jin and X.-Y. Guo, *ACS Catal.*, 2015, **5**, 3836-3840.
301. Y. Wang, Y. Zhao, J. Liu, Z. Li, G. I. N. Waterhouse, R. Shi, X. Wen and T. Zhang, *Adv. Energy Mater.*, 2020, **10**, 1902860.
302. X. Li, S. Zhao, X. Duan, H. Zhang, S.-z. Yang, P. Zhang, S. P. Jiang, S. Liu, H. Sun and S. Wang, *Appl. Catal., B* 2021, **283**, 119660.
303. Y. Wu, Y. Sun, W. Fu, X. Meng, M. Zhu, S. Ramakrishna and Y. Dai, *ACS Appl. Nano Mater.*, 2020, **3**, 2713-2722.
304. R. Verma, S. K. Samdarshi, S. Bojja, S. Paul and B. Choudhury, *Sol. Energy Mater. Sol. Cells*, 2015, **141**, 414-422.
305. L. Shi, Y. He, X. Wang and Y. Hu, *Energy Convers. Manage.*, 2018, **171**, 272-278.
306. J.-H. Kim, K. M. Twaddle, J. Hu and H. Byun, *ACS Appl. Mater. Interfaces,* 2014, **6**, 11514-11522.
307. B.-H. Lai, Y.-R. Lin and D.-H. Chen, *Chem. Eng. J.*, 2013, **223**, 418-424.
308. D. Zhu, L. Cai, Z. Sun, A. Zhang, P. Héroux, H. Kim, W. Yu and Y. Liu, *Sci. Total Environ.*, 2021, **787**, 147536.

 

309. J. Ni, D. Liu, W. Wang, A. Wang, J. Jia, J. Tian and Z. Xing, *Chem. Eng. J.*, 2021, **419**, 129969.
310. S. Dong, Y. Zhao, J. Yang, X. Liu, W. Li, L. Zhang, Y. Wu, J. Sun, J. Feng and Y. Zhu, *Appl. Catal., B* 2021, **291**, 120127.
311. R. Ma, J. Sun, D. H. Li and J. J. Wei, *Int. J. Hydrogen Energy,* 2020, **45**, 30288-30324.
312. F. Wang, Y. Huang, Z. Chai, M. Zeng, Q. Li, Y. Wang and D. Xu, *Chem. Sci.*, 2016, **7**, 6887-6893.
313. J. Hong, C. Xu, B. Deng, Y. Gao, X. Zhu, X. Zhang and Y. Zhang, *Adv. Sci.*, 2022, **9**, 2103926.
314. A. V. Tavasoli, M. Preston and G. Ozin, *Energy Environ. Sci.*, 2021, **14**, 3098-3109.
315. J. Albero, E. Dominguez, A. Corma and H. García, *Sustain. Energy Fuels*, 2017, **1**, 1303-1307.
316. J. U. Kim, S. Lee, S. J. Kang and T.-i. Kim, *Nanoscale*, 2018, **10**, 21555-21574.
317. Z. Aqachmar, H. Ben Sassi, K. Lahrech and A. Barhdadi, *Int. J. Hydrogen Energy,* 2021, **46**, 30790-30817.
318. F. Bayrak, N. Abu-Hamdeh, K. A. Alnefaie and H. F. Öztop, *Renew. Sustain. Energy Rev.*, 2017, **74**, 755-770.
319. H. I. Villafán-Vidales, C. A. Arancibia-Bulnes, D. Riveros-Rosas, H. Romero-Paredes and C. A. Estrada, *Renew. Sustain. Energy Rev.*, 2017, **75**, 894-908.
320. Y. Li, J. Hao, H. Song, F. Zhang, X. Bai, X. Meng, H. Zhang, S. Wang, Y. Hu and J. Ye, *Nat. Comm.*, 2019, **10**, 2359.
321. M. Mecklenburg, W. A. Hubbard, E. R. White, R. Dhall, S. B. Cronin, S. Aloni and B. C. Regan, *Science*, 2015, **347**, 629-632.
322. F. Menges, P. Mensch, H. Schmid, H. Riel, A. Stemmer and B. Gotsmann, *Nat. Comm.*, 2016, **7**, 10874.
323. D. Wang, Y. R. Koh, Z. A. Kudyshev, K. Maize, A. V. Kildishev, A. Boltasseva, V. M. Shalaev and A. Shakouri, *Nano Lett.*, 2019, **19**, 3796-3803.
324. P. Ren and X. Yang, *Sol. RRL*, 2018, **2**, 1700233.
325. X. Niu, Y. Li, Y. Zhang, Z. Zhou and J. Wang, *ACS Appl. Mater. Interfaces,* 2019, **11**, 17987-17993.